Università degli Studi di Napoli Federico II
Ph.D. Program in
Information Technology and Electrical Engineering
XXXV Cycle

Thesis for the Degree of Doctor of Philosophy

Disturbance rejection in optimal control for limbed parallel robots

by

Viviana Morlando

Advisor: Prof. Fabio Ruggiero

Scuola Politecnica e delle Scienze di Base
Dipartimento di Ingegneria Elettrica e delle Tecnologie dell'Informazione

To my parents

and

to my beloved grandfather

Disturbance rejection in optimal control for limbed parallel robots

Ph.D. Thesis presented
for the fulfillment of the Degree of Doctor of Philosophy
in Information Technology and Electrical Engineering
by

Viviana Morlando

January 2023

Approved as to style and content by

Prof. Fabio Ruggiero, Advisor

Università degli Studi di Napoli Federico II
Ph.D. Program in Information Technology and Electrical Engineering
XXXV cycle - Chairman: Prof. Stefano Russo

http://itee.dieti.unina.it

Candidate's declaration

I hereby declare that this thesis submitted to obtain the academic degree of Philosophiæ Doctor (Ph.D.) in Information Technology and Electrical Engineering is my own unaided work, that I have not used other than the sources indicated, and that all direct and indirect sources are acknowledged as references.
Parts of this dissertation have been published in international journals and/or conference articles (see list of the author's publications at the end of the thesis).

Napoli, March 10, 2023

Viviana Morlando

Abstract

Over the years, robot started to be used in broad but cluttered environments to accomplish different tasks. For this reason, the research in field and service robotics has been directed towards robots able to traverse large spaces. These robots have to operate in highly complex terrains, and need to move in wide spaces. For this reason they are characterized by a mobile platform. Despite the most used mobile robots are the wheeled one, they could encounter some difficulties when moving on challenging and irregular terrain. For this reason, other kind of robots started to be used, able to overcome obstacles and move in complex environments. Nevertheless, these kinds of robots are more unstable and subject to external disturbances. For this reason, in this thesis, our main focus will be to investigate disturbance rejection strategies for a particular type of mobile base robots: the limbed parallel robots. These robots comprise a mobile floating base that is connected to a fixed base by some independent kinematic chains, referred to as limbs. This category encompasses both legged and cable-driven parallel robots, which have demonstrated the ability to overcome many of the limitations associated with wheeled robots. These robots are highly maneuverable and can navigate challenging terrains and obstacles with relative ease.

- **Quadruped robots**. External disturbances, such as hitting the ground, can cause their fall. For this reason, a disturbance observer-based control is presented in this thesis. It presents a novel momentum-based observer that can deal with disturbances applied both to swing and stance legs. Then, an extension is developed, realizing a novel hybrid observer that integrates the previous estimation on the legs with a double observer on the center of mass. In this way, all kinds of disturbances acting on the robot are taken into account and compensated.

- **Cable-driven parallel robots**. By replacing rigid links with cables, cable-driven parallel robots can expand their workspace and increase their load capacity. However, this modification comes at a cost of significant vibrations resulting from cable flexibility, which makes the robot susceptible to external disturbances that can disrupt its stability. To address this issue, this thesis proposes a model predictive controller for underconstrained cable-driven parallel robots that takes into account tension limits. This controller implementation enables the robot to approach the equilibrium point safely and smoothly, reducing the oscillatory movements caused by cable flexibility.

Keywords: legged robots, cable-driven parallel robots, disturbance rejection, optimal control, model predictive controller, whole-body controller

Sintesi in lingua italiana

Nel corso degli anni, i robot hanno iniziato ad operare in ambienti vasti e pieni di ostacoli. Per questo motivo, la robotica di campo e di servizio ha iniziato a sviluppare robot capaci di attraversare ampi spazi. Questi robot devono operare in luoghi complessi, e, data la necessità di muoversi in spazi ampi, solitamente sono dotati di una piattaforma mobile.
Nonostante i robot mobili più usati siano dotati di ruote, questi ultimi possono incontrare difficoltà quando operano in ambienti complessi ed irregolari, pieni di ostacoli.
Per questo motivo, altri robot hanno cominciato ad essere usati, capaci di superare gli ostacoli e muoversi in ambienti complessi. Nonostante la loro capacità di operare in ambienti non strutturati e sconnessi, questi robot sono più instabili e soggetti a disturbi esterni. Per questo motivo, questa tesi si concentra sulle strategie di reiezione dei disturbi per una sottoclasse di robot mobili: i robot paralleli dotati di arti. Questi robot comprendono una base mobile connessa ad un sistema fisso tramite almeno due catene cinematiche indipendenti. Questa categoria include i robot su gambe ed i robot paralleli azionati dai cavi. Entrambe queste tipologie di robot riescono a superare il problema presente nel caso dei robot dotati di ruote, potendo superare agilmente gli ostacoli e navigare terreni complessi. La tesi può essere suddivisa in due sezioni principali:

- **Robot quadrupedi.** Disturbi esterni, come l'urto al suolo, possono provocarne la caduta. Per questo motivo, questa tesi presenta un controllore basato sull'osservatore del disturbo. Verrà dapprima presentato un nuovo osservatore basato sul momento in grado di trattare i disturbi applicati sia alle gambe in movimento che a quelle ferme. Successivamente, viene sviluppata un'estensione, realizzando un nuovo osservatore ibrido che integra la precedente stima sulle gambe con un doppio osservatore sul centro di massa. In questo modo vengono presi in considerazione e compensati tutti i tipi di disturbo che agiscono sul robot.

- **Robot paralleli guidati da cavi (CDPR).** Sostituire i link rigidi con i cavi si introducono significative vibrazioni dovute alla loro flessibilità, rendendo il robot vulnerabile ai disturbi esterni che possono inficiare l'equilibrio del robot. In questa tesi viene presentato un controllore predittivo basato sul modello per CDPR sottovincolati, ovvero con numero di cavi inferiore al numero di gradi di libertà. L'utilizzo di questo controllore, tenendo conto dei limiti di tensione, consente al robot di avvicinarsi al punto di equilibrio in modo controllato e sicuro, attenuando i movimenti oscillatori causati dalla flessibilità dei cavi.

Parole chiave: robot su gambe, robot paralleli guidati da cavi, controllo ottimo, reiezione dei disturbi, controllo predittivo basato sul modello, controllo whole-body

Contents

Abstract ii

Sintesi in lingua italiana iv

Acknowledgements viii

List of Acronyms ix

List of Figures xv

List of Symbols 1

1 Introduction **1**

1.1 Limbed parallel robots 4

1.2 Disturbance rejection 6

1.3 Optimal Control 9

1.4 Contribution of the Thesis 10

1.5 Thesis Structure 12

2 Disturbance Rejection in Optimal Control for Quadruped Robots **13**

2.1 State of the art 13

2.2 Main Contributions 18

2.3 Dynamic model of quadruped robots 19

2.4 Whole-Body Controller 22

2.4.1 Foot Scheduler and motion planner 23

2.4.2 Disturbance Observer 25
2.4.3 Optimization-based Controller 30
2.5 Case Studies 36
2.5.1 Setup 36
2.5.2 Disturbance rejection through observer on the legs . 37
2.5.3 Disturbance rejection with hybrid observer with momentum-based acting on the legs 54
2.5.4 A possible application: A Guide Dog to Help Visually Impaired People 61

3 Disturbance Rejection in optimal control for cable-driven parallel robots 73
3.1 State of the art 73
3.2 Main Contributions 78
3.3 Dynamic model of a cable-driven parallel robot 78
3.4 Model Predictive Controller 81
3.5 Experiments 84
3.5.1 Floating robot 84
3.5.2 Inverse Geometric Problem of a Cable-Driven Parallel Robot with four cables 85
3.5.3 Experiments results 87

4 Conclusions and future study 95
4.1 Main Results 95
4.2 Future Developments 97

Bibliography 99

Author's Publications 111

Acknowledgements

After three years of dedicated study and hard work, I am grateful to be concluding this journey, and I would like to express my sincere appreciation to the many people who have supported me throughout this experience.

Firstly, I must thank my supervisor, Prof. Fabio Ruggiero, for providing me with this incredible opportunity to continue my learning. He has been an outstanding instructor, always patient and available to help me overcome any difficulties that I faced.

I would also like to extend my heartfelt gratitude to Prof. Marco Hutter, for his warm hospitality in his Robotic System Lab at ETH Zurich. It was an incredible six months full of discoveries, and I had the privilege of working with a fantastic group of people. Additionally, the city of Zurich will always hold a special place in my heart.

To my dear friend, Matteo, I am grateful for your unwavering support during both the good and the bad times. I hope to always have you by my side in the future.

To my best friend, Chicca, thank you for always being there for me, through thick and thin. Your support and friendship have been invaluable.

To my parents, who have given me everything I need to build my future, and to my brother, whose constant presence assures me that I am never alone, I am forever grateful.

Lastly, I would like to thank Prof. Bruno Siciliano and all the members of the PRISMA Lab, who have become like family to me over the past few years.

Finally, I must express my gratitude to Jonathan, the best gift that this PhD has given me. From the moment we met, he has been my closest friend, always brightening my days and filling them with joy. Thank you for being the perfect companion that everyone deserves by their side.

The research leading to these results has been supported by both the

PRINBOT project (in the frame of the PRIN 2017 research program, grant number 20172HHNK5 002) . The authors are solely responsible for its content.

List of Acronyms

The following acronyms are used throughout the thesis.

CoM	Center of mass
CDPR	Cable-Driven Parallel Robot
DoF	Degree of freedom
IMU	Inertia Measurement Unit
LQ	Linear Quadratic
MPC	Model Predictive Control
QP	Quadratic Problem
SLQ	Sequential Linear Quadratic
WBC	Whole-Body Control
WCW	Wrench Closure Workspace
WFW	Wrench Feasible Workspace
ZMP	Zero Moment Point

List of Figures

1.2 On the left, a mobile manipulator during an assembly task in an industrial application [58]. On the right, a vacuum cleaner robot [77]. 3

1.3 A cable-driven parallel robot with 4 cables. In red one of the closed loop created by two cables (dashed red segments). Blue circles highlights the fixed points of these cables on the wall. 4

1.4 A quadruped during the walking. The feet in contact with the ground creates a closed loop. 5

2.1 DogBot, the platform used for simulations. The reference frames for the robot are shown. Ground reaction forces need to stay in the cones. 20

2.2 Conceptual block scheme of the devised whole-body controller. 22

2.3 Analysis on the order of the estimator. (a) Estimation's error for first (blue) and second (orange) order. (b) Estimation's error for second (blue), third (green), fourth (yellow) and fifth (violet) order. 39

2.4 Case Study A1. In this simulation, external forces on swing legs are not compensated. These pictures show instants when the disturbance is around its peaks. The yellow arrow indicates the application point and direction of the force. The green circle represents the planned foothold, the drift of the foot is evident. At 11.3 s, the robot loses its balance. 39
2.5 Case Study A1. Error norm of the robot's CoM using the proposed whole-body controller. 41
2.6 Case Study A1. Estimation of the disturbance through the proposed momentum-based observer. In blue the estimated force, in orange the actual force. 41
2.7 Case Study A1. Error norm of the ground reaction forces for front left leg, using the proposed whole-body controller. 42
2.8 Case Study A2. Comparison between several control techniques. The plot show the error norm of the robot's CoM for each of the considered observer. From left to right: the results obtained with the proposed controller; the results obtained using [36]; the results obtained through [23]. 42
2.9 Case Study A2. Comparison between several control techniques. The plot shows the error norm of the front left foot position for each of the considered observer. From left to right: the results obtained with the proposed controller; the results obtained using [36]; the results obtained through [23]. 43
2.10 Case Study A3: Error norm of the front right foot position using the proposed whole-body controller. 44
2.11 Case Study A3: Estimation of the disturbance through the proposed momentum-based observer. In blue the estimated force, in orange the actual force. 45
2.12 Case Study A3: Error norm of the robot's CoM using the proposed whole-body controller. 45

2.13 Case Study A4: Error norm of the robot's CoM using the proposed whole-body controller. (a) Ideal situation. (b) White Gaussian noise added on the joint torque measurement. 47
2.14 Case Study A4-Ideal situation. (a),(c),(e),(g) Estimation of the disturbance on the four legs, in blue the estimated force, in orange the actual force. (b),(d),(f),(h) Error norm of respective feet. 48
2.15 Case Study A4-White Gaussian noise added on the joint torque measurement. (a),(c),(e),(g) Estimation of the disturbance on the four legs, in blue the estimated force, in orange the actual force. (b),(d),(f),(h) Error norm of respective feet. 49
2.16 Case Study A5: Error norm of the robot's CoM using the proposed whole-body controller. 50
2.17 Case Study A5. (a),(c),(e),(g) Estimation of the disturbance on the four legs, in blue the estimated force, in orange the actual force. (b),(d),(f),(h) Error norm of respective feet. . . 52
2.18 Case Study A6: Environment of the Case Study 6. The friction coefficient is: 0.4 for blue blocks, 0.6 for green blocks, 0.8 for red blocks, and 1 for the ground. The height of the blocks is: 0.015 m for blue blocks, 0.04 m for green blocks, and 0.02 m for red blocks. 53
2.19 Case Study A6. Error norm of the feet. 54
2.20 Case Study A6: Error norm of the robot's CoM using the proposed whole-body controller. 55
2.21 Scenario used for Case Study B1. 55
2.22 Case Study B1. Error on the $x-$axis (a) and on the $z-$axis (b). 57
2.23 Case Study B1. Estimation of $\hat{f}_c$ (a) and $\hat{\tau}_c$ (b). 58

2.24 Case Study B2. Error norm of the robot's CoM using the proposed controller. 59
2.25 Case Study B2. Estimation of $\hat{f}_c$ (a) and $\hat{\tau}_c$ (b). 60
2.26 Case Study B2. Estimation of $\hat{f}_e$ for the rear right leg. . . . 61
2.27 Case Study B3. Error norm of the robot's CoM using the proposed controller. 62
2.28 On the left, a guide dog helping a visually impaired person. On the right, a quadruped is connected to a human through a leash in the Gazebo simulation environment. 63
2.29 Conceptual block scheme of the devised framework. 64
2.30 Case study C1. Estimated force (blue) and actual force (red). 67
2.32 Case study C1. Distance l between the robot and the human. 68
2.31 Case study C1. Human (blue) and robot (red) positions. . . 68
2.33 Case study C1. Human (blue) and robot (red) velocities in the sinusoidal trend. 69
2.34 Case study C2. Estimated force (blu) and actual force (red). 69
2.35 Case study C2. Human (red) and robot (blu) trajectories. The arrows indicate the starting points. 70
2.36 Case Study C3. Scenario and movements. 70
2.37 Case Study C3. Estimated force along the $x-$ (a) and the $y-$ (b) axes. 71

3.1 Scheme of a CDPR with n_c cables. In the figure, the main frame are shown: $\mathscr{B}$ is the frame attached to the floating base's CoM, $\mathscr{W}$ is the inertial fixed frame. The black parallelogram represents the environment on which the cables are attached. The red figure represents the moving platform of the robot. 79
3.2 The floating robot, used for the experiments, during a locomotion task within a vineyard. 85

3.3 The setup of the experiments, the four cables are attached to the wall with four hooks, that are positioned in order to create a parallelogram whose dimension is 7×9 m. 88

3.4 Force of cable 1 during the task: (a) MPC with no desired input (b) MPC with equilibrium input (c) PD. 90

3.5 Force derivative for cable 1. 91

3.6 Euler angles during the task: (a) MPC with no desired input (b) MPC with equilibrium input (c) PD. 92

3.7 Linear acceleration during the task: (a) MPC with no desired input (b) MPC with equilibrium input (c) PD. 93

3.8 x and y component during the task: (a) MPC with equilibrium input (b) PD. 93

3.9 Euler angles during the task: (a) MPC with equilibrium input (b) PD. 94

Chapter 1

Introduction

The origins of robotics can be found firstly in the literature and imagination of human beings and only later in science. Indeed, the word "robot" was introduced in 1920 through the play "Rossum's Universal Robots" written by the Czech Karel Capek with the meaning of executive labour.

Starting from the first robotics manipulators employed in industries (Fig. 1.1), humans have always tried to build new machines to help them with heavy and repetitive tasks and ultimately replace them with the riskiest work. Over the years, robots passed from the structured and closed spaces of industries to unstructured and open spaces full of obstacles. The branch involved in realizing technologies operating in these environments is called field robotics [87], which encompasses the automation in applications such as search and rescue, agriculture, underwater exploration, and patrolling.

Besides the work in unstructured but isolated environments, robots started to dominate also fields where interaction with human beings is predominant. Indeed, in recent years, different robots have also been developed and deployed in service fields ranging from tourism and hospitality to home care assistance [41]. In all these applications, robots must be able to dexterously and safely interact in a usually broad but cluttered environment to accomplish different tasks. For this reason, the research in field and service robotics has been directed towards robots able to traverse large spaces. These robots should operate in places where dextrous and safe interaction with humans is required, or in highly complex terrains

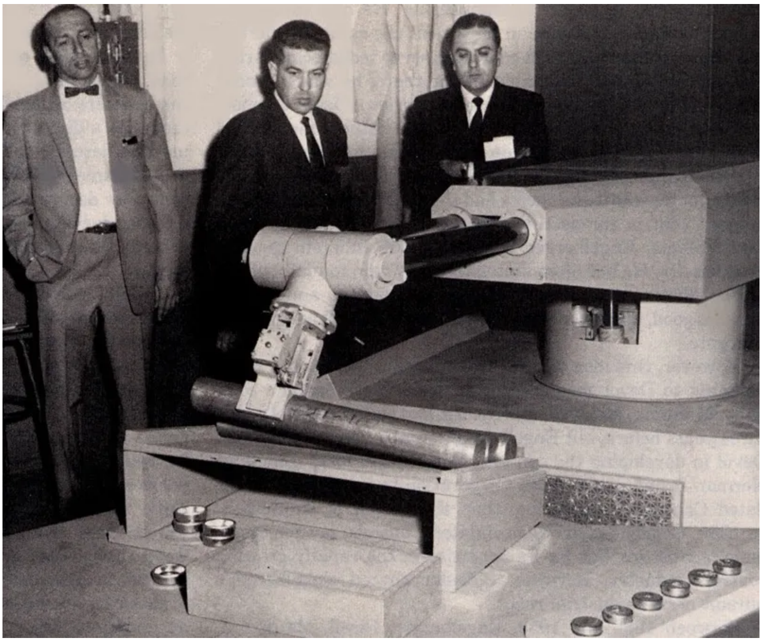

Figure 1.1. Unimate, the first industrial robot in 1950s, a precursor of the machines that now automate assembly lines all over the world [37].

where agility and robust performance are the main requirements. The main characteristic that a robot capable of operating in an unstructured and broad space needs to have is a mobile platform [73], that can change its position and orientation relative to an inertial frame. In this way, the robot can move around in the environment, unlike the typical robotic manipulator used in industries constrained to a fixed base.

Different kinds of robots with a mobile base have been realized over the years, and the first one to be introduced in real-life environments has been the wheeled mobile robot (Fig. 1.2) [15, 58, 77], in which the base is endowed with wheels. Using wheels allows navigation in a wide space in small time. It also guarantees an intrinsic balance since the robot is continuously in contact with a surface. However, despite their capability to traverse great distances in a relatively short time and the ease of retaining balance, wheeled robots can encounter difficulties whenever they need to move in challenging terrains. On complex and uneven ground, the wheels

Figure 1.2. On the left, a mobile manipulator during an assembly task in an industrial application [58]. On the right, a vacuum cleaner robot [77].

can easily remain stuck, and they can not overcome obstacles if present, but they need to circumnavigate them. Other mobile base robots have been developed to improve mobility over rough terrains, with different methods of actuation.

- Aerial robots: endowed with propellers allowing them to fly over challenging terrain, solving the problem of remaining stuck [34].
- Legged robots: they move through the legs, kinematic chains that allow to can adapt their gait to the irregularities of the terrain, modulating the ground reaction forces [46].
- Cable-driven parallel robots: they are wired-driven robots able to traverse large spaces, which perimeter is delimited from some anchor points for the cables [69].

Despite their ability to navigate in complex environments, these types of robots are often more prone to instability and external disturbances. These disruptions can come from a variety of sources, including the ground and the external environment, especially in severe atmospheric conditions or cluttered spaces where collisions between the robot and its surroundings are more likely.

In this work of thesis, the focus will be on the disturbance rejection strategies for a subclass of mobile base robots: the limbed parallel robots, including legged and cable-driven parallel robots.

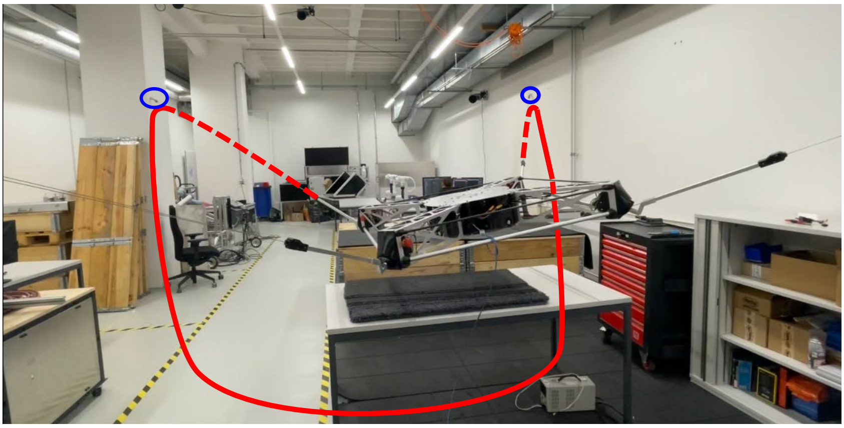

Figure 1.3. A cable-driven parallel robot with 4 cables. In red one of the closed loop created by two cables (dashed red segments). Blue circles highlights the fixed points of these cables on the wall.

1.1 Limbed parallel robots

Legged and cable-driven robots belong to the class of limbed parallel robots. These robots can be defined as a closed-loop mechanism composed of a floating base linked to a fixed base by some independent kinematic chains [67]. The serial chains between the mobile base and the fixed one are usually called limbs.

Parallel robots are developed in order to substitute serial manipulators in dull and heavy tasks, thanks to their load-carrying capacity. A large workpsace may be obtained using wire transmissions, constituting cable-driven parallel robots (CDPRs) [69, 71]. Cables are mechanical components that can withstand a large tensile force. In a cable-driven parallel robot, a certain number of cables is attached to the floating base and driven by actuated winches mounted on the base frame. On the other side, cables are attached to some fixed point, ensuring to maintain tension within a given workspace. The advantages are that cables allow motion ranges larger than those produced by conventional articulated systems. Moreover, since cables can only resist tensile forces, they are much thinner and lighter than conventional mechanical components.

The limbs of a CDPR are then composed of cables in place of rigid-

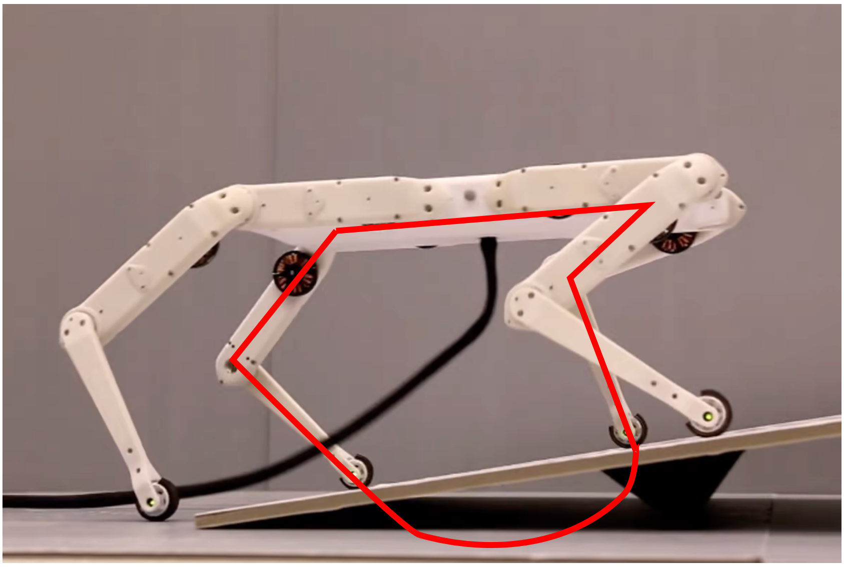

Figure 1.4. A quadruped during the walking. The feet in contact with the ground creates a closed loop.

link serial chains. Generally speaking, CDPRs can be divided into three categories: *under-constrained* if they own less cables than DoFs; *fully constrained* if they own as many cables as DoFs; *redundantly constrained* if the number of cables is greater than the degrees of freedom (DoFs). The under-constrained CDPRs usually approach the minimum gravitational potential energy to determine the position and orientation of the floating base, whose state can be easily changed by any external disturbance. In fully or redundantly CDPRs the position and orientation are instead completely determined by the lengths of the cables. The movement of the floating base is obtained through the modulation of the tension forces in the cables. The modulation of cable forces creates a net that commands the wrench at the center of mass of the floating base, pushing it along a desired trajectory.

Similar approaches are employed for the locomotion of legged robots. In this case, the limbs are composed of rigid-links serial kinematic chains. A legged robot can be assimilated to a parallel mechanism too. Indeed, whenever the legs are in contact with the ground, multiple closed loops are created [56]. Then, in a legged robot, the trunk is the floating base, while the legs are the limbs. Depending on the number of legs, the control of these robots presents different challenges. Robots with two or four legs are easily subject to external disturbances. Instead, robots with more than four legs have high stability, but coordinating the legs becomes more difficult. Different from the CDPR, legged robots have no constant point attached to the fixed base. Closed parallel loops are created by the contact of the feet with the ground (Fig. 1.4). Then, these contact points are continuously changing according to a foot scheduler and the desired trajectory, making the robot move in a workspace that is, theoretically, infinite. Similarly to CDPR, the locomotion is commanded through the modulation of the ground reaction forces. The magnitude of these forces always needs to be positive along the normal direction to the ground. Moreover, the ground reaction forces have to be contained inside the friction cone to avoid the foot sliding.

1.2 Disturbance rejection

In order to reach a significant integration of robots into the human world, there is a need to make them safe. Indeed, during interaction with human beings, the robot needs to preserve the safety of everyone and move in an environment full of obstacles. Moreover, with the final goal of replacing humans in repetitive tasks needing precise execution, the robots need to increase their thoroughness.

Classical control strategies used in many robotic applications consider simplified mathematical models subject to different uncertainties. The performance is greatly affected neglecting these uncertainties and external disturbances. Since the presence of disturbances and uncertainties leads to a weak performance of the robot, the research in the last years mainly pointed towards the development of control strategies able to reduce the entity of disturbance and the influence of the model uncertainties [32]. Different control philosophies have been implemented to improve performance with uncertain robotic systems. One of the most applied approaches is adaptive control, which continuously adjusts the controller parameters based on variations in the system dynamics. When the aim is to mitigate plant disturbances and uncertainties, having precise prior knowledge of plant dynamics is crucial for optimal performance of adaptive control. A different controller developed in the field of disturbance rejection is the robust control method, which explicitly deals with uncertainties without continuously adjusting the controller parameters. This controller, differently from an adaptive one, does not need to have an accurate knowledge of the plant uncertainties. However, it is designed to achieve good performance considering the assumption that disturbances are bounded in a compact set. In this way, the robust control approach tends to be over-conservative.

Although adaptive and robust controllers are able to attenuate the effect of disturbances in case of accurate knowledge of the system, they can not guarantee similar performance when coping with nonlinearities, unknown uncertainties, and disturbances arising from the environment. To tackle this problem some observer-based control approaches have been proposed to successfully control robotic systems. This approach guarantees to cope with the plant uncertainties and disturbances, that are not only large and unknown, but also unmeasurable [83, 19, 79]. The main idea of this approach is to design an observer to estimate disturbances acting on the robots. Then, the obtained estimations are fed back to the controller to have a robust control law rejecting the disturbances.

The success of observer-based controllers highly depends on the reliability of the estimations, whose quality depends on the knowledge of the model used in the observer design. It means that, to have a better estimation, the observer needs to take into account all the possible uncertainties not considered during the modelling of the system. In this way, the observer also includes internal uncertainties that arise from unknown parameters and unmodeled dynamics, together with external variations and disturbances. The estimation of the disturbance observer needs to be fed back to a control algorithm to be compensated for. Disturbance observers have been integrated with different control methods, from traditional PID to a more complex controller, such as sliding mode [19, 7]. In the field of limbed parallel robots, especially legged ones, one of the most used approaches for locomotion is optimal control, which aims to find a control policy leading the system to the equilibrium point in an optimal way, with respect to a performance cost function [83]. It usually requires knowledge of the system dynamics, and, also for this case, an observer is often implemented to compensate for uncertainties and external disturbances. In the range of optimal control approaches, another method finds a wide application in the case of limbed parallel robots: the model predictive controller (MPC) [52, 17, 59]. It uses the dynamical model to predict the future behaviour of the process based on a set of inputs and control actions. The controller then optimizes the control action based on a predefined objective function, which could be minimizing the cost of production, maximizing the yield, or minimizing the energy consumption. One of the key benefits of MPC is its ability to handle constraints on inputs and outputs. The controller can be designed to ensure that the inputs and outputs of the process remain within the specified limits, which can improve the stability and reliability of the process. In this case, the model is employed to obtain a predicted behaviour. Compensating the model with the estimated disturbance would lead to an inaccurate prediction unless the dynamic of the disturbance is known and it could be predicted along with the state. If the robot moves within an unstructured environment, the dynamic of the disturbances is usually unknown. In this case, the disturbance attenuation only relies on the MPC's intrinsic stability. Indeed, being the MPC a feedback control method, it has some inherent robustness, as analyzed by several researchers. However, if the description of the model uncertainty is available, the approach can consider all possible future trajectories under the given uncertainty description in the optimal control calculation. The first works considering a model with uncertainty description formulated robust MPC as a min-max problem, which aims to minimize the worst-case error over the output trajectories possible for the given model set. However, it was demonstrated that the receding horizon control law resulting from such a formulation was not robust at all. Moreover, the lack of robustness was given by the failure to account for the fact that the control calculation would be repeated in a receding horizon fashion, with feedback updates. Then, an MPC algorithm that solves a convex program at each time has been proposed starting from the dynamic programming [53]. Through this formulation, the MPC can be used in case of disturbances, guaranteeing robust stability.

1.3 Optimal Control

Optimal control has attracted huge attention from research and industries since the beginning of the '80s. Optimal controllers exploit the model of the system to find a control policy that minimizes an objective function, which represents the system's performance. The cost function takes into account the initial and final state of the system and the control input applied to the system over a given period. There are two main types of optimal control problems: open-loop and closed-loop. In an open-loop problem, the control input is not based on the current system's state but rather on a predetermined set of inputs. In a closed-loop problem, the control input is based on the current state of the system and the goal is to drive the system to the desired state.

One of the most commonly used methods for solving optimal control problems is the Pontryagin's maximum principle [54, 47]. This method, based on the calculus of variations, provides the conditions for optimal control input. The necessary conditions are expressed through the Hamiltonian, a function of the state and control variables, and the co-state variables, related to the cost function.

Another popular method for solving optimal control problems is the dynamic programming approach [74]. This method is based on the principle that optimal solutions can be found by breaking a problem into subproblems and solving them recursively. Dynamic programming can be used to solve both open-loop and closed-loop problems, but it is particularly helpful for problems with a large number of states and control inputs. In addition to these methods, several numerical methods can be used to solve optimal control problems. The choice of the method depends on the specific case and the requirements of the application. Then, optimal control is a powerful tool for designing systems that perform efficiently and effectively. The methods used to solve optimal control problems are based on a combination of mathematical optimization and numerical techniques. With the ever-growing computational power, the application of optimal control problems has been used in various fields to solve the most difficult control problems.

Over the years, optimal control demonstrated to be a powerful tool in robotics. In this field, usually, optimal control is used to find the best control inputs for the robot to achieve a specific goal, such as minimizing energy consumption or maximizing performance. One of the main challenges in robotic optimal control is dealing with the complexity of the robot's dynamics. Many robotic systems have a high number of degrees of freedom, which makes it difficult to model and control the system. Additionally, the presence of uncertainty, such as unmodeled dynamics or sensor noise, can further complicate the control problem.

One of the most widely used methods for solving optimal control problems in robotics is the linear quadratic regulator (LQR) method [70, 90]. LQR is a type of model-based control that uses a linearized model of the robot's dynamics to design the controller. LQR is well-suited for robotic systems with linear dynamics and small uncertainties. Also the MPC is a popular method in robotics. MPC is a model-based control method that uses a model of the robot's dynamics to predict its future behaviour. The controller uses this prediction to determine the best control input at each time step. MPC is particularly useful for systems with nonlinear dynamics or large uncertainties and can handle constraints on the control inputs and states. In addition to these methods, there are several other techniques used in robotic optimal control, such as iterative LQR, feedback linearization, and nonlinear model predictive control. Each of these methods has advantages. Limitations and the choice of method depends on the specific problem at hand and the application's requirements.

In conclusion, optimal control is a crucial tool for designing robotic systems that perform efficiently and effectively. There are a variety of methods available for solving optimal control problems in robotics, each with its advantages and limitations. With the advancements in computation and machine learning, it is possible to apply new techniques to tackle more complex robotic problems.

1.4 Contribution of the Thesis

This thesis contributes to develop control architectures that enhance the stability and safety of robotic systems. By doing so, it will facilitate technological advancement and enable limbed parallel robots to be introduced more effectively into real-life situations. Indeed, despite the great recent developments in robust control and disturbance rejection to integrate robots in real-life situations and unstructured environments, robots are still mostly confined to industrial or research scenarios. While simple wheeled mobile robots such as robotic vacuums are gradually becoming more prevalent in human environments, other types of robots still struggle to establish themselves due to their inherent instability. The aim of this thesis is to address some of the numerous challenges that remain in achieving stable and safe control for these robots. The contribution of this thesis can be divided into two main sections:

- **Quadruped robots**. Quadruped robots are not so robust in the presence of challenging terrain and significant external disturbances. For this reason, different solutions have been realized, like disturbance observers and model predictive controllers. This thesis contributes to solve the problem of disturbance rejection for quadruped robots using the previously mentioned approach of disturbance observer-based control. It will be first presented a novel momentum-based observer that can deal with disturbances applied both to swing and stance legs, differently from existing approaches that usually consider only disturbances acting on the CoM. Then, an extension is developed, realizing a novel hybrid observer that integrates the previous estimation on the legs with a double observer on the CoM. In this way, all kinds of disturbances acting on the robot are taken into account and compensated. Robust control and a disturbance rejection allow the robots to start making their way into the real-life environment and tasks, especially for the safety of the humans working in the same environment. For this reason, the natural evolution of this work has been an application in real life for a human-robot interaction task, useful in the field of care assistance.

- **Cable-driven parallel robots**. Replacing rigid links with cables enables CDPRs to achieve a wider workspace and larger load capacity, but it also poses challenges for control due to their inherent flexibility, which causes significant vibrations during motion. Typically, the robot's desired wrench is computed and commanded for movement. However, the minimum and maximum cable tension limits are crucial, as slack cables must be avoided. Unfortunately, conventional control strategies are often unable to handle these constraints within the motion controller, and they are usually addressed in a cable tension distribution algorithm that acts after the controller computes the desired wrench. Consequently, if the desired wrench is unfeasible with the cable tension limits, the robot's movement cannot be executed. To solve this problem, MPC has been introduced, but it has only been applied to fully and redundantly constrained CDPRs. This thesis contributes to solve these challenges realising an MPC for underconstrained CDPRs, which considers the tension limits and allows the robot to approach the equilibrium point smoothly and safely, attenuating the oscillatory movements caused by cable flexibility. The results are compared with other controllers that have limited capabilities in handling vibrations.

1.5 Thesis Structure

A brief outline of the thesis is given in the following.

The disturbance rejection problem for quadruped robot is addressed in 2. A description of different control and disturbance rejection approaches in the literature is given, along with a description of the dynamic model of the robot. Then, the framework and the proposed observers are introduced. Different case studies are shown along with the obtained results.

A review of the state of the art of cable-driven parallel robots is provided in Chapter 3. Then, the dynamic model of these robots is described, followed by the proposed model predictive controller. Finally, the results and the comparisons with other kinds of the controller are provided.

The conclusions and the perspective of future works in this field can be found in Chapter 4.

Chapter 2

Disturbance Rejection in Optimal Control for Quadruped Robots

Life is like riding a bicycle. To keep your balance, you must keep moving.

Albert Einstein

This chapter deals with the part of this thesis related to the legged robots. It first presents the state of the art of control approaches for biped and quadruped robots and the importance of taking into account possible external disturbances. Then, the main contribution of this thesis about legged robotics is highlighted. Afterwards, the dynamic model of a legged robot is presented, along with the whole-body controller and the novel approaches for disturbance rejection. Finally, the obtained results for different case studies are presented.

2.1 State of the art

The main advantage of legged robots is the capability to navigate through complicated and challenging terrains to accomplish different tasks, from inspection or search and rescue to care assistance. This is possible because of their capability to adapt their footstep and overcome obstacles, which allows these robots to move in unstructured environments full of stairs, holes and obstacles. For this reason, these robots are expected to start collaborating with humans in daily life tasks and being an essential resource in dangerous situations like search and rescue after environmental disasters, but also to start having a central role in care assistance tasks, such as helping visually impaired people in moving around.

In recent years, research has focused on realizing highly dynamic gaits and improving the ability to maintain a stable balance during motion to recreate the natural movement of living beings. Despite the significant advances made in motion planning and control methods on real hardware, legged robots cannot yet cope with all the difficulties of unstructured environments. These robots have started to be recently used in tasks such as inspection or patrolling. Thus, they need to be able to move in confined or cluttered environments, where it is difficult retaining balance and adapt their foothold to the slope and the roughness of the terrain but also to reject external disturbances.

The first challenge in robust control for legged robots is related to their structure. As seen in Chapter 1, the structure of a legged robot is determined by the number of legs. Indeed, robots with only two legs have an inherently unstable structure, meaning that controlling this kind of robot requires a high knowledge of the dynamic model and complex controller architecture with a certain computational complexity.

Quadruped robots are characterized by a high instability if they are executing gaits with at least two legs swinging at the same time, for example: trot gait, when diagonal pairs of legs move together; pace gait, with lateral pairs of legs moving contemporary; gallop gait, when either the front legs or the rear ones are swinging simultaneously. Given this instability, similar to the behaviour of biped robots, controllers explicitly realized for bipedal locomotion are often modified and adapted for quadrupeds.

A common approach for quadrupedal locomotion control is to exploit a reduced model, in which the quadruped robot is assimilated to a biped. An example is the approach employed in [24], where the quadruped is modeled as a biped using the concept of virtual legs. Then, the virtual biped model is reduced to a linear inverted pendulum, considered able to swing in a planar workspace. This modelling makes it possible to react against pushes along both the forward and lateral directions. Then, an estimator is designed to calculate the desired position of the legs, based on the concept of capture points. The obtained results are used within a model predictive control algorithm, which redesigns the reference path of the robot's footsteps and center of mass such that the robot can recover after a sudden push applied to its body. However, in this case, only the trot gait has been considered, since using this gait it is easier to model the quadruped as a virtual biped.

Modelling the robot as a biped allows one to employ standard controllers to exploit these reduced models, like controllers for a linear inverted pendulum. However, these approximations neglect some aspects of the quadruped dynamics, making it possible to move the robot only in an easy and flat environment. Indeed, in [94], the quadruped robot is modeled as a cart-table, which does not fully capture the dynamics of the real system. In order to account for this, the ZMP is required to stay away from the edge of the support polygon. The design complexity and the computation overhead are actually reduced using these approximated dynamics, but the dynamism could be limited. To avoid this situation, most controllers usually take into account the full dynamic of the robot.

In order to realize a highly dynamic gait, the full dynamic of the robot should be employed. A widely used approach that considers the full dynamic of the robot employs operational-space control. Usually, within these frameworks, a desired motion is imposed for relevant points, such as the CoM or a reference point for feet and hands. This approach found wide application both for biped and quadruped robots. It has been employed in [72] for a biped robot. In this case, the inverse dynamics control is used and uses the center of mass and its future prediction as a criterion for balance control. It enables the robot to perform fast whole-body movements without falling: the robot keeps its balance taking steps only whenever the CoM and its prediction remain within the foot reachable limits.

In the field of quadrupedal locomotion, the full dynamic of the robot has been employed in different whole-body controllers, usually exploiting quadratic problems that involve inverse dynamics for the movement of the feet [43, 96, 97, 26]. The framework usually exploits the inverse dynamics imposing various priorities for different tasks. The task with higher priority always regards the equation of motion, guaranteeing dynamic consistency, while secondary tasks can track a desired motion, force, or torque. Techniques based on null space projection or a standard constrained quadratic problem (QP) ensure that priorities are respected.

Always considering the desired motion of a specific point, different approaches involve the zero moment point (ZMP), where the influence of all forces acting on the mechanism can be replaced by one single force. Even in this case, the optimal control, employing QP methodology, is often used, such as in [4], where a ZMP-based optimization problem is solved to find optimal joint torques and acceleration that guarantee the tracking of the previously generated trajectory.

Nevertheless, in the previously cited approaches, there is usually no modulation of the ground reaction forces, a meaningful aspect for robust control and locomotion on rugged terrains. For this reason, a ZMP-based optimal control is presented in [5, 6], method that relies on an online motion planner that computes the reference motion trajectory as a function of the foot schedule and the state of the robot. The planner is employed together with a hierarchical whole-body controller, optimizing the whole-body motion and contact forces, and solving a cascade of prioritized tasks. Through this framework, optimal joint accelerations and contact forces are founds, obtaining better results in terms of robustness, given the modulation of ground reactions. In this way, the robot can approach the ground in a smooth and gentle way, reducing impacts, and being able to modify its step based on the irregularities of the terrain. A heuristic-based planning approach, always based on ZMP, was presented in [36], assuming a quasi-static dynamic without achieving highly dynamic gaits.

In recent years, the model predictive control found wide application in legged robotics. It considers the full dynamic of the robot to predict the movements over a finite horizon to stabilize the robot. Sometimes a nonlinear predictive optimization is used instead in order to cope with the nonlinearity of the legged robots dynamic [9, 49, 65, 86].

All these whole-body controllers consider a motion planner decoupled from the control, meaning that a desired trajectory is firstly computed and then injected into the controller. There is often the possibility of online re-planning, in order to compute a new desired trajectory after a certain period, to cope with the roughness of the terrain and all the external disturbances.

The robustness against external disturbances has been widely investigated, over the years, for both quadruped and biped robots. Most of the studies concentrated on the external forces given by the touchdown phase of the feet. This is because one of the main capabilities of a legged robot is to traverse challenging terrain. Indeed, given its irregularity, the foot could have an anticipated impact on the ground, causing external forces acting on the system [10, 57]. A solution to this problem is provided in [42], where an impedance control approach using contact forces is performed to obtain references for feet such that contact with the ground is modeled as desired to have a smooth and safe interaction. This impedance controller has also been used for quadrupeds in [96], adding an impedance estimation of external forces on swing legs.

In order to allow the robots to move in unstructured environments with a good balance and rejecting external disturbances, a powerful tool for robust control is the disturbance observer. This kind of observer can handle external forces acting on the robot through the dynamic model, and it is often employed given its simple structure and high performance. In [8], a momentum-based observer detects the anticipated touchdown of the foot, sending this information to a framework of Kalman filtering to increase robustness. A disturbance observer model for floating base robots using kinematic constraints on fixed contact positions, such as the supporting foot, is proposed in [51]. In most cases, the observer's estimation is integrated into a controller acting on the position of the center of mass.

In most of these cases, only the disturbances applied to the CoM are taken into account [30, 36, 51, 31], assuming that there is no external force on legs that are moving. For example, a nonlinear disturbance observer is presented in [25, 23] as a virtual force sensor, assuming there is no disturbance on the swing legs. This observer is applied in combination with sliding control, and coupling forces between the legs and the torso of the robot are estimated.

Observing only disturbances acting on the center of mass can robustify the locomotion on uneven terrains. Nevertheless, if the robot is subject to severe impact on swing legs, estimating only disturbances acting on the CoM could not be enough. In this case, the robot could not be prevented from falling. Indeed, in similar situations, the foot of the hit leg can drift from the desired motion, and the touchdown could happen far away from the planned foothold, reducing the support polygon and unbalancing the robot. In worst cases, the swing leg may not touch the ground or may impact another leg, making the robot fall. For this reason, it is necessary to estimate external forces acting on swing legs and compensate for the disturbance. An estimation of the external forces through impedance control on swing legs has been carried out in [96]. However, such a methodology is not integrated with an observer and is used only for static or quasi-static situations.

Hence, during their locomotion, the legged robot can encounter unknown obstacles and can be subject to external disturbances acting both on the trunk of the robot and on the legs that are moving. Then, it is necessary to estimate and compensate for the disturbances acting on the legs, but this compensation alone could not be enough whenever major forces are acting directly on the CoM. This brings to the need to combine the action of different observers, acting on both the legs and the CoM.

2.2 Main Contributions

On the base of the state of the art presented in the previous section, and with the aim to advance the disturbance rejection strategies for the legged robot, the main contribution of this thesis, in this field, is the realization of two observers.

As previously seen, disturbance rejection strategies for legged robots take usually into account only forces acting on the CoM. With this in mind, the first observer has been designed in order to reject mainly disturbances acting on the legs, with the final goal to make the robot robust against irregularities of the terrain [64]. However, if major forces acting on the CoM, the use of this observer alone could not be enough. For this reason, a second observer acting directly on the CoM will be presented. It is composed of an acceleration-based observer for the translational part and a momentum-based observer for the angular one. Given its combination of two observers, it is here identified as *hybrid* [63].

The combined action of these two observers takes into account both disturbances acting on swing legs and on the center of mass, having a good retaining of the balance and an optimal rejection of external disturbances in almost all situations. These observers are employed within a whole-body controller to realize the locomotion of the robot. The performance and the validity of this framework will be demonstrated through some numerical case studies in a simulation enviroment endowed with a physics engine (i.e., Gazebo).

2.3 Dynamic model of quadruped robots

Legged robots are usually modelled as a free-floating base with some legs attached. The floating base can be usually modelled through six virtual joints that endow the robot with six additional degrees of freedom (DoFs) with respect to a fixed world frame $\mathscr{W}$ (see Fig. 2.1). The number of legs attached depends on the kind of robot. More generally, $n_l \geq 2$ legs are attached to the floating base, giving other nn_l additional DoFs to the structure, where $n > 0$ is the number of joints for each leg.

In order to describe the dynamic model of a legged system, let consider $\mathscr{B}$ as the frame whose position is attached to the CoM of the robot (see Fig. 2.1). It is worth noticing that this point is not fixed, but it changes during the movement with the change of the configuration of the robot. The orientation of the frame $\mathscr{B}$ can be instead represented through the one of a fixed frame on the trunk of the robot. Let consider $x_{com} = \begin{bmatrix} x_c & y_c & z_c \end{bmatrix}^T \in \mathbb{R}^3$, $\dot{x}_{com} \in \mathbb{R}^3$, and $\ddot{x}_{com} \in \mathbb{R}^3$ as the position, velocity, and acceleration of the frame $\mathscr{B}$'s origin with respect to $\mathscr{W}$, respectively. Besides, let $\omega_{com} \in \mathbb{R}^3$ and $\dot{\omega}_{com} \in \mathbb{R}^3$ be the angular velocity and the angular acceleration of $\mathscr{B}$ with respect to $\mathscr{W}$, respectively. The angular velocity can be computed from the rate of change of ZYX Euler Angles, stacked in the vector $\Theta = \begin{bmatrix} \phi & \theta & \psi \end{bmatrix}^T$ [22], that can be extracted from the rotation matrix $R_b \in SO(3)$.
Finally, let's indicate with $q \in \mathbb{R}^{nn_l}$ the vector collecting the legs' joints. Then, the state of the legged robot is represented not only by the joint variables relative to the actuated joints of the legs but also by the pose of the floating base that is often represented by a chosen fixed point on the trunk and a chosen orientation reference. However, starting from a fixed point on the trunk, the model can be transformed in order to be formulated in terms of the global CoM, meaning the center of mass of the whole robot. The transformation to apply in order to obtain the dynamic model expressed in terms of the CoM has been introduced in [66].

With this transformation, the inertia matrix assumes a decoupled struc-

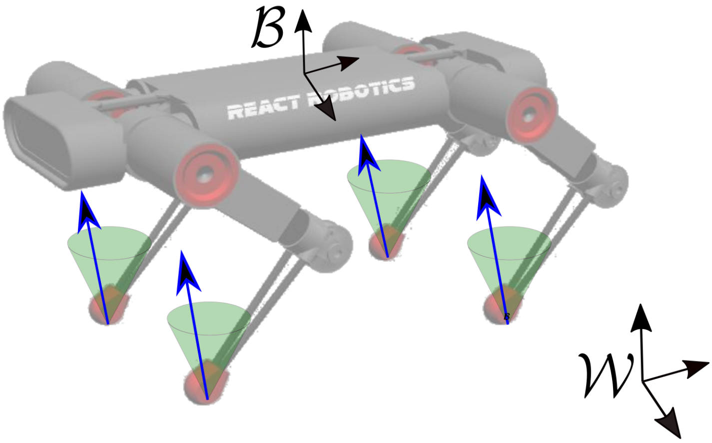

Figure 2.1. DogBot, the platform used for simulations. The reference frames for the robot are shown. Ground reaction forces need to stay in the cones.

ture

$$M(q) = \begin{bmatrix} M_{com}(q) & O_{6\times nn_l} \\ O_{nn_l\times 6} & M_q(q) \end{bmatrix} \in \mathbb{R}^{6+nn_l\times 6+nn_l}. \tag{2.1}$$

In this way, it is clear the decoupling of the inertia term relative to the CoM $M_{com}(q) \in \mathbb{R}^{6\times 6}$ from the one related only to the legs $M_q(q) \in \mathbb{R}^{nn_l\times nn_l}$. Moreover, also the inertia term relative to the CoM is diagonal $M_{com}(q) = \begin{bmatrix} M_{com,l}(q) & O_{3\times 3} \\ O_{3\times 3} & M_{com,a}(q) \end{bmatrix}$, with $M_{com,l}(q)$ relative to the linear part of the CoM, and $M_{com,a}(q)$ relative to the angular part. To obtain a similar decoupled structure for the vector accounting for Coriolis and centrifugal forces, it is necessary to assume that the angular motion of the robot's main body is slow and that the leg mass is negligible with respect to the total mass of the robot. In this way, the coupling between the angular dynamics of the robot's CoM and the legs' joints dynamics can be supposed negligible. As a consequence of these assumptions, the Coriolis and centrifugal terms related to the angular part of the CoM can be neglected [40, 22], obtaining the vector

$$h(q, \upsilon) = \begin{bmatrix} O_{6\times(6+nn_l)} \\ C_q(q, \upsilon) \end{bmatrix} \upsilon + \begin{bmatrix} mg \\ 0_{nn_l} \end{bmatrix}, \tag{2.2}$$

as the sum of Coriolis and centrifugal forces, $C_q(q,\upsilon) \in \mathbb{R}^{nn_l\times(6+nn_l)}$, and gravitational forces where $\upsilon = \begin{bmatrix}\dot{x}_{com}^T & \omega_{com}^T & \dot{q}^T\end{bmatrix}^T \in \mathbb{R}^{6+nn_l}$ is the stacked velocity; vector $m > 0$ is the total mass of the robot, $g = \begin{bmatrix}g_0^T & 0_3^T\end{bmatrix}^T \in \mathbb{R}^6$, and $g_0 \in \mathbb{R}^3$ the gravity vector; $0_\times$ and $O_\times$ the zero vector and matrix of proper dimensions, respectively. The resultant model can be written as

$$M(q)\dot{\upsilon} + h(q,\upsilon) = S^T\tau + J_{st}(q)^T f_{gr} + J(q)^T f_{ext} + S_w^T w_{e,c}, \qquad (2.3)$$

with $S = \begin{bmatrix}O_{nn_l\times 6} & I_{nn_l}\end{bmatrix}$ a selection matrix for the terms relative to the legs' joints; $\tau \in \mathbb{R}^{nn_l}$ the joint actuation torques; $f_{gr} \in \mathbb{R}^{3n_{st}}$ are the ground reaction forces, with $0 < n_{st} \leq n_l$ the number of stance legs; $J_{st}(q) = \begin{bmatrix}J_{st,com}(q) & J_{st,j}(q)\end{bmatrix} \in \mathbb{R}^{3n_{st}\times 6+nn_l}$ where $J_{st,com}(q) \in \mathbb{R}^{3n_{st}\times 6}$ and $J_{st,j}(q) \in \mathbb{R}^{3n_{st}\times nn_l}$ are those Jacobians whose transpose map the ground reaction forces into the acceleration of the CoM and the legs' joints, respectively; $f_{ext} \in \mathbb{R}^{3n_l}$ is the stacked vector containing the resultant effect at the legs' tips of all external forces accounting for unmodelled dynamics and disturbances at any point of the robot; $J(q) = \begin{bmatrix}J_{com}(q) & J_j(q)\end{bmatrix} \in \mathbb{R}^{3n_l\times 6+nn_l}$ where $J_{com}(q) \in \mathbb{R}^{3n_l\times 6}$ and $J_j(q) \in \mathbb{R}^{3n_l\times nn_l}$ are those Jacobians whose transpose map such external forces into the acceleration of the CoM and the legs' joints, respectively. The Jacobian matrix J includes a matrix J_{com} representing the centroidal dynamics and a matrix J_j related to the legs' dynamics $J = \begin{bmatrix}J_{com} & J_j\end{bmatrix}$, and it can be divided into a matrix referring to support legs $J_{su} = \begin{bmatrix}J_{su,com} & J_{su,j}\end{bmatrix}$ and a matrix referring to swing legs
$J_{sw} = \begin{bmatrix}J_{sw,com} & J_{sw,j}\end{bmatrix}$.
Differently from [31], the assumption that all the external forces are ground reaction ones is no longer made. For this reason in (2.3), there is a distinction between the ground reaction forces f_{gr} and the external forces f_{ext}. The former act only on the stance legs, while the latter accounts for the effects at the legs' tip, including the swing legs, of the disturbances acting at any structure level. As an assumption, the external torques resulting at the legs' tip are negligible. In (2.3), the ground reaction forces are taken into account in the following term $\begin{bmatrix}J_{su,com}^T \\ J_{su,j}^T\end{bmatrix} f_{gr}$; while external forces apart from the ground reaction are considered in the term $\begin{bmatrix}J_{com}^T \\ J_j^T\end{bmatrix} f_{ext}$.

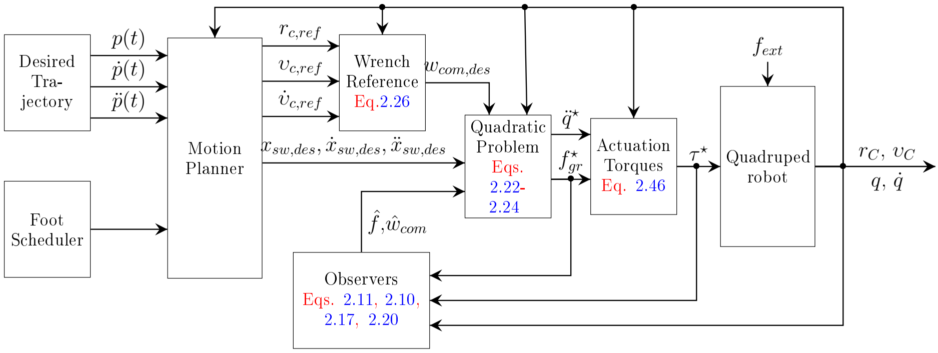

Figure 2.2. Conceptual block scheme of the devised whole-body controller.

Finally, $S_w = \begin{bmatrix} I_{6\times 6} & O_{6\times nn_l} \end{bmatrix}$ is a selection matrix of the unactuated part; while $w_{e,c} = \begin{bmatrix} f_{e,c}^T & \tau_{e,c}^T \end{bmatrix}^T \in \mathbb{R}^6$ is the external wrench acting directly on the CoM. In conclusion, it can be noticed that the dynamics of the CoM are decoupled from the ones of the legs, so that the CoM's dynamics, also called centroidal dynamics, are included in the first six rows of (2.3), while the remaining rows take into account the dynamics of the joints. It should also be noticed that the resultant external forces at the legs' tip, f_{ext}, can be considered as contacts that dictate a net wrench delivered to the CoM, while the external wrench directly applied to the CoM, $w_{e,c}$, influences only the centroidal's dynamics.

2.4 Whole-Body Controller

In order to realize the locomotion of the quadruped robot, a whole-body controller has been used. This controller finds the optimal joint torques and joint accelerations by solving an optimization problem. Along with the optimization problem, the whole-body controller (WBC) is composed of a foot scheduler, a motion planner and the hereby presented observers. These last are the main contributions of this thesis in this chapter. In Fig. 2.2 the block scheme of the whole-body controller is presented. In the following, the various blocks of the scheme are explained in detail.

2.4.1 Foot Scheduler and motion planner

Given high-level user commands, the foot scheduler defines a contact schedule for all the legs. The schedule is depending on the chosen gait. Usually, four different gaits are used for quadruped robots:

- **crawl**: in each instant, there is only one leg moving;
- **trot**: diagonal pairs of legs move at the same time;
- **pace**: lateral pairs of legs move simultaneously;
- **gallop**: either the front legs or the rear ones are moving together.

Based on the chosen gait, a schedule for each leg is computed, that establishes the events of lift-off and touchdown for the leg so that in every instant it is established which ones are the stance legs and which are the swing legs. This is important in order to have a known support polygon [5] that will be used inside the motion planner for the planning of references that allow retaining the balance of the robot. Indeed, starting from a desired trajectory, that is simply computed as a spline from the current position to the target position, a new trajectory for the robot is continuously replanned by the motion planner module. This replanning is made such that the ZMP, $x_{zmp} = \begin{bmatrix} x_z & y_z & z_z \end{bmatrix}^T \in \mathbb{R}^3$ expressed in $\mathscr{W}$, is always contained inside the support polygon.

From now on, the position and the orientation of the CoM will be combined into the vector $r_c = \begin{bmatrix} x_{com}^T & \phi^T \end{bmatrix}^T \in \mathbb{R}^6$, while the velocity and the acceleration will be considered as $v_c = \begin{bmatrix} \dot{x}_{com}^T & \omega_{com}^T \end{bmatrix}^T \in \mathbb{R}^6$ and $\dot{v}_c = \begin{bmatrix} \ddot{x}_{com}^T & \dot{\omega}_{com}^T \end{bmatrix}^T \in \mathbb{R}^6$.

For each footstep, the motion is split into two phases, replanning the desired trajectory for the CoM at the beginning of each footstep, with a period T_{fs}.

Stance phase

All the legs are in contact with the ground, ensuring an intrinsic balance. Therefore, the reference of the CoM, $r_{c,ref} \in \mathbb{R}^6$ can be computed as a 3-rd order spline that brings it at the center of the support polygon with the desired orientation [6].

Swing phase

At least one leg is swinging. The motion could be quasi-static if only one leg is moving, or highly dynamic if two legs are swinging and the support polygon degenerates into a line. During this phase, both the references for the CoM and the swing feet need to be planned. The reference $x_{sw,des} \in \mathbb{R}^{3(n_l - n_{st})}$ for the swing feet is computed using two splines: the first one to lift the foot, the second to lower it. Considering $T_{sw} > 0$ the duration of the swing phase, each spline lasts $0.5T_{sw}$ [100]. The linear reference of the CoM is instead computed solving an optimization problem, having as variables the coefficients of a third-order spline for each coordinate of the CoM [5].

The problem penalizes the deviation from a regularized path $p(t) \in \mathbb{R}^3$, expressed in $\mathscr{W}$, approximated as a sequence of splines, such that:

- the initial state $p(0)$, $\dot{p}(0)$ and $\ddot{p}(0)$ coincides with $x_{com}(0)$, $\dot{x}_{com}(0)$, and $\ddot{x}_{com}(0)$, respectively;
- the position $p(t_f)$, where $t_f > 0$ is the final time, is set to be at the center of the planned support polygon, while $\dot{p}(t_f)$ and $\ddot{p}(t_f)$ are zero so that the robot can stop and stand up at the end of the support polygon sequence.

An important constraint during this phase regards the ZMP, which can be written in the function of the CoM as follows

$$x_z = x_c - \frac{1}{(g_z + \ddot{z}_c)} \left(z_c \ddot{x}_c + \frac{\dot{L}_y}{m} \right), \tag{2.4}$$

$$y_z = y_c - \frac{1}{(g_z + \ddot{z}_c)} \left(z_c \ddot{y}_c - \frac{\dot{L}_x}{m} \right), \tag{2.5}$$

with $g_z > 0$ the gravity acceleration and $L = \begin{bmatrix} L_x & L_y & L_z \end{bmatrix}^T \in \mathbb{R}^3$ the angular momentum at the CoM. In the following, it will be assumed $\dot{L} = 0$, since there is no optimization for rotations within the trajectory computation.

Considering (2.4) and (2.5), the ZMP can be limited inside the support polygon adding a constraint for each of its edges [5]. The angular reference of the CoM is computed as a 3-rd order spline, bringing the robot to the desired orientation.

2.4.2 Disturbance Observer

As previously discussed, there is the need to reject external disturbances to obtain good locomotion.
The approach followed in this thesis is disturbance observer based. The estimated disturbance is compensated within the whole-body controller, as can be seen by the block scheme.
However, although for a legged robot only the disturbances acting on the center of mass are usually compensated for, severe external forces acting on the legs can lead the robot to a severe unbalance and a consequent falling. Section 2.5.2 will provide an example of this scenario to demonstrate the significance of compensating for these forces.
With the aim to prevent similar situations, this work of thesis presents firstly a momentum-based observer for the robot's legs, demonstrating its capability to reject external disturbances acting on the legs [64].
Then, a hybrid observer for rejecting disturbances acting both on legs and on the CoM is presented [63] in order to demonstrate the importance of rejecting both disturbances in severe irregularities conditions that can have a major impact on the whole structure.

Momentum-based Observer for robot's legs

The observer presented in this section is based on the legs system's momentum and differs from those already employed in legged robotics. It takes inspiration from estimators already applied in aerial robotics [76]. Such an estimator creates a linear relationship in the Laplace domain and can be extended to any desired order.
This estimator can reconstruct unknown forces arising for several reasons, such as unmodelled or inaccurate model parameters, external pushing actions, collision with obstacles, and so on. Some of these uncertainties can not be avoided or predicted in the real world.
The objective of this observer is to consider the momentum of all the legs, whether they are stance or swing legs. This is different from observers in the literature of legged robots, such as the ones investigated in [30, 36].

To take into account the legs momentum, the observer considers the last nn_l rows of (2.3). Suppressing dependencies to compact the notation, the generalized momentum of the legs from (2.3) can be expressed as

$$\rho = M_q \dot{q}, \tag{2.6}$$

Taking into account (2.3), the time derivative of (2.6) is

$$\dot{\rho} = C_q^T \dot{q} + \tau + J_{st,j}^T f_{gr} + J_j^T f_{ext}, \tag{2.7}$$

where the property $\dot{M}_q = C_q + C_q^T$ has been taken into consideration in the calculations [82]. Here the general procedure of momentum-based estimator design in [76] is being followed, which is investigated in [75] .
Let consider $\hat{f} \in \mathbb{R}^{3n_l}$ as the estimation of the vector f_{ext}, that accounts for the resultant effects at the legs tips of the external forces acting on the structure of the robot. The observer aims to reduce the difference between the estimated forces and the real ones.
Without loss of generality, the effect at the joint torques of the resultant force at the legs' tips can be considered as $F_{ext} = J_j^T f_{ext} \in \mathbb{R}^{nn_l}$, while its estimation can be written as $\hat{F} = J_j^T \hat{f} \in \mathbb{R}^{nn_l}$.
The observer is explicitly designed to achieve a linear relationship between the estimated external forces and the real ones in the Laplace domain

$$\hat{F} = G(s) F_{ext}, \tag{2.8}$$

with $s \in \mathbb{C}$ the complex Laplace variable and $G(s) \in \mathbb{C}^{(nn_l)\times(nn_l)}$ a diagonal matrix of transfer functions.These transfer functions should have poles located in the left-half plane.
The i-th diagonal element of $G(s)$ is

$$G_i(s) = \frac{k_0}{s^r + c_{r-1}s^{r-1} + \cdots + c_1 s + c_0}, \tag{2.9}$$

with $i = 1, \ldots, nn_l$, $r > 0$ the desired degree of the estimator, $k_0 > 0$ a gain, and c_j the coefficients of a Hurwitz polynomial, with $j = 0, \ldots, r-1$. Notice that, in principle, the Hurwitz polynomial can change among the single $G_i(s)$.
To obtain (2.9) in the Laplace domain, taking into account (2.7), the esti-

mator is designed in the time domain as follows

$$\gamma_1(t) = K_1 \left(\rho_j(t) - \int_0^t (\hat{F}(\sigma) + \alpha(\sigma)) \mathrm{d}\sigma \right), \tag{2.10}$$

$$\gamma_i(t) = K_i \int_0^t (-\hat{F}(\sigma) + \gamma_{i-1}(\sigma)) \mathrm{d}\sigma, \quad i = 2, \ldots, r, \tag{2.11}$$

where $\hat{F} = \gamma_r$, $K_i \in \mathbb{R}^{(6+nn_l)\times(6+nn_l)}$ are positive definite gain matrices, with $i = 1, \ldots, r$, and

$$\alpha(\sigma) = C_q^T \dot{q} + \tau + J_{st,j}^T f_{gr}, \tag{2.12}$$

In practical implementation, integrals in (2.10) and (2.11) are discretized, while $\hat{F}(\sigma)$ is referred to the estimation obtained at the previous time step.

Notice that, if $r = 1$, only (2.10) is relevant. Besides, notice that the elements of K_i, with $i = 1, \ldots, r$, are related to the coefficients c_j in (2.9), with $j = 0, \ldots, r-1$, and it is assumed that $\rho(0) = \gamma_i(0) = 0$, with $i = 1, \cdots, r$, meaning that the estimator's kick-off should be prior to the robot control.

Having in mind (2.3) and (2.7), the estimator's dynamics in the time domain can be written in the following compact form

$$\sum_{i=0}^{r} \left(\prod_{j=r}^{i+1} K_j \right) \hat{F}^{(i)} = \prod_{i=1}^{r} K_i F_{ext}, \tag{2.13}$$

where $\hat{F}^{(i)} = \gamma_{r-i}$ is the i-th time derivative of the $\hat{F}$, with $\hat{F}^{(0)} = \hat{F}$ and $\prod_{j=r}^{r+1} K_j = I_{nn_l}$, with $I_\times$ the identity matrix of proper dimensions.

It should be noticed that the estimation of the external forces at the legs tips can be retrieved through $\hat{f} = J_j^{T^\dagger} \hat{F}$. Here, the pseudo-inversion is indicated for the general case, in which ad-hoc solutions can be employed [25, 8, 55, 21]. For the quadruped adopted in this thesis, the matrix $J_j \in \mathbb{R}^{12\times12}$ is squared, so this is simply an inversion. Singularities are instead avoided through the gait generator.

Some quantities need to be fed back into the observer, as can be seen from (2.12). In particular, there is the need to have the joints position, q, and velocity, $\dot{q}$; the legs' input torques, τ; and the ground reaction forces,

f_{gr}. The joints position and velocity can be easily obtained from the motors' encoder. The input torques should be measured after feeding the command. However, in this work, it is thus assumed that the reference torque input $\tau^\star$, obtained from the optimization problem, is perfectly followed (i.e, $\tau^\star = \tau$). Finally, the ground reaction forces can be obtained by embedded sensors on the robot's feet.

Hybrid Observer

The previously presented momentum-based observer estimates disturbances deploying only the leg's dynamics, neglecting the CoM's ones. This approximation might be crucial whenever the robot is stressed by major forces acting directly on the CoM. For this reason, a hybrid observer that sees the combination of an estimation employing centroidal dynamics with the one deploying legs' dynamics will be presented in this section.

Together with the momentum-based for the legs presented in the previous section, a novel hybrid observer for the centroidal dynamics is used. This observer is inspired by aerial robotics once again [89], which aims to employ only direct measurements from an inertial measurement unit (IMU). Indeed, usually, a momentum-based observer estimating the external wrench acting on the CoM [36, 30] requires the CoM's translational velocity knowledge. Such a velocity is indirectly obtained through the transformation presented in [66] and not directly from a sensor. Robots with a mobile base, as the ones introduced in 1, are usually endowed with an IMU, that provides the floating base's angular velocity and translational acceleration, leaving the translational velocity to a numerical estimation. If the centroidal's dynamics introduced in 1 is employed for a legged robot there is the need to report every measurement to the CoM's frame. Thus, using an IMU that can not provide the translational velocity, leaving it to a numerical estimation, there is the need to

- compute the floating base's translational velocity;
- transform the obtained quantity into the CoM's translational velocity.

These computations, alongside the approximation made to obtain the centroidal's dynamics, can bring significant mistakes in estimating the external wrench. To avoid such mistakes, the hybrid observer here presented comprises a momentum-based observer for the CoM's angular term and an acceleration-based observer for the translational one. Therefore, here, with hybrid is intended the combination of two different kinds of observers, the momentum-based and the acceleration-based.

As already seen for the observer acting on the legs, let consider the angular centroidal's dynamics composed of the second set of three rows in (2.3). The generalized angular momentum is expressed as

$$\rho_{com} = M_{com,a}\omega_{com}. \tag{2.14}$$

Then, taking into account (2.3), the time derivative of (2.14) is

$$\dot{\rho}_{com} = J^T_{st,com,a} f_{gr} + J^T_{com,a} f_{ext} + \tau_{e,c}, \tag{2.15}$$

with $J_{st,com,a} \in \mathbb{R}^{3n_{st}\times 3}$ and $J_{com,a} \in \mathbb{R}^{3n_l\times 3}$ the Jacobians whose transpose map the ground reaction and the external forces into the angular acceleration of the CoM, respectively. Without loss of generality, from (2.3), define $\tau_c = J^T_{com,a} f_{ext} + \tau_{e,c} \in \mathbb{R}^3$ as the total external torques acting at the CoM, and $\hat{\tau}_c$ as its estimation. The straightforward objective is to achieve

$$\hat{\tau}_c \simeq \tau_c. \tag{2.16}$$

The estimator is explicitly designed to achieve a linear relationship between the estimated external torques and the real ones in the Laplace domain.

Taking inspiration from the observer already designed for the legs, the design of the estimator in the time domain is

$$\hat{\tau}_c(t) = K_a \left(\rho_{com}(t) - \int_0^t (\hat{\tau}_c(\sigma) + J^T_{st,com,a} f_{gr}) \mathrm{d}\sigma \right), \tag{2.17}$$

where $K_a \in \mathbb{R}^{3\times 3}$ is a positive definite gain matrix. Moreover, it is assumed that $\rho_{com}(0) = 0$, meaning that the estimator's kick-off should be prior to the robot control. In this case, only the angular velocity, available from the IMU, is required. The estimator's dynamics can be written as

$$\dot{\hat{\tau}}_c + K_a \hat{\tau}_c = K_a \tau_e, \tag{2.18}$$

that represents a linear exponentially stable system.

To compute the translational component of the wrench acting on the CoM, an acceleration-based observer can be used employing the measurement of the translational acceleration of the floating base given by the IMU. Considering the linear centroidal's dynamics composed of the first set of three rows in (2.3), it can be obtained

$$J_{com,l}^T f_{ext} + f_{e,c} = M_{com,l}\ddot{x}_{com} + mg - J_{st,com,l}^T f_{gr}, \tag{2.19}$$

with $J_{st,com,l} \in \mathbb{R}^{3n_{st}\times 3}$ and $J_{com,l} \in \mathbb{R}^{3n_l\times 3}$ the Jacobians whose transpose map the ground reaction and the external forces into the linear acceleration of the CoM, respectively. From (2.3), consider $f_c = J_{com,l}^T f_{ext} + f_{e,c} \in \mathbb{R}^3$ as the current total external force at the CoM, and $\hat{f}_c \in \mathbb{R}^3$ as the estimated one. Also in this case, the estimator is designed to achieve a linear relationship between the estimated external force and the real ones in the Laplace domain. The following first-order stable filter can be applied

$$\hat{f}_c(t) = K_l \int_0^t (M_{com,l}\ddot{x}_{com} + mg - J_{st,com,l}^T f_{gr} - \hat{f}_c)\mathrm{d}\sigma \tag{2.20}$$

to obtain the estimator's dynamics, that is

$$\dot{\hat{f}}_c + K_l\hat{f}_c = K_l f_c, \tag{2.21}$$

where $K_l \in \mathbb{R}^{3\times 3}$ is a positive definite gain matrix.

2.4.3 Optimization-based Controller

The core of the whole-body controller is the optimization problem, which, with the feedback of various variables previously introduced, computes optimal joint acceleration and ground reaction forces to retain the balance and realize the locomotion.

The employed optimization problem is wrench-based, and within the cost, the function employs the centroidal dynamics only, that is the first six rows of (2.3).To create a comprehensive whole-body controller, the remaining dynamics have been incorporated into both the equality and inequality constraints. This means that the optimization aims to compute the optimal solution in order to reduce the error between the current wrench at the CoM with the desired one obtained from the reference trajectory.

The chosen vector of control variables for the problem is $\zeta = \begin{bmatrix}\ddot{r}_c^T & \ddot{q}^T & f_{gr}^T\end{bmatrix}^T \in \mathbb{R}^{6+nn_l+3n_{st}}$.

The problem described in the following has the form

$$\begin{aligned} \underset{\zeta}{\text{minimize}} \quad & f(\zeta) && (2.22)\\ \text{subject to} \quad & A\zeta = b, && (2.23)\\ & D\zeta \le c. && (2.24) \end{aligned}$$

The detail for each term of the above minimization problem is detailed in the following.

Cost function

The CoM's reference obtained from the motion planner is tracked through the cost function, with the aim to reduce as much as possible the control effort. Since the problem is wrench-based, it is useful to consider the first six equations of (2.3)

$$M_{com}(q)\dot{v} + mg_0 = w_{com} = J_{st,com}(q)^T f_{gr} + J_{com}(q)^T f_{ext} + w_{e,c}, \quad (2.25)$$

where $w_{com} \in \mathbb{R}^6$ is the wrench at the robot's CoM including inertial and gravity terms. Using the references $r_{c,ref}$, $v_{c,ref}$, and $\dot{v}_{c,ref}$ from the motion planner, the desired wrench $w_{com,des} \in \mathbb{R}^6$ can be written as

$$w_{com,des} = K_p(r_c - r_{c,ref}) + K_d(\dot{r}_c - \dot{r}_{c,ref}) + mg + M_{com}(q)\ddot{r}_{c,ref}, \quad (2.26)$$

with $K_p, K_d \in \mathbb{R}^{6\times 6}$ positive definite matrices. Let $\hat{w}_{com}$ be the estimated external wrench at the CoM, the cost function minimizing the desired wrench and compensating for the disturbance can be written as

$$f(\zeta) = \left\| J_{st,com}^T \Sigma\zeta - (w_{com,des} - \hat{w}_{com}) \right\|_Q + \left\|\zeta\right\|_R, \quad (2.27)$$

with $\Sigma \in \mathbb{R}^{3n_{st}\times(6+nn_l+3n_{st})}$ a matrix selecting the last $3n_{st}$ elements of ζ, $Q \in \mathbb{R}^{6\times 6}$ and $R \in \mathbb{R}^{(6+nn_l+3n_{st})\times(6+nn_l+3n_{st})}$ two symmetric and positive definite matrices that can be used to specify the relative weight between the components of the cost function, and $\|\cdot\|_\times$ the quadratic form with a proper matrix.

Equality constraints

Two equality constraints are imposed to guarantee dynamic consistency and satisfy the dynamic constraint relative to the position of the stance feet. Then, the first equality is the equation of the motion and its constraints on the control variables to be consistent with the floating base dynamic in the absence, or perfectly compensated, of external disturbances. Such a dynamic regards the first six rows of (2.3) as follows

$$\begin{bmatrix} M_{com}(q) & 0_{6\times nn_l} & J_{st,com}(q)^T \end{bmatrix} \zeta = -mg. \tag{2.28}$$

The second equality constraint guarantees that the support feet remain in their position. Indeed, in order to avoid slippage of the robot it is of main importance that the stance feet do not slip maintaining the support polygon as it is. This holds by imposing the velocity of the feet equal to zero as $J_{st,com}(q)\dot{r}_c + J_{st,j}(q)\dot{q} = 0_{3n_{st}}$, whose time derivative is

$$J_{st,com}(q)\ddot{r}_c + \dot{J}_{st,com}(q,\dot{q})\dot{r}_c + J_{st,j}(q)\ddot{q} + \dot{J}_{st,j}(q,\dot{q})\dot{q} = 0_{3n_{st}}. \tag{2.29}$$

In terms of control variables the above constraint becomes

$$\begin{bmatrix} J_{st,com} & J_{st,j} & O_{3n_{st}\times 3n_{st}} \end{bmatrix} \zeta = -\dot{J}_{st,com}(q,\dot{q})\dot{r}_c - \dot{J}_{st,j}(q,\dot{q})\dot{q}. \tag{2.30}$$

Collecting (2.28) and (2.30), the terms in (2.23) are

$$A = \begin{bmatrix} M_{com}(q) & O_{6\times nn_l} & J_{st,com}(q)^T \\ J_{st,com}(q) & J_{st,j}(q) & O_{3n_{st}\times 3n_{st}} \end{bmatrix}, \tag{2.31}$$

and

$$b = -\begin{bmatrix} mg \\ \dot{J}_{st,com}(q,\dot{q})\dot{r}_c + \dot{J}_{st,j}(q,\dot{q})\dot{q} \end{bmatrix}. \tag{2.32}$$

Inequality constraints

Together with the equality constraint imposed on the position of the stance feet, an inequality constraint on ground reaction forces must be

considered in order to avoid the sliding of the supporting feet.
Ground reaction forces need to be constrained inside the friction cone to avoid slipping. For control design purposes, the friction cone is approximated as a pyramid to obtain linear constraints in the optimization problem. Considering the i-th ground reaction force $f_{gr,i} \in \mathbb{R}^3$, with $i = 1, \dots, n_{st}$, and indicating with $\bar{n}_i \in \mathbb{R}^3$ the i-th normal vector, $\bar{l}_{1,i}, \bar{l}_{2,i} \in \mathbb{R}^3$ two tangential vectors related to the i-th contact with the ground, and $\mu > 0$ the friction coefficient, the contact constraints can be written as follows [4]

$$\begin{aligned} (\bar{l}_{1,i} - \mu\bar{n}_i)^T f_{gr,i} &\leq 0, \\ -(\bar{l}_{1,i} + \mu\bar{n}_i)^T f_{gr,i} &\leq 0, \\ (\bar{l}_{2,i} - \mu\bar{n}_i)^T f_{gr,i} &\leq 0, \\ -(\bar{l}_{2,i} + \mu\bar{n}_i)^T f_{gr,i} &\leq 0. \end{aligned} \tag{2.33}$$

Then, for mechanical and safety reasons, joint torques need always to be limited based on the minimum and maximum reachable torques, that are τ_{min} and $\tau_{max} \in \mathbb{R}^{nn_l}$, respectively. Considering the last nn_l rows of (2.3) regarding the robot's legs, the constraints about limited torques can be expressed as follows

$$\tau_{min} - C_q(q, v)\dot{q} \leq \begin{bmatrix} M_q(q) & -J_{st,j}(q)^T \end{bmatrix} \begin{bmatrix} \ddot{q} \\ f_{gr} \end{bmatrix} \leq \tau_{max} - C_q(q, v)\dot{q}. \tag{2.34}$$

The last addressed constraint allows the swing feet to follow the desired trajectory planned. Let $v_{sw} \in \mathbb{R}^{3(n_l - n_{st})}$ be the vector collecting the linear velocity of the swing feet. Besides, let $J_{sw} \in \mathbb{R}^{3(n_l - n_{st}) \times (6 + nn_l)}$ be the Jacobian related to the swing feet. The following relation holds $v_{sw} = J_{sw,com}(q)\dot{r}_c + J_{sw,j}(q)\dot{q}$, whose time derivative is $\dot{v}_{sw} = J_{sw,com}(q)\ddot{r}_c + \dot{J}_{sw,com}(q, \dot{q})\dot{r}_c + J_{sw,j}(q)\ddot{q} + \dot{J}_{sw,j}(q, \dot{q})\dot{q}$. This last constraint compensates for the external forces acting on swing legs, estimated through the observer. These disturbances can heavily affect the respective foot's motion, so it is necessary to compensate for them. For this purpose, operational space formulation for swing feet is now employed. Having (2.3) in mind, the contact constraints $J_{st}^T f_{gr}$ can be eliminated using an orthogonal projection operator $P \in \mathbb{R}^{6+nn_l \times 6+nn_l}$, such that $PJ_{st}^T = 0$, $P = P^2$, and $P =$

P^T [43, 62]. Although different valid choice can be used for P [1, 73], the matrix P in this thesis has been chosen as in [62], that is $P = I_{6+nn_l} - J_{st}^{\dagger} J_{st}$. Pre-multiplying both sides of (2.3) by P yields

$$P\left(M\dot{\upsilon} + h\right) = PS^T\tau + PJ_{sw}^T f_{sw,ext}. \tag{2.35}$$

It is worth noticing that, since $PJ_{st}^T = 0$, the only remaining term related to external forces is $J_{sw}^T f_{sw,ext}$, which regards the swing legs. Following [62], equation (2.35) can be transformed into

$$M_c\dot{\upsilon} + Ph - C\upsilon = PS^T\tau + PJ_{sw}^T f_{sw,ext}, \tag{2.36}$$

where $M_c = PM + I_{6+nn_l} - P$ and $C = -J_{st}^{\dagger}\dot{J}_{st}$. As discussed in [62], M_c is always invertible, provided that M is invertible. Let $x_{sw} \in \mathbb{R}^{3(n_l - n_{st})}$ be the position of the swing feet. The following relations hold

$$\dot{x}_{sw} = J_{sw}\upsilon, \tag{2.37}$$

$$\ddot{x}_{sw} = J_{sw}\dot{\upsilon} + \dot{J}_{sw}\upsilon. \tag{2.38}$$

Pre-multiplying both sides of (2.36) by $J_{sw}M_c^{-1}$ and substituting (2.38) into (2.36), the following operational space configuration for the swing legs can be recovered

$$\ddot{x}_{sw} - \dot{J}_{sw}\upsilon + J_{sw}M_c^{-1}\left(Ph - C\upsilon\right) = J_{sw}M_c^{-1}PS^T\tau + J_{sw}M_c^{-1}PJ_{sw}^T f_{sw,ext}. \tag{2.39}$$

Let $\ddot{x}_{sw,des} \in \mathbb{R}^{3(n_l - n_{st})}$, $\dot{x}_{sw,des} \in \mathbb{R}^{3(n_l - n_{st})}$ and $x_{sw,des} \in \mathbb{R}^{3(n_l - n_{st})}$ be the swing feet references from the motion planner. The command acceleration for the swing feet $\ddot{x}_{sw,c} \in \mathbb{R}^{3(n_l - n_{st})}$ can be chosen as

$$\ddot{x}_{sw,c} = \ddot{x}_{sw,des} + K_{d,sw}(\dot{x}_{sw,des} - \dot{x}_{sw}) + K_{p,sw}(x_{sw,des} - x_{sw}), \tag{2.40}$$

with $K_{p,sw}, K_{d,sw} \in \mathbb{R}^{3(n_l - n_{st}) \times 3(n_l - n_{st})}$ positive definite matrices. To compensate for disturbances, the term related to external forces on swing legs in (2.39) must be taken into account. Therefore, the command acceleration needs to become

$$\ddot{x}_{sw,cmd} = \ddot{x}_{sw,c} - J_{sw} M_c^{-1} P J_{sw}^T \hat{f}_{sw}. \tag{2.41}$$

To follow the trajectory, the following equality constraint should be imposed, replacing (2.41) into (2.38)

$$\ddot{x}_{sw,cmd} = J_{sw,com}(q)\ddot{r}_c + \dot{J}_{sw,com}(q,\dot{q})\dot{r}_c + J_{sw,j}(q)\ddot{q} + \dot{J}_{sw,j}(q,\dot{q})\dot{q}. \tag{2.42}$$

Although an equality constraint should be imposed, the constraint is softened by adding slack variables $\gamma \in \mathbb{R}^{3(n_l - n_{st})}$ within the optimization problem. The addressed inequality constraint is thus chosen as [31]

$$\begin{aligned} \ddot{x}_{sw,cmd} - \gamma \leq J_{sw,com}(q)\ddot{r}_c + \dot{J}_{sw,com}(q,\dot{q})\dot{r}_c + \\ + J_{sw,j}(q)\ddot{q} + \dot{J}_{sw,j}(q,\dot{q})\dot{q} \leq \ddot{x}_{sw,cmd} + \gamma. \end{aligned} \tag{2.43}$$

Therefore, collecting (2.33), (2.34), and (2.43), the terms in (2.24) are

$$D = \begin{bmatrix} O_{4n_{st}\times 6} & O_{4n_{st}\times nn_l} & D_{fr} \\ O_{nn_l\times 6} & M_q(q) & -J_{st,j}^T \\ O_{nn_l\times 6} & -M_q(q) & J_{st,j}^T \\ J_{sw,com} & J_{sw,j} & O_{3(n_l-n_{st})\times 3n_{st}} \\ -J_{sw,com} & -J_{sw,j} & O_{3(n_l-n_{st})\times 3n_{st}} \end{bmatrix}, \tag{2.44}$$

$$c = \begin{bmatrix} 0_{4n_{st}} \\ \tau_{max} - C_q(q,\upsilon)\dot{q} \\ -(\tau_{min} - C_q(q,\upsilon)\dot{q}) \\ \ddot{x}_{sw,cmd} + \gamma - \dot{J}_{sw,com}(q,\dot{q})\dot{r}_c - \dot{J}_{sw,j}(q,\dot{q})\dot{q} \\ -\ddot{x}_{sw,cmd} + \gamma + \dot{J}_{sw,com}(q,\dot{q})\dot{r}_c + \dot{J}_{sw,j}(q,\dot{q})\dot{q} \end{bmatrix}, \tag{2.45}$$

where $D_{fr} \in \mathbb{R}^{4n_{st}\times 3n_{st}}$ is a diagonal matrix containing the friction cone constraints expressed in (2.33) for each stance leg [31].

Control torques

The result of the optimization problem is the desired vector $\zeta^* = \begin{bmatrix} \ddot{r}_c^{\star T} & \ddot{q}^{\star T} & f_{gr}^{\star T} \end{bmatrix}^T$. The control torques can be computed using the second part of (2.3), considering that all the external forces have been compensated for inside the quadratic problem

$$\tau^{*} = M_q(q)\ddot{q}^{\star} + C_q(q,v)\dot{q} - J_{st,j}(q)^T f_{gr}^{\star}. \tag{2.46}$$

2.5 Case Studies

In the following, the setup used to test the case studies is presented. Then, the performance of different case studies is analysed:

- the sole momentum-based observer acting only on the legs is used within the WBC, its performance is compared with two other solutions available within the state of the art;
- the momentum-based observer acting only on the legs is used in combination with the hybrid observer for the CoM. Even in this case, the performance is compared with other solutions;
- a possible application of the observers for care assistance is presented.

2.5.1 Setup

Simulations have been carried out through the ROS middleware, in combination with the dynamic simulator *Gazebo*. This choice has been made since Gazebo uses a high-performance physics engine to make the movement and external conditions as realistic as possible. The quadruped used for simulations in Gazebo is DogBot from React Robotics, an open-source platform. The structure of the robot is shown in Fig. 2.1. It presents three actuated revolute joints for each leg: the first one connects the body with the leg, and its axis is parallel to the longitudinal axis of the body, realizing all the lateral movement; the second and the third ones allow the lift-off of the foot from the ground and coincide with the hip and the knee, respectively, and their axis are both normal to the plane of the leg. Then, for this robot, $n_l = 4$ and $n = 3$. DogBot's configuration has all the legs pointing backward so that the push-off impulse is facilitated, while fast motions are easy to realize. It weighs 21 kg, the mass is mainly concentrated in the body, which has a weight of 12 , while each leg is 2 kg.

Both the upper and the lower segments of each leg have a length of around 0.3 m.

All the simulations were performed on a standard personal computer. The references for the CoM and the swing feet were generated using *Towr* [93], a C++ library for trajectory optimization for legged robots. A fixed planned step's height for the swing feet has been set to 0.05 m, and the maximum step length is chosen to avoid a complete stretching or retraction of the legs: at the planning level, this avoids singularities in J_j. Besides, these references were replanned at the beginning of each footstep, with a period $T_{fs} = 0.26$ s. The quadratic problem was solved using the C++ library *ALGLIB*. The gains for the desired wrench in (2.26) have been experimentally tuned to $K_p = \text{diag}(250, 250, 250, 250, 250, 250)$ and $K_d = \text{diag}(50, 50, 50, 50, 50, 50)$. The gains for the command acceleration for swing feet in (2.40) have been experimentally tuned to $K_{d,sw} = 100 I_{3n_l - n_{st}}$ and $K_{p,sw} = 25 I_{3n_l - n_{st}}$. The gains for the optimization have been set as $Q = \text{diag}(100, 100, 100, 100, 100, 100)$, $R = I_{6+nn_l+3n_{st}}$, while $\mu = 1.0$, $\tau_{min} = -60$ Nm, and $\tau_{max} = 60$ Nm.

2.5.2 Disturbance rejection through observer on the legs

This section will present the results obtained using only the observer on the legs, without any compensation for external disturbances acting directly on the CoM. For these simulations, the stance phase has been chosen to last 0.15 s, while the swing phase lasts 0.115 s. Numerical integration for dynamics is set in Gazebo as $\delta\, t = 0.001$ s.The torque control loop, the state estimation and the momentum-based observation have a frequency of 1 kHz, while the optimization problem runs at a frequency of 400 Hz. The various operations of the control scheme are applied sequentially.

In order to test the whole-body control design, six case studies have been considered:

- a sinusoidal disturbance with an amplitude of 20 N has been applied on the front left knee within the first case study;

- in the second case study, the same sinusoidal disturbance has been applied to carry out a comparison against two state-of-the-art solutions;

- in the third case study, instead, a disturbance of 80 N has been applied for a small portion of time, 0.2 s, on the front right knee during his swing phase, simulating a sudden impact;
- in the fourth case study, a random disturbance is injected every two seconds on a randomly chosen leg. The force is applied at different points of the limb to show the effectiveness of the approach;
- the situation of the previous case is repeated in the fifth case study, where this random disturbance is combined with parametric uncertainties in the model known by the controller;
- the robot is tested on irregular terrain in the last case.

Although the estimated vector accounts for the effects at the legs' tips of external forces acting at any point of the robot (information that is unknown by the controller), the plots presented in the following show the estimated force vector reported back to the application point of the disturbance. This is obtained after offline post-processing of the results. The presented simulations can be found in the video [1].

Analysis on the order of the estimator

Firstly, a series of simulations have been done to choose the estimator's order, considering a constant external force. The estimation's error for different orders is reported in Fig. 2.3. In Fig. 2.3a, a comparison has been made between first-order and second-order estimators. It can be noticed that the former presents a higher overshoot of the error. Results for the next orders are shown in Fig. 2.3b. From the third-order, it is not possible to appreciate any significant improvement. Anyway, the overshoot of the error is higher for the fourth and second order. For this reason, the best choices are the third and fifth orders. In this work, as a result of the analysis carried out, the degree r is set to 3, while coefficients K_1, K_2 and K_3 have been chosen as $17.5I_{12}$, $6.28I_{12}$ and $2.25I_{12}$, respectively, in a trade-off between desired results and the computational time leading to delays.

[1] https://youtu.be/styHnKxOot8

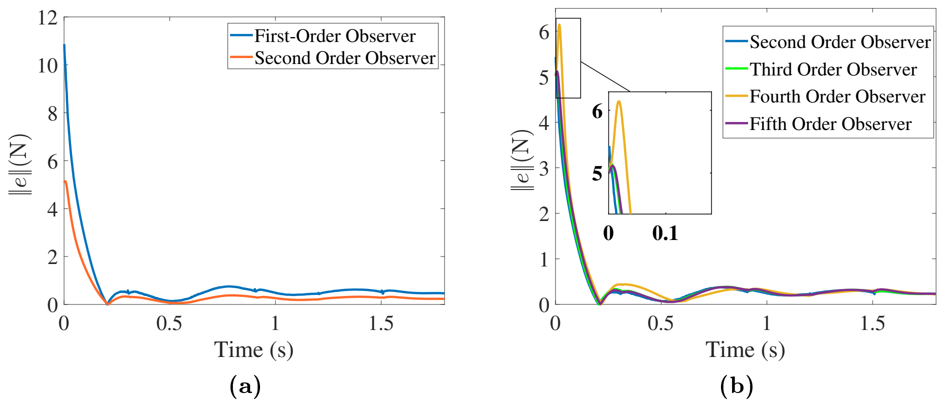

Figure 2.3. Analysis on the order of the estimator. (a) Estimation's error for first (blue) and second (orange) order. (b) Estimation's error for second (blue), third (green), fourth (yellow) and fifth (violet) order.

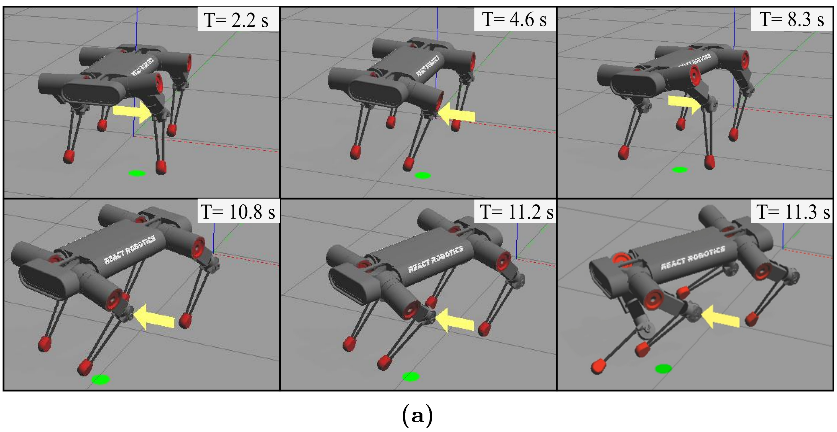

Figure 2.4. Case Study A1. In this simulation, external forces on swing legs are not compensated. These pictures show instants when the disturbance is around its peaks. The yellow arrow indicates the application point and direction of the force. The green circle represents the planned foothold, the drift of the foot is evident. At 11.3 s, the robot loses its balance.

Case Study A1

The first case study has been carried out by considering a sinusoidal disturbance along the x-axis, with an amplitude of 20 N and a period $T = 2\pi$ s, on the front left knee during all the simulation.
This choice is made to see the effect of time-varying disturbances on a leg during both the stance and the swing phase. In this case study, the robot is guided to follow a trajectory of 5.5 m composed of alternating sequences of rectilinear and curvilinear motions. The forward velocity is 0.12 m/s and, during curvilinear motions, the angular velocity is 0.05 rad/s.

A simulation of this case study without counterbalancing for disturbances on the swing legs is performed and presented in video to stress the importance of having such compensation. It could be observed that, although the robot can retain the balance for a while, the drift of the perturbed leg's foot is evident. It brings the robot to fall after 11.3 s. Fig. 2.4 shows in detail this situation with a series of pictures of salient instants of the movement.

Using the proposed framework, this situation can be avoided. The norm of CoM error for a portion of the path is shown in Fig. 2.5. It can be noticed that, although the error is at most 0.01 m, some peaks can be noticed: these are produced during the swing phase regarding the front leg subject to the external disturbance. In general, the CoM error components have sinusoidal trend. This is given by the continuous change of support legs, so the motion of the CoM is replanned to reach the center of the current support polygon. During the swing phase, the support line has been enlarged to a rectangle to soften the constraint about the ZMP. The disturbance reconstructed by the observer is depicted in Fig. 2.6. Small uncertainties can be noticed, probably given by some parametric inaccuracies in the model.

Fig. 2.7 shows the norm of the error between the ground reaction forces computed by the QP (2.22)-(2.24) and the ones measured by some sensors put under the feet within the Gazebo environment. The time history is referred to the front left leg so as to prove the framework's effectiveness in tracking the ground reaction forces. The average of such error remains under 5 N, which is an improvement with respect to existing works [36].

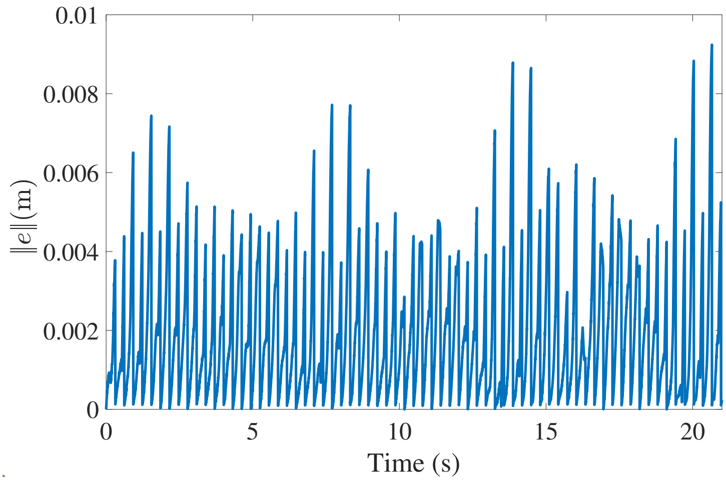

Figure 2.5. Case Study A1. Error norm of the robot's CoM using the proposed whole-body controller.

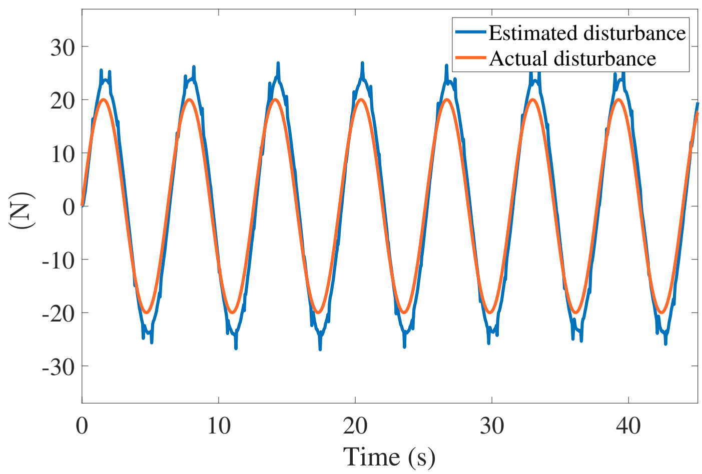

Figure 2.6. Case Study A1. Estimation of the disturbance through the proposed momentum-based observer. In blue the estimated force, in orange the actual force.

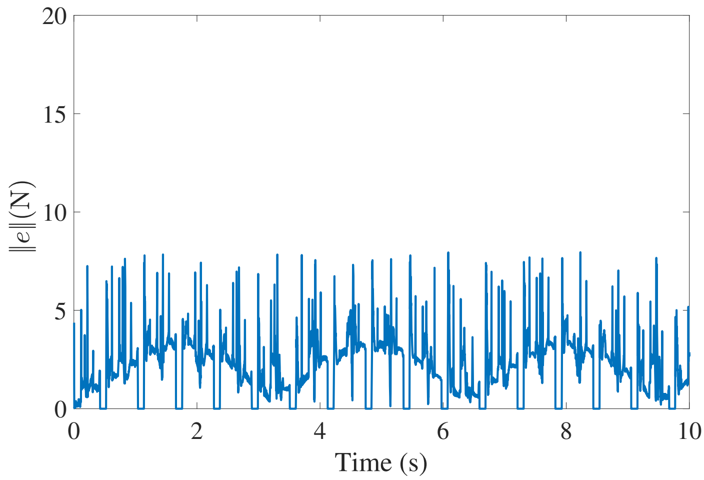

Figure 2.7. Case Study A1. Error norm of the ground reaction forces for front left leg, using the proposed whole-body controller.

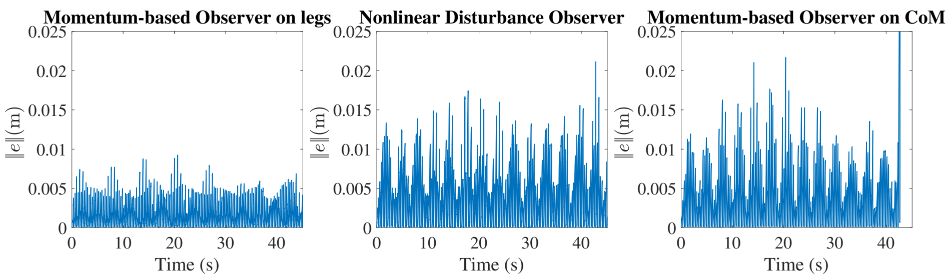

Figure 2.8. Case Study A2. Comparison between several control techniques. The plot show the error norm of the robot's CoM for each of the considered observer. From left to right: the results obtained with the proposed controller; the results obtained using [36]; the results obtained through [23].

Case Study A2

A comparison with state-of-the-art observers is now accomplished to validate the envisaged whole-body controller's performance further. Both the trajectory and the external disturbance are the ones considered in case study A1. The observers chosen for comparison are picked up from [36]

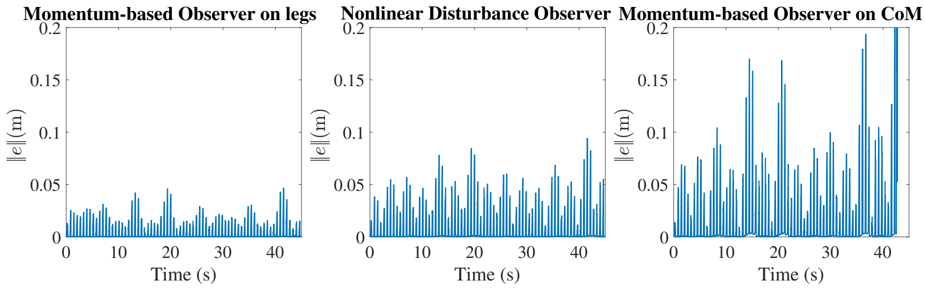

Figure 2.9. Case Study A2. Comparison between several control techniques. The plot shows the error norm of the front left foot position for each of the considered observer. From left to right: the results obtained with the proposed controller; the results obtained using [36]; the results obtained through [23].

and [23]. The former is a first-order momentum observer that considers only the external wrench of the CoM and can deal with disturbance applied to the stance legs only. This is reasonable in those cases where the only source of errors comes from the unknown terrain. This observer employs the first six rows from (2.3). The latter observer is a nonlinear disturbance observer taking into account the four legs' dynamics, but it is not based on the system's momentum. To the best of the author's capabilities, the gains for the first observer were chosen as $G_{lin} = 25I_3$ and $G_{ang} = 10I_3$ [36], while for the second observer the gain matrix was set as $X = 10I_{12}$. The gains of the optimization problem remain unchanged.

The norm of the CoM errors of the three considered observers is compared in Fig. 2.8. It can be noticed that observer from [36] and the one from [23] have similar CoM error norm. Nevertheless, the former is not able to follow the full trajectory. Indeed, the robot loses its balance. An explanation of this imbalance can be found in Fig. 2.9, where the error norm of the front left foot position is represented. It can be seen that the highest error norm of the foot position is obtained using the observer proposed in [36]. As it was already said, this is the only observer, here tested, that considers only the external wrench of the CoM. Using this observer, the disturbance on the leg causes a significant drift of the foot during the swing phase, which, although the CoM error remains small, brings to the loss of balance. It is highlighted once again the importance of considering leg dynamics and compensating for external forces on all the legs. Given the author's ability to implement and tune the addressed state-of-the-art observers, the proposed observer seems to outperform the others thanks to explicitly addressing the errors on the swing legs. This is evident since the error norm on the robot's CoM is less than 0.01 m and the error norm of the foot position subject to the disturbance is always less than 0.05 m.

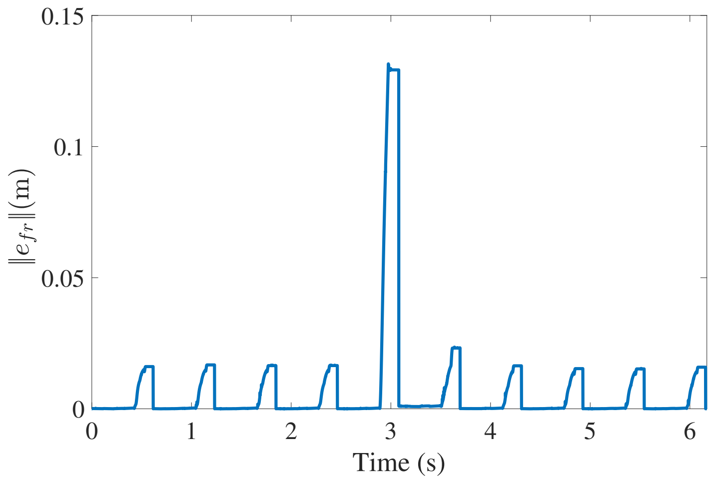

Figure 2.10. Case Study A3: Error norm of the front right foot position using the proposed whole-body controller.

Case Study A3

Within the third case study, a brief but severe disturbance is applied along the x-axis on the front right knee during its swing phase. The planned trajectory is a rectilinear path and the forward velocity is 0.12 m/s. The disturbance has a magnitude of 80 N, it lasts for 0.2 s, and it is injected at 2.8 s from the planned trajectory's start. The instant of the injection has been chosen so that it goes to apply on the leg during its swing phase, demonstrating that the control framework can handle unexpected impulsive disturbances. Such a disturbance causes a considerable drift of the front right foot while it is swinging, unbalancing the robot. The controller here presented can instead cope with such a disturbance by

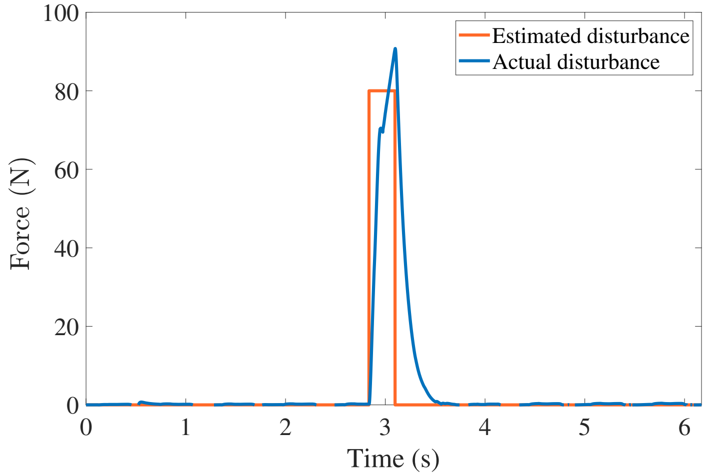

Figure 2.11. Case Study A3: Estimation of the disturbance through the proposed momentum-based observer. In blue the estimated force, in orange the actual force.

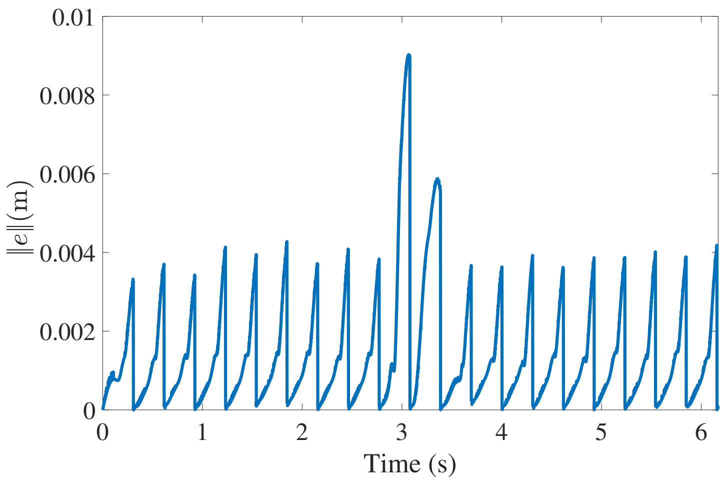

Figure 2.12. Case Study A3: Error norm of the robot's CoM using the proposed whole-body controller.

minimizing the leg's drift and recovering the given trajectory in the next footsteps. This can be appreciated in Fig. 2.10, where the foot position's error is shown. The highest peak coincides with the application of the disturbance. Fig. 2.11 shows the estimation of the external force, while in Fig. 2.12 the CoM's error norm can be observed. In this case, there are two peaks: the first one is caused by the external force, while the second coincides with the recovery footstep, a phase in which the support polygon is not optimal given the former drift of the foot subject to the disturbance. However, the CoM's error is still less than 0.01 m, guaranteeing the recovery of the balance after the impact. This third case study demonstrates that the designed architecture can effectively estimate a large disturbance, also if it happens on a leg during its swing phase. In this way, the legged robot can work in various scenarios: for instance, in severe atmosphere conditions or during collisions with the environment during the swinging. The disturbance's magnitude has been chosen so large on purpose to bolster the performance of the envisaged observer that can cope with a broader range of disturbances than other state-of-art observers, which can handle only small external forces acting on swing legs.

Case Study A4

The fourth case study has been carried out considering a random disturbance. Every two seconds, the force's magnitude changes randomly between 10 N and 35 N. Moreover, both the leg subject to the perturbation and the height of the application point change too. The direction of the disturbance forces is shown in the video. In this case study, the robot is guided to follow a trajectory of 3.7 m composed of alternating sequences of rectilinear and curvilinear motions. The forward velocity is 0.12 m/s and, during curvilinear motions, the angular velocity is 0.05 rad/s. This case study aims to demonstrate the validity of the proposed method for a wide range of disturbances. The approach results robust against a random perturbation and also against an unexpected variation of the application point. The location of the external force is chosen along all the length of the legs. It could be from the top (so it can be considered a disturbance on the torso) to the bottom (at the foot). In this way, the observer helps with general disturbance rejection where external forces can be applied anywhere on the robot. In Fig. 2.13a the plot about the error norm of the

CoM is reported. It can be observed that the peaks of error are always around 0.01 m. Nevertheless, in previous cases has been highlighted the importance of foot position error, that can cause a loss of balance even if the CoM error is small. For this reason, in Fig. 2.14, the disturbances for each leg are represented on the right. On the left, the norm errors of the respective foot can be observed, so that it can be noticed that the highest peaks correspond to the application of the external force on the leg. In particular, it can be observed that the error is always under 0.035 m except for cases when the start of disturbance application coincides with the beginning of the swing phase. This situation verifies for the front left foot at 10 s and the rear right foot at 26 s. In these instants, the unexpected and instantaneous disturbance is applied to the leg while its foot lifts off the ground. Since this external force is not compensated, the foot is subject to an initial drift higher than usual. Anyway, the observer demonstrates to estimate the disturbance in a short time so that the balance can be retained.

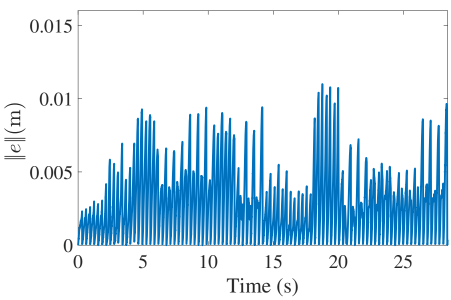

(a)

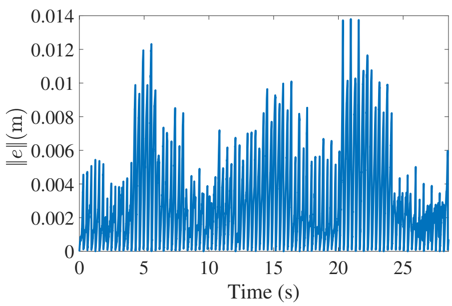

(b)

Figure 2.13. Case Study A4: Error norm of the robot's CoM using the proposed whole-body controller. (a) Ideal situation. (b) White Gaussian noise added on the joint torque measurement.

Until now, all the cases have been simulated in an ideal situation. In a real situation, some sensor noise could influence the estimation of the observer, adding uncertainty. For this reason, this case has also been tested in a non-ideal condition, adding a white Gaussian noise on both the

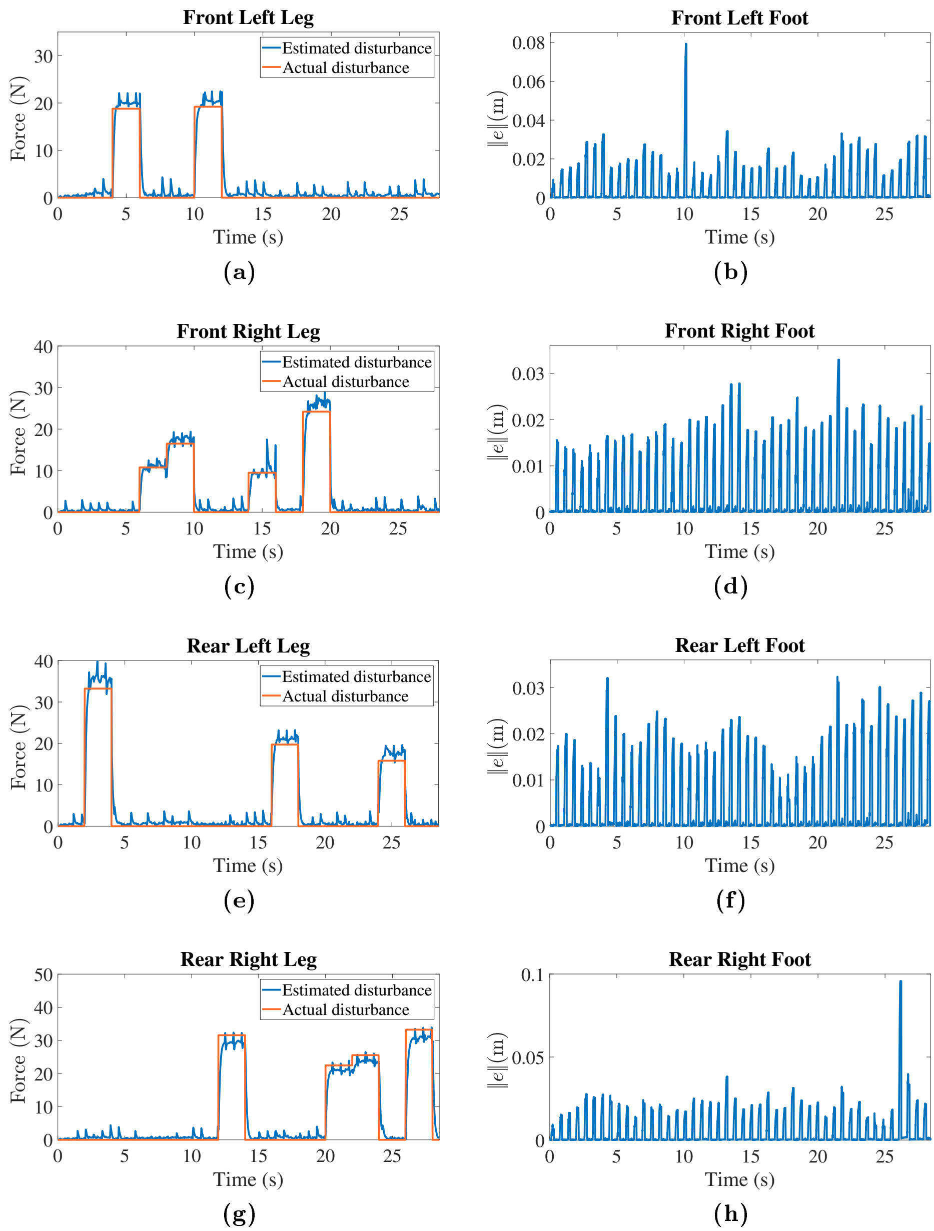

Figure 2.14. Case Study A4-Ideal situation. (a),(c),(e),(g) Estimation of the disturbance on the four legs, in blue the estimated force, in orange the actual force. (b),(d),(f),(h) Error norm of respective feet.

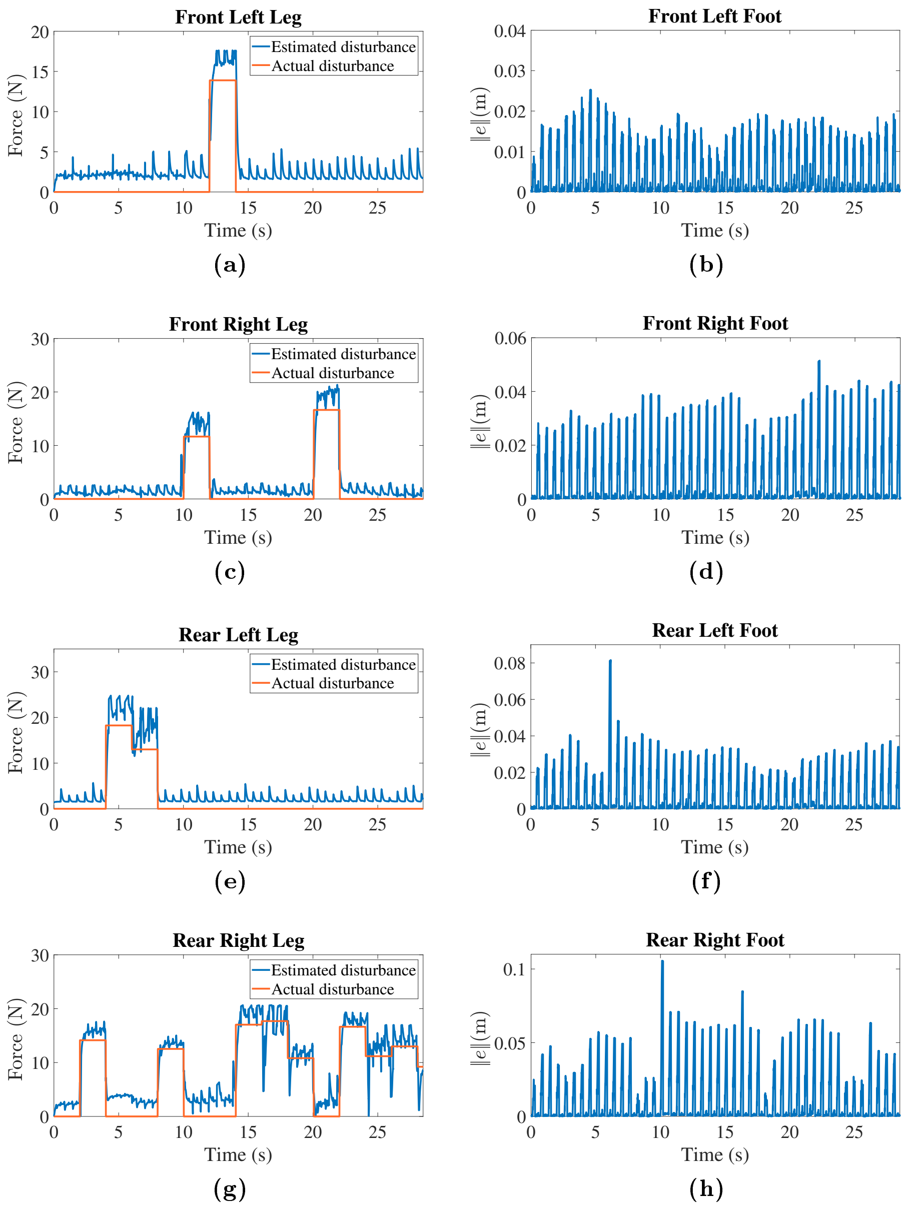

Figure 2.15. Case Study A4-White Gaussian noise added on the joint torque measurement. (a),(c),(e),(g) Estimation of the disturbance on the four legs, in blue the estimated force, in orange the actual force. (b),(d),(f),(h) Error norm of respective feet.

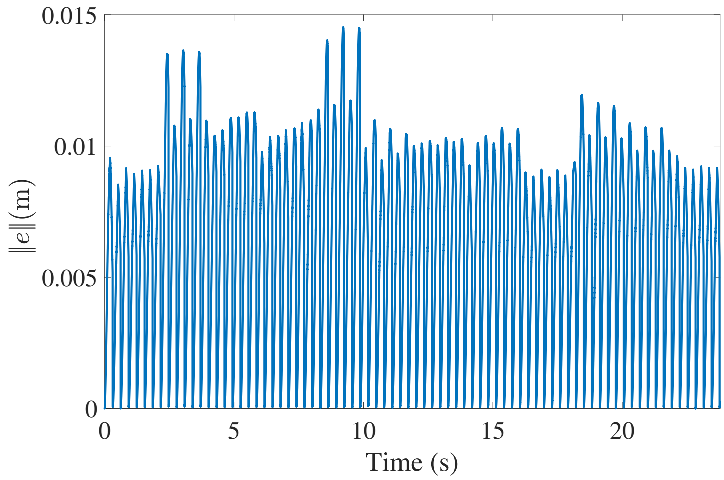

Figure 2.16. Case Study A5: Error norm of the robot's CoM using the proposed whole-body controller.

joint torque and the ground reaction forces measurements with a standard deviation of 10% of the measured signal. This situation has been tested to analyze further the robustness of the controller. In Fig. 2.15 the plot about the disturbance estimation for each leg is reported alongside the norm error of the respective foot. In this case, it can be noticed that the presence of noise inevitably leads to a noisy estimation. However, the controller can still guarantee an optimal tracking of the feet position. Its error is below 0.06 m, except for cases when the disturbance application coincides with the swing phase's beginning. Also, good tracking of the CoM is performed, as can be observed in Fig. 2.13b, where the peaks of error are always less than 0.014 m.

Case Study A5

The fifth case study considers the same random disturbance of the fourth case study. Now, to add a parametric uncertainty, the total mass known by the controller is changed by 30%. While the goal of case study 4 was to demonstrate the validity of the approach for external forces applied at different points, this case study aims to extend the range of disturbances considering parametric uncertainties in the model. As in the previous case, the disturbances for each leg and the respective foot's norm errors are represented in Fig. 2.17. It is worth noticing that, this time, the estimated force has an offset due to the parametric error, which is seen as a disturbance even when there is no physical force applied to the robot. This can be appreciated in Fig. 2.17g: no perturbation is acting on the rear right leg, but the estimation is never equal to zero. The norm error of the feet position is always less than 0.035 m, guaranteeing a precise tracking of the support polygon desired. As highlighted in the previous case, some peaks of the error happen when the beginning of the swing phase and the disturbance's application coincide. In Fig. 2.16 the plot about the error norm of the CoM is reported. It can be observed that the peaks of error are now higher, but always less than 0.015 m. This small increment of the error can be considered the result of the parametric uncertainty, which can still be handled.

Case Study A6

The sixth case study focuses on the capability of the whole-body controller to work on irregular terrain. For this purpose, some blocks with different heights have been added to the environment to reproduce the terrain's irregularities, as it is shown in Fig. 2.18. Moreover, all the blocks have different friction coefficients to simulate various kinds of soils. With reference to the figure, the heights of the blocks are 0.015 m for blue blocks, 0.04 m for green blocks, and 0.02 m for red blocks. Instead, the friction coefficients are 0.4 for blue blocks, 0.6 for green blocks, 0.8 for red blocks, and 1 for the ground. These friction coefficients have been chosen after different simulations, which demonstrated the approach could not guarantee good performance for coefficients lower than 0.4. For smaller coefficients, it is possible to retain the balance, but there is a foot slipping after the impact phase. The friction coefficient inside the whole-body controller has been chosen, in a conservative way, as 0.4. This is crucial to improve robustness so that the controller can step over different soils without slipping, maintaining the ground reaction forces inside the friction cone. In this case, the path is rectilinear and the forward velocity is 0.12 m/s. The results of this case study demonstrate the capability of the proposed approach to reject disturbances given by an irregular terrain.

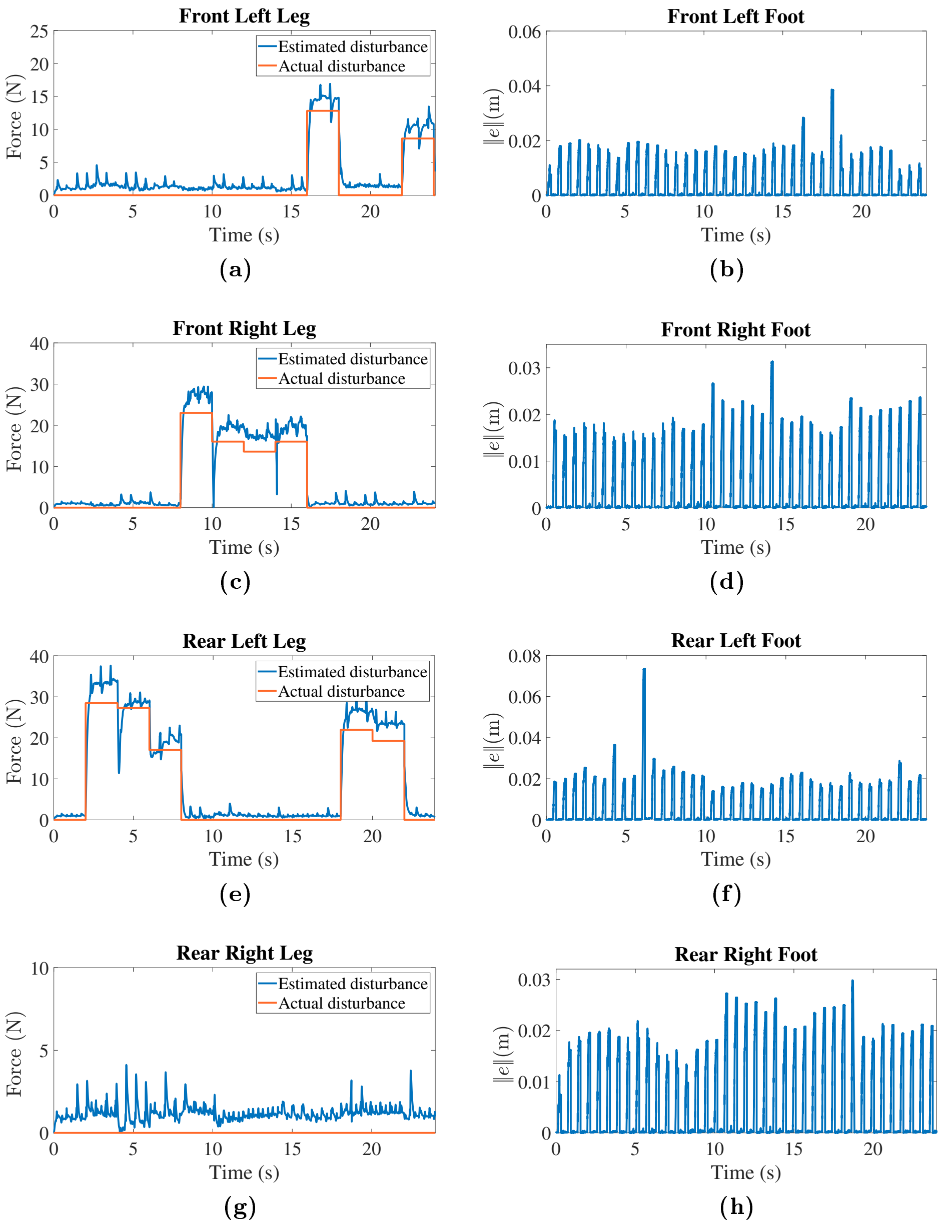

Figure 2.17. Case Study A5. (a),(c),(e),(g) Estimation of the disturbance on the four legs, in blue the estimated force, in orange the actual force. (b),(d),(f),(h) Error norm of respective feet.

In particular, these external forces are given by the anticipated touchdown caused by different heights of the soil. Indeed, the reference foothold is planned for a flat ground, and the unexpected difference in the height causes an asymmetric gait, unbalancing the robot. This concept can be appreciated in Fig. 2.19, where the foot's norm error for each leg is shown. It can be noticed that, differently from other cases, there are some intervals where the foot's norm error never goes to zero despite the re-planning (e.g., from instant $t_1 = 10$ s to $t_2 = 20$ s in Fig. 2.19a). Comparing the figure with the video shows that these intervals coincide with the stepping of the respective foot on one of the blocks. During these phases, the block's height constitutes a continuous disturbance since the reference foothold is planned for a flat ground. Observing the figure, it could be noticed that the height of different blocks can be retrieved from the position error. It should also be noticed that the heights of the blocks have been chosen considering the planned step's height. In the case of a high block, there would be the need for a strategy for recognition of the height and a consequent adjustment of the gait. However, this is out of the scope of this work. In Fig. 2.20, it can be observed that the controller, despite the irregularities, guarantees a good tracking of the CoM position, with an error always less than 0.01 m. In the video, some instants are highlighted when a foot impact the edge of a block or slide down between two blocks. Nevertheless, in all these cases, the balance is retained, demonstrating the robustness of the controller.

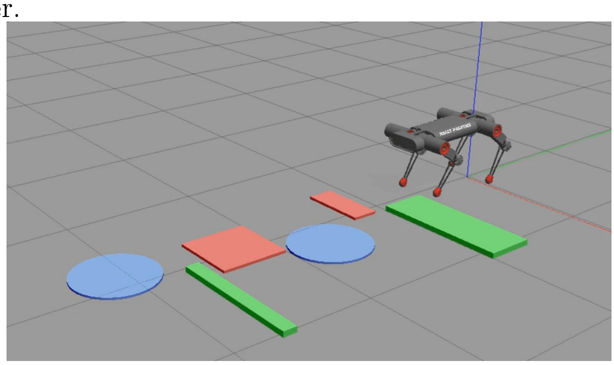

Figure 2.18. Case Study A6: Environment of the Case Study 6. The friction coefficient is: 0.4 for blue blocks, 0.6 for green blocks, 0.8 for red blocks, and 1 for the ground. The height of the blocks is: 0.015 m for blue blocks, 0.04 m for green blocks, and 0.02 m for red blocks.

2.5.3 Disturbance rejection with hybrid observer with momentum-based acting on the legs

This section will present the results obtained using the hybrid observer on the CoM in combination with the momentum-observer acting on the legs. All the simulations were performed on a standard personal computer. The stance phase has been chosen to last 0.15 s, while the swing phase lasts 0.115 s. Numerical integration for dynamics is set in Gazebo as $\delta\ t = 0.001$ s. The torque control loop, the state estimation, and the observation have a frequency of 1 kHz, while the optimization problem runs at a frequency of 400 Hz. In order to test the whole-body control design, three case studies are considered in the following. The case studies can be appreciated in the video[2].

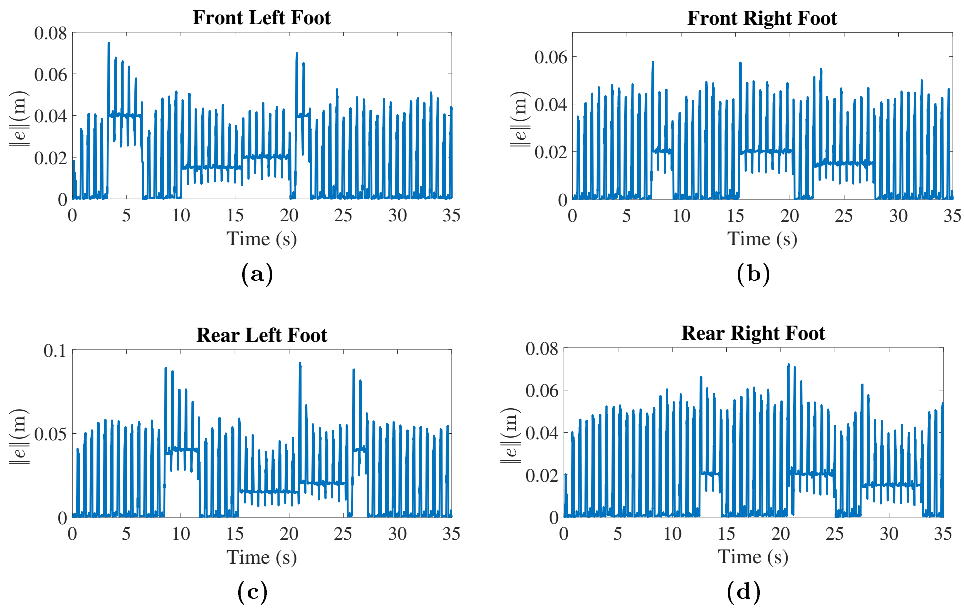

Figure 2.19. Case Study A6. Error norm of the feet.

[2] https://youtu.be/wbtoAo3Y6Xc

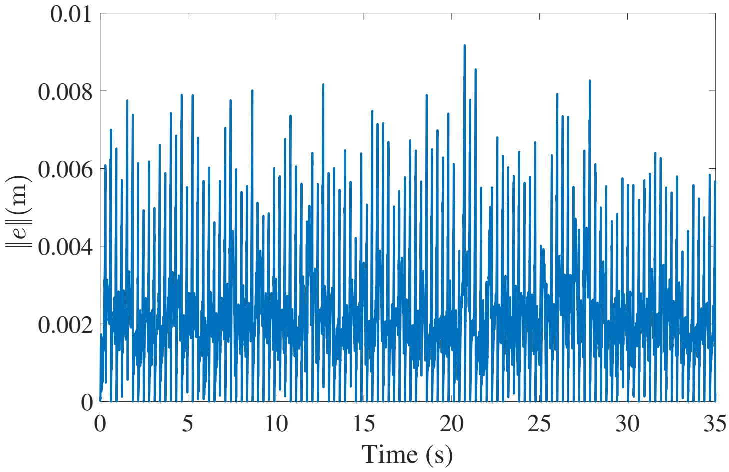

Figure 2.20. Case Study A6: Error norm of the robot's CoM using the proposed whole-body controller.

Case study B1

This case study aims to test the controller in a realistic scenario, presented in Fig. 2.21, where some blocks with different heights and friction coefficients have been added to reproduce an irregular terrain. With reference to Fig. 2.21, the heights of the blocks are 0.015 m for the blue blocks, 0.035 m for the green ones, and 0.02 m for red blocks. Instead, in Gazebo, the friction coefficients between the legs and the blocks are set to 0.4, 0.6, 0.8, respectively, while 1 is the friction coefficient with the ground.

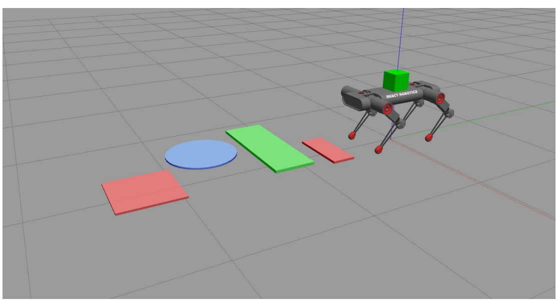

Figure 2.21. Scenario used for Case Study B1.

To test robustness, the friction coefficient inside the whole-body controller has been chosen, in a conservative way, as 0.4. An object of 23 kg has been put on the robot's torso for further stress. It should be noticed that the objective of this case study is not the object transportation but to test the capability of the controller to handle such a disturbance. Combining an irregular terrain with an object on the torso is a suitable scenario for testing disturbances on the CoM and the legs. In this case study, the forward direction is along the $y-$axis, with a velocity of 0.12 m/s. The controller here presented (CoM and legs) is compared with the one using only the estimation on the legs, as in section 2.5.2 and the controller employing only the estimation on the CoM [31], thus without the compensation of disturbances on swing legs implemented in (2.41).

The results showed that this kind of stress is difficult to handle using only the estimation on the legs. Indeed, it can be seen in Fig. 2.22b that the error along the $z-$axis is one order of magnitude higher than the error obtained when the observation on the CoM is present. This is plausible since the object impresses a significant disturbance on the CoM that cannot be seen through the legs' observer, making the robot lower its torso and, eventually, fall. Comparing the two controllers addressing the estimation on the CoM, their errors on the $z-$axis are similar, while on the $x-$axis the here presented hybrid estimator has better performance. This can be explained because the presence of irregular terrains causes anticipated touchdowns that can be better handled using observation on the legs. Irregular terrain may thus unbalance the robot if it used an observer on the CoM only. In Fig. 2.23 the estimation of the wrench at the CoM is reported. It can be seen that the most important estimation is the one regarding the force acting along the $z-$axis, whose mean is -228.0635 N. This is given by the object's weight, which, given the gravity acceleration, imposes a force of around -225.6300 N. The estimation demonstrates to be valid enough to handle this force retaining the balance.

Case study B2

The second case study has been carried out considering two random disturbances: the first acting on the CoM and the second acting on a randomly chosen point of one of the legs. Every four seconds, the force's magnitude changes randomly between 2.5 N and 40 N. The direction of the

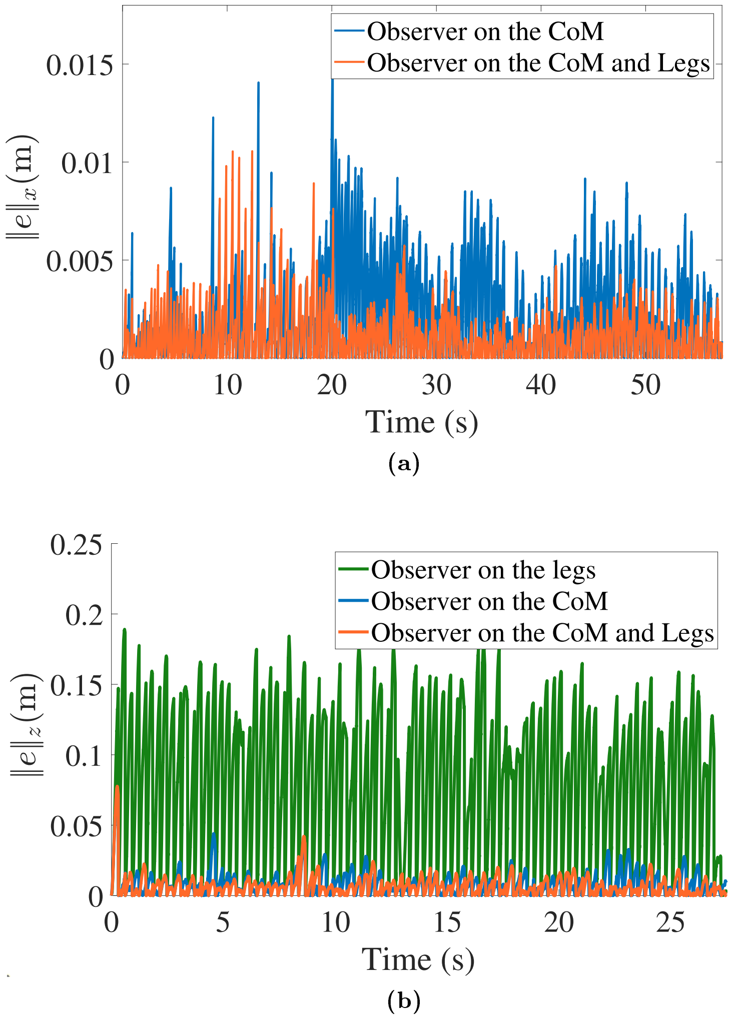

Figure 2.22. Case Study B1. Error on the $x-$axis (a) and on the $z-$axis (b).

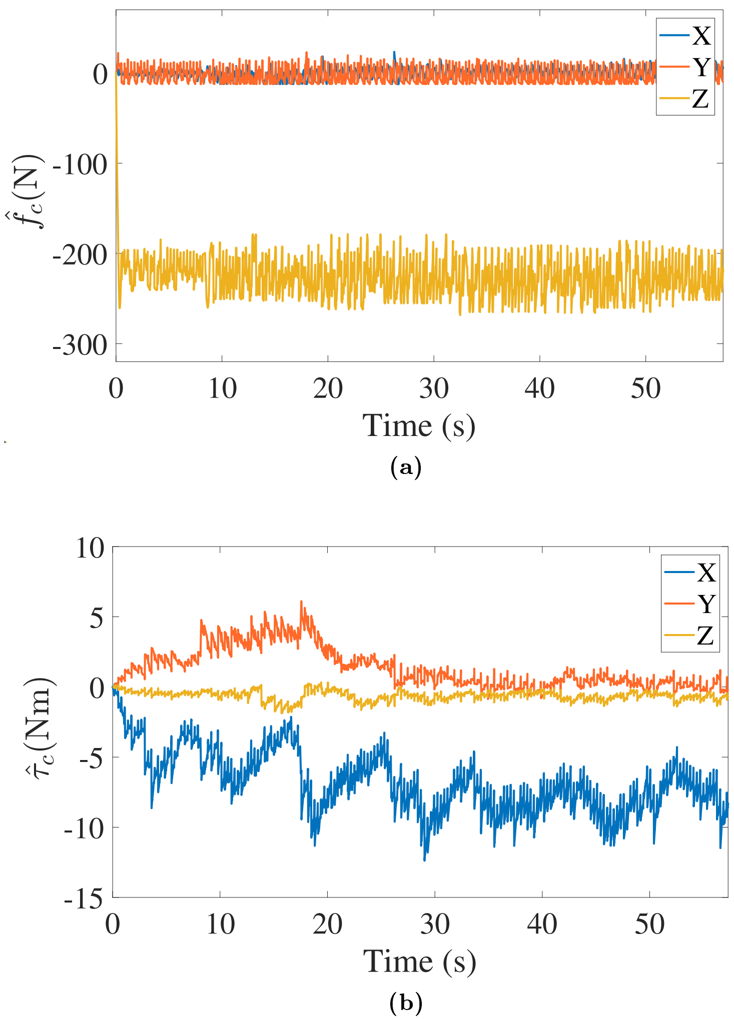

Figure 2.23. Case Study B1. Estimation of $\hat{f}_c$ (a) and $\hat{\tau}_c$ (b).

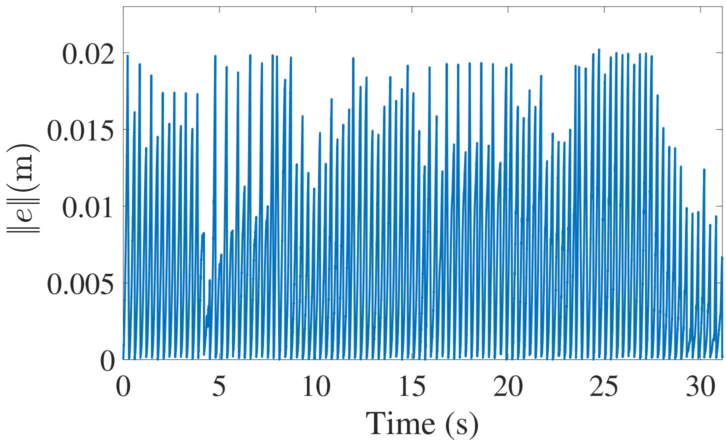

Figure 2.24. Case Study B2. Error norm of the robot's CoM using the proposed controller.

disturbance forces is shown in the video. The forward direction is along the $y-$axis, with a velocity of 0.12 m/s.

This case study aims to demonstrate the validity of the proposed hybrid observer, acting on both the CoM and the legs. The following results can be discussed. Using the observer only on the CoM, the robot seems unable to reject the disturbance acting on the legs, with a significant drift of the foot that causes the fall. Using the observer only on the legs, the robot, differently from the previous situation, seems to have good tracking of the planned foothold. However, it is unable to reject the disturbance on the CoM with a consequent fall. Finally, using the hybrid estimator, the robot can reject the disturbance on the CoM and have good tracking of the planned foothold at the same time. This case study has been tested in a non-ideal situation. Adding a white Gaussian noise on the joint torque and the ground reaction forces measurements, with a standard deviation of 10% of the measured signal, simulates sensors noise. The approach results robust, with a maximum error in the tracking of the CoM of 0.02 m, as it can be seen in Fig. 2.24. The estimation of the magnitude acting on the CoM and the rear right leg are presented in Figs. 2.25 and 2.26, respectively. In this way, good tracking of the actual disturbances can be

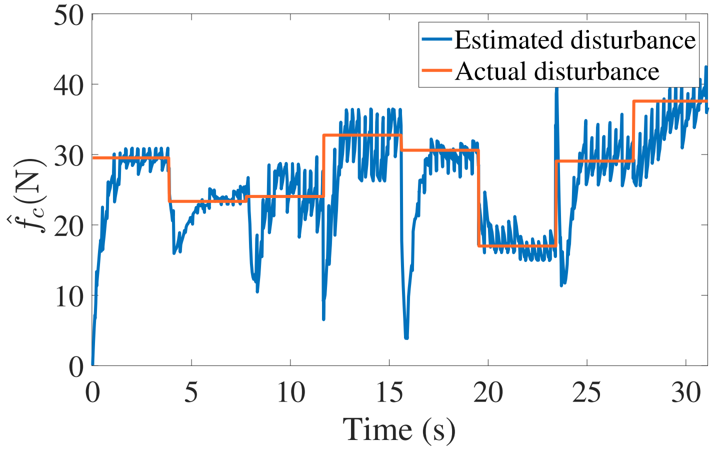

(a)

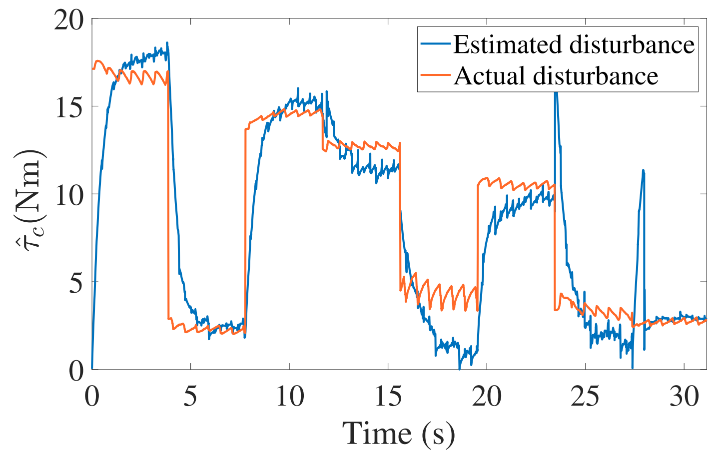

(b)

Figure 2.25. Case Study B2. Estimation of $\hat{f}_c$ (a) and $\hat{\tau}_c$ (b).

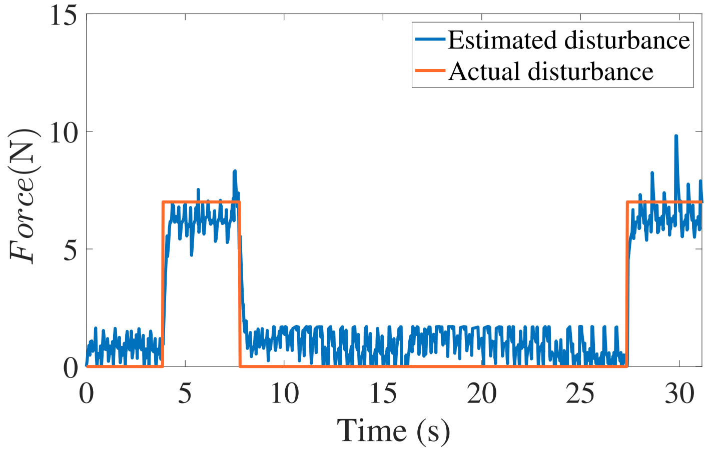

Figure 2.26. Case Study B2. Estimation of $\hat{f}_e$ for the rear right leg.

observed.

Case Study B3

The third case study considers the same random disturbances of the previous case study plus a parametric uncertainty of the total mass known by the controller, which is changed by 30%. Besides, the same blocks already employed in case B1 are used to simulate an irregular terrain. The capabilities of the controller are now tested in a complex situation where: (i) the robot is stressed by high external forces, simulating impact with objects or pushes; (ii) there is a rough terrain; and (iii) parametric uncertainties are present. The error norm's plot of the CoM is reported in Fig. 2.27. It can be observed that the peaks are now higher but always less than 0.025 m. However, this small error increment can be considered the result of the parametric uncertainty and the presence of irregular terrain, which can still be handled.

2.5.4 A possible application: A Guide Dog to Help Visually Impaired People

The presented observers can open the path to some new applications in which a legged quadruped could be involved. This last section aims

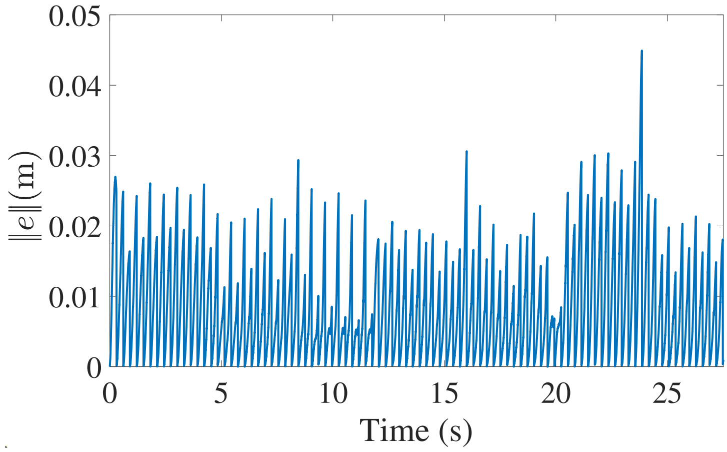

Figure 2.27. Case Study B3. Error norm of the robot's CoM using the proposed controller.

to demonstrate this possibility, modifying the previously presented framework to be employed in a care assistance case study. The focus of this section is on people suffering from a visual disease. To this end, different robotic systems were developed, usually employing wheeled robots. One of the first examples was presented in [84], where the robot has an internal map of the environment, can detect obstacles using onboard sensors, and communicates to the blind individual the clear path to follow. Another guiding device employing a wheeled robot is the GuideCane [11]. It is equipped with sonar sensors to detect obstacles, while the computer inside the cane reads the information and constructs a rudimentary map of the environment. Then, it computes a path to guide the cane around obstacles [14].

In the cases mentioned above, the connection between humans and robots always happens through a rigid link, limiting the human-robot interaction's flexibility and ability to operate in narrow spaces. For this reason, recent works started to explore the possibility of using a leash to connect the robot with the person [95, 88, 39, 99]. The leash can be considered a hybrid system, switching from a taut to a slack condition. The human-robot system's dimensions change whenever the leash becomes

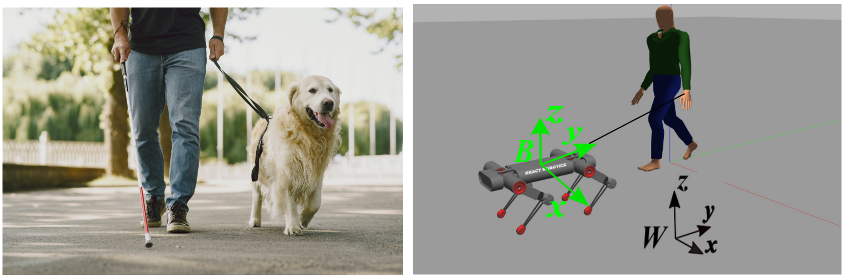

Figure 2.28. On the left, a guide dog helping a visually impaired person. On the right, a quadruped is connected to a human through a leash in the Gazebo simulation environment.

slack, allowing the robot to guide the human through narrow spaces [95]. A leash-guided interaction is used in [88], in which a physical connection tightly couples a human and an aerial robot. In this case, the human holds a handle which is in turn connected to an aerial vehicle through a cable.

The robots considered in the literature above have evident problems guiding visually impaired people. Wheeled robots have problems adapting to irregularities of the terrain. They are unfeasible in anthropic environments, usually designed for not disabled people with stairs, holes, and obstacles. The propellers' noise of aerial robots interferes instead with human hearing, which is a vital resource for visually impaired people. Indeed, it is often used to understand the dangers around them: for example, before crossing a road, the guide dog stops and waits for the human to give it the order to cross the street after having heard that there are no cars. A quadruped robot can quickly adapt to terrain irregularities and go up and down stairs, and it usually produces less noise than aerial vehicles [95].

In this section, the framework is adapted for using a tethered robot quadruped as a guide dog (Fig. 2.28), exploiting the previously presented hybrid observer to retrieve the information about the leash force. The observer for the legs is instead used to deal with terrain irregularities acting directly on the quadruped's legs. An admittance filter is also employed to guarantee a safe human-robot interaction. Besides, a supervisor is designed and placed side by side with the quadruped whole-body control to understand human needs and handle realistic situations. The resulting framework can be observed in Fig. 2.29.

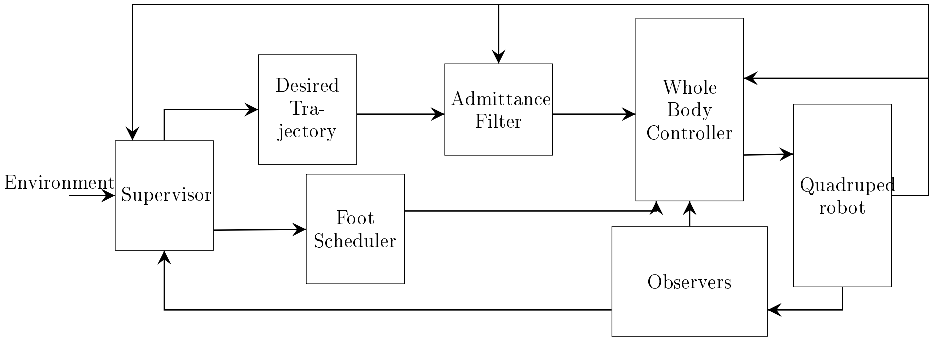

Figure 2.29. Conceptual block scheme of the devised framework.

Human-robot system

The relation between the human and the robot can be defined as a function of the two connection points of the leash: $p_h \in \mathbb{R}^3$ for the human's hand, and $x_r \in \mathbb{R}^3$ for the robot, considering it as a fixed point of the main body $p_h = x_r - l\bar{v}_l$, where $l > 0$ is the distance between the robot and the human, and $\bar{v}_l \in \mathbb{R}^3$ is the unit vector pointing from the human to the robot along the leash. It is important to consider the interaction between the human and the robot. As reported in [88], such kind of tasks can be performed considering the human's dynamics as a mass-spring-damper system. Let $m_h \in \mathbb{R}_{>0}$ be the human's mass; $C_h \in \mathbb{R}^{3\times3}_{>0}$ be the system's damping; $g_h = m_h g_0 \in \mathbb{R}^3$; $f_{h,ext} \in \mathbb{R}^3$ be the vector containing external forces acting on the human and $v_h \in \mathbb{R}^3$ be the human's linear velocity. The human's dynamics can be written as

$$m_h \dot{v}_h + C_h v_h + g_h = f_{h,ext} - f_{e,c}. \tag{2.47}$$

Given the assumption in Section 2.3 about the slowness of the main's body angular motion, it can be considered that most of the leash wrench is contained in the translational force, representing the most critical information about the human-robot interaction. For this reason, the leash can be modeled as a spring with stiffness $k > 0$ through the Hooke's law, so that the leash force is

$$||f_{e,c}|| = \begin{cases} k(l-\bar{l}) \quad if \quad (l-\bar{l}) > 0 \\ 0 \quad if \quad (l-\bar{l}) \leq 0 \end{cases} \tag{2.48}$$

where $\bar{l}$ represents the nominal length of the leash. Whenever the leash is taut, $(l - \bar{l}) > 0$, and a force is applied between the robot and the human, so that the human is guided by the robot.

Admittance filter

The idea of an admittance control scheme is to modify the reference position of the robot $x_{com,ref} \in \mathbb{R}^3$ based on the leash force. It should be observed that this control is performed only for the translational part, given the above assumption that the essential information about the human-robot interaction is given through the linear force.

The admittance controller guarantees a safe human-robot interaction so that the robot's motion adapts to the human one. In this way, the robot can accelerate or decelerate based on the cable's tension, avoiding overcoming human capabilities. To obtain the modified reference trajectory, $x_{com,mod} \in \mathbb{R}^3$, the desired admittance model can be considered as

$$M_a \ddot{\tilde{x}} + D_a \dot{\tilde{x}} + K_a \tilde{x} = f_d - \hat{f}_c, \tag{2.49}$$

where $\ddot{\tilde{r}} = x_{com,mod} - x_{com,ref}$, and M_a, D_a, and $K_a \in \mathbb{R}^{3\times3}$ are the desired inertia, damper, and stiffness matrices of the desired admittance model, respectively. In order to achieve a desired human-robot behaviour, $f_d \in \mathbb{R}^3$ is the desired leash force empirically chosen to maximize the velocity of the robot without pulling too much the human.

Supervisor

A supervisor is employed to decide how the robot should act based on the intention of the human or the environment. Such a supervisor is inspired by the training of guide dogs in reality. Whenever the dog meets an obstacle or a dangerous situation, it usually: (*i*) stops its motions; (*ii*) waits for the human to understand the situation; (*iii*) waits for an input to continue the path and, eventually, some information about the new trajectory to follow [28, 27]. Usually, visually impaired people are trained to understand the situation by using a cane or hearing. They are also trained to understand what is better to do afterwards, telling the dog the new command. In the following, the robot is supposed to be endowed

Algorithm 1 SUPERVISOR

if $||\hat{f}_c|| > \bar{\sigma}$ **and** $MOVE$ **then**
    $STOP$
else if $||\hat{f}_c|| > \bar{\sigma}$ **and** $STOP$ **then**
    $MOVE$ **and** *new direction*
else if env **and** $MOVE$ **then**
    $STOP$
else
    keep doing what is doing
end if

with sensors and algorithms allowing it to detect obstacles or dangerous situations: the implementation of these skills are out of the scope of this work.

The devised supervisor should not only start and stop the movement of the robot based on the leash tension, but it should also change the robot forward direction based on the estimated cable's force $\hat{f}_c$. The supervisor's behaviour can be resumed in Algorithm 1. It is based on the following states and commands: $MOVE$, the state indicating that the robot is moving; $STOP$, the state indicating that the robot is not moving; *new direction*, the new direction the dog must follow and that is computed based on the estimated force $\hat{f}_c = \begin{bmatrix} \hat{f}_{c,x} & \hat{f}_{c,y} & \hat{f}_{c,z} \end{bmatrix}^T$, meaning that the desired yaw angle for the robot is computed as $\varphi = Atan2(\hat{f}_{c,x}, \hat{f}_{c,y})$, where $Atan2$ is the arctangent function of two arguments [82]; $\bar{\sigma} > 0$, a threshold for the leash force indicating the pulling of the leash by the human; env, a Boolean variable indicating the detection of obstacles or dangerous situations.

Simulations

Simulations have been carried out through the ROS middleware and the physics-engine-based simulator Gazebo, as described in Section 2.5.1. Using a Gazebo plugin, the human is simulated by approximating the model to a mass-spring-damper system. Another plugin simulates the leash's force through the equation (2.48). In the following, it is experimentally

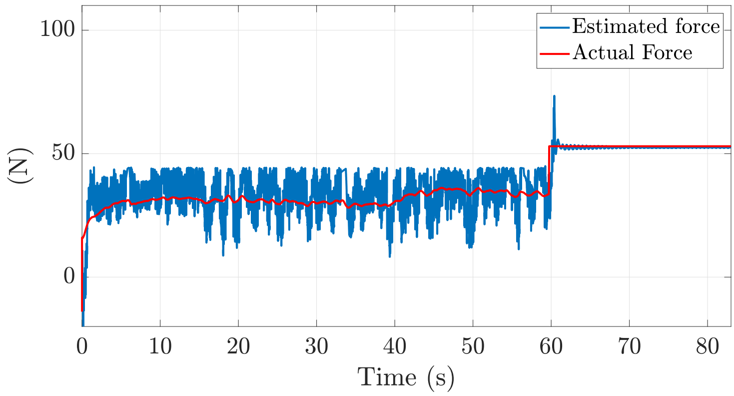

Figure 2.30. Case study C1. Estimated force (blue) and actual force (red).

chosen $\bar{\sigma} = 50$ N.

Case study C1

This case study tests the framework's capabilities on a rectilinear trajectory, characterized by a change in the velocity profile of the human and a sudden stop, testing the robot's capabilities to adapt its motion to the human. The robot is forced to follow a rectilinear trajectory along the y-axis of $\mathscr{W}$. The desired force f_d presented in the admittance filter in (2.49) has been empirically chosen in the forward direction y as $f_{d,y} = 30$ N. This force keeps the cable in tension, applying reasonable force on the human. As shown in Fig 2.30, the actual applied force remains bounded around this chosen value, overcoming the threshold at the instant $t = 62$ seconds when the human suddenly stops. It can also be observed that the reconstructed force has some oscillations and uncertainties, probably given by parametric uncertainties and the approximations made to obtain the decoupled model in (2.3). However, this estimation helps the robot retain balance and maintain a good gait also in the presence of the leash tension. In order to show the capability of the framework to adapt the robot's velocity to the human one, the same case on a rectilinear trajectory has been tested considering a human's velocity with a sinusoidal trend. The velocities for both the human and the robot can be appreciated in Fig. 2.33.

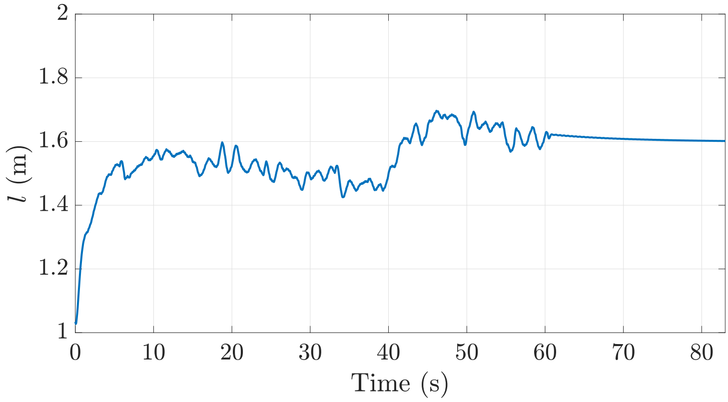

Figure 2.32. Case study C1. Distance l between the robot and the human.

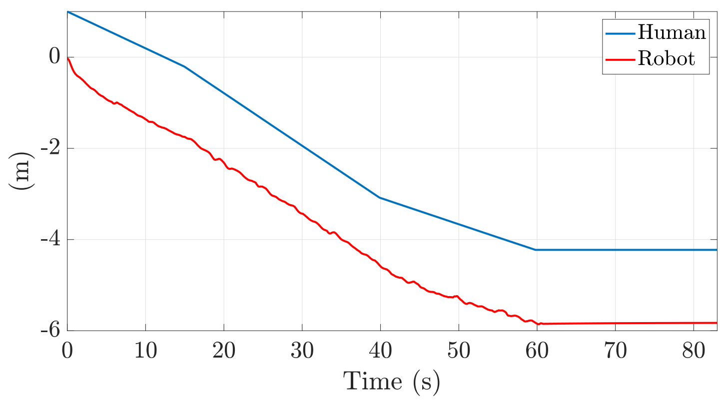

Figure 2.31. Case study C1. Human (blue) and robot (red) positions.

The human's velocity change can be appreciated in Fig. 2.31, observing the slope of his position. The distance l between the human and the robot can be observed in Fig. 2.32, as introduced in (2.48). Notice that it remains constant, validating the performance of the admittance controller that adapts the robot's velocity to the human, guaranteeing a safe motion.

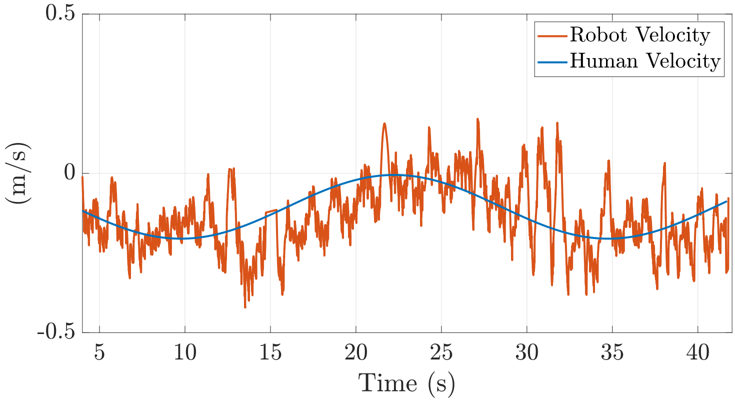

Figure 2.33. Case study C1. Human (blue) and robot (red) velocities in the sinusoidal trend.

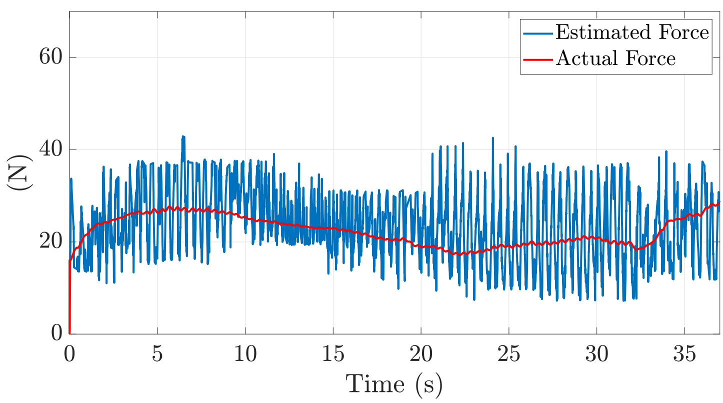

Figure 2.34. Case study C2. Estimated force (blu) and actual force (red).

Case study C2

This case study aims to demonstrate the framework capabilities along a curved trajectory. In order to guide the human, the robot can not immediately change its orientation while standing at the same point. Otherwise, the human will not understand where it is going, and the leash could also be slack without giving the human any information regarding the direction.

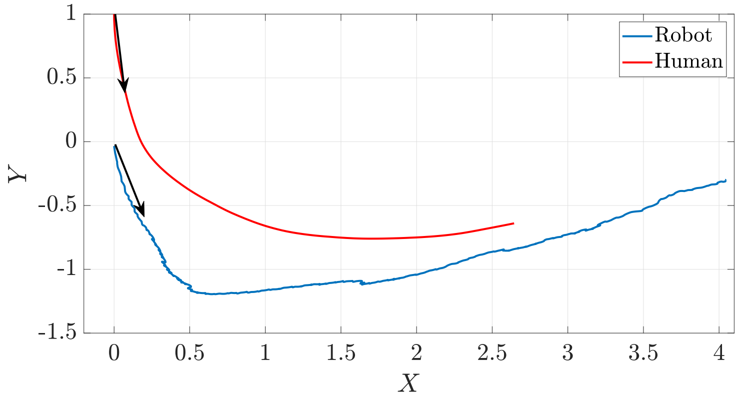

Figure 2.35. Case study C2. Human (red) and robot (blu) trajectories. The arrows indicate the starting points.

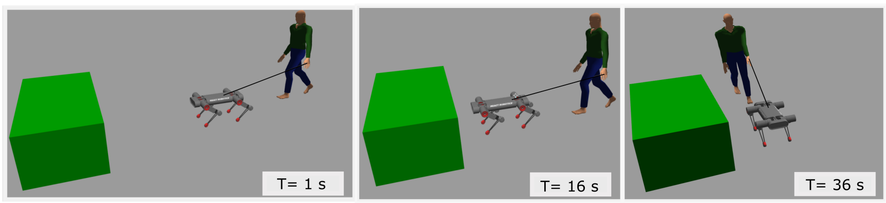

Figure 2.36. Case Study C3. Scenario and movements.

For this reason, the robot should perform a curved trajectory to change its direction, constantly imposing a force on the leash that, even if it changes the orientation, can guide the human through a similar curved trajectory. The resultant trajectories performed by both the human and the robot can be seen in Fig. 2.35, noticing that the human can finally smoothly change direction. Also in this case, the resultant leash force is bounded thanks to the admittance controller (see Fig. 2.34) with its estimation.

Case study C3

Suppose the dog meets an obstacle on the path ($env = 1$). In this case, it usually stops its walking, waits for the human to understand the situation or a signal to continue, and some information about the new trajectory to follow.

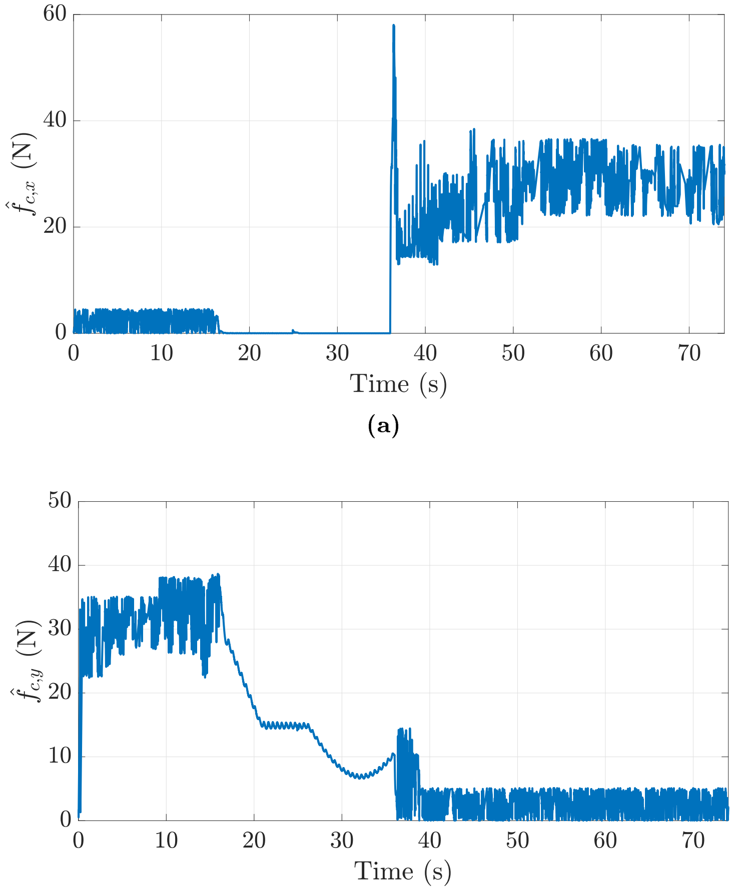

(a)

(b)

Figure 2.37. Case Study C3. Estimated force along the $x-$ (a) and the $y-$ (b) axes.

This case study aims to test the observer to understand when the robot should restart. However, it uses this estimation to retrieve the direction of the new trajectory decided by the human (i.e., the impressed leash force). In this case, a simple scenario with only one obstacle is considered (see Fig. 2.36). In Fig. 2.37, the estimations for both x-axis and y-axis can be observed. It can be noticed that for the first part of the path, most of the leash force is along the y-axis since this is the direction of the path. From instant $t = 16$ to $t = 36$ seconds, the estimated force is lower regarding the movement phase, so the leash can be considered almost slack, and the human understands that the dog has stopped. Afterwards, the human understands which is the best direction to follow, rotates to align with it, and gives the robot a pull along the x-axis to start moving in that direction. Indeed, at instant $t = 36$ seconds, the estimated force $\hat{f}_{c,x}$ along the x-axis is greater than 50 N, which is the threshold for the leash force. For the rest of the path, most of the leash force is along the x-axis because the robot is now moving in this direction.

Chapter 3

Disturbance Rejection in Optimal Control for Cable-Driven Parallel Robots

Experience is the hardest kind of teacher: it gives you the test first and the lesson afterward.

Oscar Wilde

This chapter deals with the part of this thesis related to cable-driven parallel robots. The state of the art of this kind of robots is firstly presented along with the difference between fully and under constrained CDPRs and an overview of the existing control strategies. Then, the main contribution presented in this chapter is highlighted. Afterwards, the dynamic model of a CDPR is presented, along with the problem of the MPC. Finally, the obtained results are presented, with a highlight of the improvement in disturbance rejection and the dampening of the oscillations caused by the flexibility of the cables.

3.1 State of the art

Cable-driven parallel robots are a particular type of parallel robot, usually employed whenever there is the need to work in a broad space or to have a high payload. Indeed, a CDPR is suspended by several flexible cables, that take the place of rigid links, and that is actuated by some winches positioned on the mobile base. These cables are usually connected to the mobile platform on one side and to some connection points that can be chosen either on a fixed or on a mobile structure.

The first CDPR has been built in 1989 in America, within the RoboCrane project [12, 13]. The realization of the RoboCrane design took inspiration from the Stewart platform parallel link manipulator, with the unicity of using for the first time cables as limbs and winches as the actuators. The RoboCrane was endowed with 6 flexible cables, with the main goal to perform land, air, water, and space applications depending on what is suspended from its work platform. With the employment of RoboCrane in a different task, especially construction one, the concept of CDPRs started to gain more and more attention and interest. Indeed, using a RoboCrane instead of a conventional gantry guarantees different advantages, such as minimal ground loading, large work volume, precise manipulator control with the possibility to change the tool on the mobile platform based on the need of the task, flexible gantry for mobility over uneven terrain.

In the last years, the research on CDPRs had great developments, highly motivated by the modern engineering demand for large load capacity and large workspace. However, although the use of cables allows for the enlargement of the workspace, it is still confined whenever the anchor points are considered fixed. For this reason, for tasks needing to have a wider workspace, there is the possibility to make mobile connection points. An example can be found in cooperative CDPR, consisting of multiple mobile cranes [102, 81]. For this kind of CDPR, the problem is not only related to the control of the mobile platform, which is mainly a dynamic problem, but it becomes a cooperation problem, including the localization of multiple mobile cranes, obstacle avoidance, and adaptive orientation control of the payload. Not only wheeled mobile robots can actuate the locomotion of the anchors, but also flying robots, such as drones as in [45, 61, 35]. This system can also be called aerial towed-cable-body systems and has been used in emergency response, and industrial, and military applications for object transport in inaccessible environments. While in the case of a mobile gantry structure, the attachment points are moving together with the whole structure, in the case of an aerial cable-driven system, the position of the pole coincide with the drone. So, the winches actuating the tension in the cables are not used in this case but are substituted by the drones.

Despite their great value on construction sites, CDPRs started to be used for most various tasks and activities. Indeed, wide applications of these robots can be found in the television field, with the use of a wire-suspended camera for videotaping and recording [20]. The first witness of a camera taping cable suspended can be found around 1990 when August Design Company developed a video tape recorder system named SkyCam. The robot is endowed with 4 cables and can reach up to 44.8 km/h at maximum speed, which is widely used for live broadcasts on large scale, especially for high-speed tracking photographs. These systems provide computer-controlled, stabilized, cable-suspended camera transporters. The systems are manoeuvred through three-dimensional space with a set of four computer-controlled winches. Both static and dynamic active stabilizations of camera carriers that ensure proper camera orientation are included in the real-time control system.

The performance of CDPRs and their dexterity highly depend on the number of cables with which it is endowed. Generally, considering that a cable-driven parallel robot is endowed with m cables and n DoFs, three types of CDPRs can be defined:

- Under-constrained: when $n + 1 > m$;
- Fully-constrained: when $n + 1 = m$;
- Redundantly-constrained: if $n + 1 < m$.

The number of cables determines not only the stability of the robot and its dexterity, but also its controllability. Indeed, in fully and redundantly constrained CDPRs, both position and orientation of the mobile platform can be controlled. Generally speaking, a CDPR moves around thanks to the wrench that is generated at the mobile base by pulling on it with the cables. For this reason, the workspace of a CDPR is defined as the set of poses of the moving platform for which a particular wrench is feasible. The set of poses of the platform for which tense cables can achieve static equilibrium is instead a particular subset of poses, called wrench feasible workspace (WFW). This workspace is determined by the geometry of the structure, the position of the anchor points and the limits of the cables' tension. Moreover, the WFW for fully constrained CDPRs depends also on the method used to compute the needed tensions in the cables. Indeed, for any desired wrench at the mobile base, there exists an infinite combination of tension forces that could exceed the limits of the maximum tension. Consequently, another subset of workspace, called wrench-closure workspace, can be identified. It corresponds to the set of poses of the platform for which any wrench can be generated at the platform by tightening the cables. For a fully-constrained robot, the WCW does not depend on the method used to generate the tensions in the cables, but it depends only on the geometry and on the positions of the connection points of the cables. It has been demonstrated that a WCW exists only if the number of cables is greater than the number of DoFs. Instead, for under-constrained CDPRs, the mobile platform usually approaches the position and orientation of minimum gravitational potential energy. Then, these robots determine the position and orientation of the platform relying on gravity. However, the state can be easily changed by any external disturbances. Under-constrained CDPRs are characterized by a coupling between the kinematics and the statics of the robot, but they are much simpler in structure with respect to fully and redundantly constrained robots. Compared with fully-constrained CDPRs, limited research has been conducted on under-constrained ones [18]. A major challenge in the kinematic study of under-constrained CDPRs comes from the fact that, when a desired cable length is reached, the floating base is still movable and the actual configuration is determined by the applied forces. For this reason, equilibrium equations must be solved, and displacement-analysis problems become geometric-static. As the floating base pose depends on the applied load, it may change due to external disturbances and equilibrium stability is essential. An equilibrium configuration is feasible only if cable tensions are positive and equilibrium is stable. Different control strategies have been presented over the years [98, 78, 16, 3], with the aim not only to move the robot but also to find an equilibrium configuration whenever a desired target is reached.

Usually, one of the main challenges to face for the control of CDPRs is related to the vibrations of the system caused by the flexibility of the cables [92, 91]. Different studies have been performed to obtain a deep knowledge of the natural oscillation frequencies of CDPRs. This knowledge can

be used to derive frequency-based trajectory planners based on periodic excitation [103] or input-shaping [68, 44], with the aim to limit oscillations.
A typical control strategy for CDPRs is the combination of feedback control with a feedforward computed torque. The computed torque allows to use of classical linear control approaches [50, 48]. Instead, a commonly nonlinear approach used for CDPR is the sliding mode control (SMC) that has been implemented successfully in CDPRs [2, 29]. The main advantages of this controller are the possibility to obtain a finite time convergence and robustness to uncertainties. However, recent and advanced SMC methods still present chattering issues in experimental setups [80].
A fully-constrained CDPR has more cables than DoFs and, for this reason, there are infinitely many possible combinations of cable tensions for the desired wrench. In order to choose the cable tensions, usually, a redundancy resolution algorithm is employed. Moreover, in computing the cable tensions, lower and upper limits should be taken into account. The lower limit is a positive tension to avoid cable slackness, while the upper one is imposed for mechanical limitations of cables and winches. In classical linear approaches [50, 48] or in the SMC approaches previously mentioned, the limits of the cable tensions are not considered within the problem. For this reason, the tension distribution problem is solved in a second moment. This could lead to having an unfeasible desired wrench. The use of an MPC as a control strategy is proposed in [78] because of the advantage of solving the tension distribution problem as an integral part of the control strategy. However, the proposed MPC strategy has been realized to be used only with fully and redundantly constrained CDPRs. For under-constrained CDPRs only either the position or the orientation is controllable, and the robot tends to reach an equilibrium that is the pose with a minimum gravity potential. Employing this concept, different strategies have been realized to solve the inverse geometric problem of under-constrained CDPRs, to obtain the orientation starting from the desired position and different trajectory planning for this kind of robots have been realized [101, 85, 60]. In this work of thesis, an MPC will be presented for CDPRs, it is combined with a strategy resolution of the inverse geometric problem to obtain the equilibrium configuration and the desired pose of the robot, in order to be employed with an under-constrained CDPR.

3.2 Main Contributions

In this chapter, an MPC is presented. It employs the kino-centroidal dynamics of the robot to realize a wrench-based controller. The MPC can be employed in combination with an algorithm of tension distribution that computes the equilibrium cables' tension for the desired position. Introducing a term for the equilibrium configuration allows the controller to obtain higher robustness against external disturbances and dampening oscillations caused by the flexibility of the cables. The validity of the MPC is demonstrated through some experiments with an under-constrained CDPR with four cables. It is also compared with a classical approach to demonstrate the improvement obtained in disturbance rejection.

3.3 Dynamic model of a cable-driven parallel robot

The dynamics of a cable-driven parallel robot can be modelled using the kino-centroidal dynamics[38].
The floating base can be usually modelled through six virtual joints that endow the robot with six DoFs with respect to a fixed world frame $\mathscr{W}$ (Fig.3.1).
Let consider $\mathscr{B}$ as the frame whose position and orientation are attached to the CoM of the robot.
Let consider $x_{com} = \begin{bmatrix} x_c & y_c & z_c \end{bmatrix}^T \in \mathbb{R}^3$, $\dot{x}_{com} \in \mathbb{R}^3$, and $\ddot{x}_{com} \in \mathbb{R}^3$ as the position, velocity, and acceleration of the frame $\mathscr{B}$'s origin with respect to $\mathscr{W}$, respectively.
Besides, let $\omega_{com} \in \mathbb{R}^3$ and $\dot{\omega}_{com} \in \mathbb{R}^3$ be the angular velocity and the angular acceleration of $\mathscr{B}$ with respect to $\mathscr{W}$, respectively.
The angular velocity can be computed from the rate of change of ZYX Euler angles, stacked in the vector $\Theta = \begin{bmatrix} \phi & \theta & \psi \end{bmatrix}^T$ [22], that can be extracted from the rotation matrix $R_b \in SO(3)$.
Finally, let consider the state vector as $q = \begin{bmatrix} x_{com}^T & \Theta^T \end{bmatrix}^T \in \mathbb{R}^6$ and the velocity vector as $\upsilon = \begin{bmatrix} \dot{x}_{com}^T & \omega_{com}^T \end{bmatrix}^T \in \mathbb{R}^6$. Let consider the centroidal momentum vector of the robot $h \in \mathbb{R}^6$, which is a composition of the robot linear and angular momentum expressed at the center of mass

$$h = A(q)\upsilon, \tag{3.1}$$

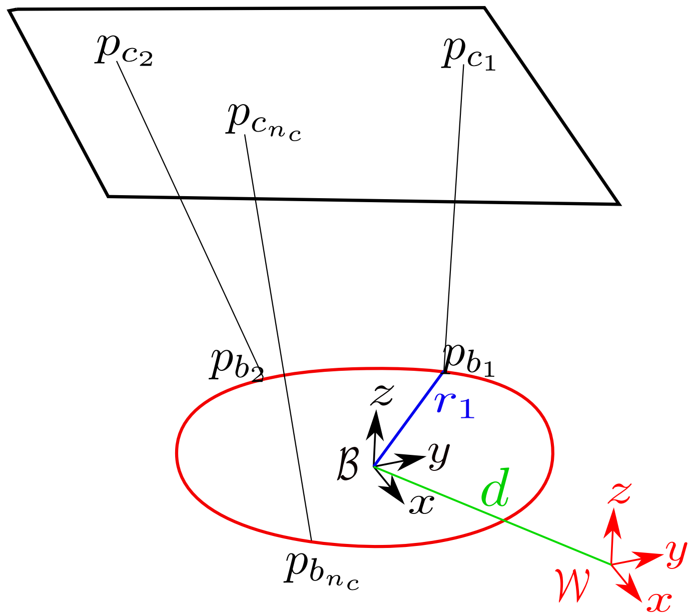

Figure 3.1. Scheme of a CDPR with n_c cables. In the figure, the main frame are shown: $\mathscr{B}$ is the frame attached to the floating base's CoM, $\mathscr{W}$ is the inertial fixed frame. The black parallelogram represents the environment on which the cables are attached. The red figure represents the moving platform of the robot.

where $A(q)$ is called the centroidal momentum matrix.
The centroidal momentum can also be expressed as

$$h = \begin{bmatrix} m\dot{x}_{com} \\ L \end{bmatrix} \tag{3.2}$$

with m the robot's total mass, and $L \in \mathbb{R}^3$ the angular momentum at the center of mass.
In order to model the action of the n_c cables on the structure, it can be considered that n_c three dimensional external forces f_{c_1}, $f_{c_2}, \dots f_{c_{n_c}}$ are applied on the floating base at n_c connection points p_{b_1}, $p_{b_2}, \dots$ $p_{b_{n_c}}$.
These forces are constrained to be in cables direction, and the only DoF for the $i-th$ cable is the applied force magnitude $\bar{f}_{c_i}$.

The cable direction can be described through the unit vector

$$\lambda_i = \frac{p_{c_i} - p_{b_i}}{\|p_{c_i} - p_{b_i}\|} \tag{3.3}$$

where $p_{c_i} \in \mathbb{R}^3$ is the $i-th$ connection point, while $p_{b_i} \in \mathbb{R}^3$ is the $i-th$ attachment point on the floating base (See Fig. 3.1). This last can also be written in function of the orientation of the robot as $p_{b_i} = R_b r_i + d$, where $r_i \in \mathbb{R}^3$ is the vector between the CoM of the moving base and p_{b_i}, depending only on the geometry of the robot. Instead, $d \in \mathbb{R}^3$ is the vector connecting the origins of the frames $\mathscr{B}$ and $\mathscr{W}$ (See Fig. 3.1). Then, the $i-th$ force vector can be computed as

$$f_{c_i} = \bar{f}_{c_i}\lambda_i. \tag{3.4}$$

The action of these forces create a net wrench on the center of mass, that allows to describe the centroidal dynamics of the robot as

$$x = \begin{bmatrix} \dot{x}_{com} \\ \bar{L} \\ x_{com} \\ \Theta \end{bmatrix} \in \mathbb{R}^{12} \tag{3.5}$$

with x the state vector, $\bar{L} = \dfrac{1}{m}L$ the normalized angular momentum at the CoM.

Moreover, the input u of the system can be defined as a vector composed of the tensions' magnitude

$$u = \begin{bmatrix} \bar{f}_{c_1} \\ \bar{f}_{c_2} \\ \dots \\ \bar{f}_{c_{n_c}} \end{bmatrix} \in \mathbb{R}^{n_c} \tag{3.6}$$

Then, considering $g \in \mathbb{R}^3$ as the vector containing the gravitational acceleration, the dynamic of the system can be written in the following form

$\dot{x} = f(x, u)$ as

$$\ddot{x}_{com} = \frac{1}{m}(f_{c_1} + f_{c_2} + ... + f_{c_{n_c}}) + g, \tag{3.7}$$

$$\dot{\bar{L}} = \frac{1}{m}(R_b r_1 \times f_{c_1} + R_b r_2 \times f_{c_2} + ... + R_b r_{n_c} \times f_{c_{n_c}}), \tag{3.8}$$

$$v = A^{-1}(q)h \tag{3.9}$$

3.4 Model Predictive Controller

The controller presented in this thesis is prediction-based, and it employs the kino-centroidal dynamics introduced in Section 3.3.
The optimal control used within the MPC has the following form

$$\begin{aligned}
\underset{u}{\text{minimize}} \quad & \phi(x(t)) + \int_0^t L(x(t), u(t), t)\, dt && (3.10)\\
\text{subject to} \quad & x(0) = x_0, && (3.11)\\
& \dot{x}(t) = f(x(t), u(t), t), && (3.12)\\
& h(x(t), u(t), t) \geq 0, && (3.13)
\end{aligned}$$

where t is the current time.
The cost function in (3.10) consists of an intermediate and a final cost, the (3.12) is the system flow map that imposes dynamic consistency, while (3.13) imposes some inequality constraints.
To set up the MPC, this optimal problem is solved repeatedly at each control instant with the latest state measurement.
In this work, the integration with a sequential linear quadratic model predictive control (SLQ-MPC) method is employed. This is based on differential dynamic programming and employs linearized dynamics and a quadratic approximation of the cost function around the latest trajectory.
In order to design the cost function employed within the MPC, let consider having a desired trajectory for the state vector of the floating base $x_{des}(t) = \begin{bmatrix}\dot{x}_{com,des}(t)^T & \bar{L}_{des}(t)^T & x_{com,des}(t)^T & \Theta_{des}(t)^T\end{bmatrix}$.
Moreover, consider as $u_{des}(t) = \begin{bmatrix}\bar{f}_{c_1,des} & \bar{f}_{c_2,des} & \dots & \bar{f}_{c_{n_c},des}\end{bmatrix}^T$ the vector of desired cable tensions. This vector could be computed using an optimal

algorithm of tension distribution in order to minimize the distance from an equilibrium configuration, given a desired pose.
Otherwise, if such an algorithm is either unavailable or requires too high computational power, it can be considered as a vector of zeros and minimizes the tensions.
The quadratic cost function of the MPC can be written as

$$J = \frac{1}{2}\int_0^T (x - x_{des})^T Q (x - x_{des}) + (u - u_{des})^T R (u - u_{des})\, dt + \\ + \frac{1}{2}(x - x_{des})^T Q_f (x - x_{des}), \tag{3.14}$$

where $Q \in \mathbb{R}^{12}$, $R \in \mathbb{R}^{n_c}$ and $Q_T \in \mathbb{R}^{12}$ are positive semi-definite state and input cost Hessian.
The second term of the function $\Phi(x(T)) = \frac{1}{2}(x - x_{des})^T Q_f (x - x_{des})$ is the final state cost, which is a heuristic to approximate the truncated infinite horizon, and it is implemented as a diagonal cost on the base pose and velocities.
Instead, the first term $L(x(t), u(t)) = \dfrac{1}{2}(x - x_{des})^T Q (x - x_{des}) + (u - u_{des})^T R (u - u_{des})$ is the intermediate cost, where a diagonal cost on all state variables and cables tension is used.
The input of the problem is composed of the cable forces. However, it should be noticed that the cables can not be subject to compression but only to tension. This means that the cables need to be always taut, otherwise it is not possible to create the adequate wrench at the CoM of the floating base.
The situation of a slack cable brings the robot to enter a configuration of singularity, since the needed tension can not be impressed on the slack cable, stacking the robot in the current pose.
For this reason, the tensions always need to be maintained positive, and the following constraint for the $i - th$ cable must be included in the function

$$\bar{f}_{c,i} \geq 0. \tag{3.15}$$

Moreover, for mechanical safety, also an upper-bound $\hat{f}_{c_i,max}$ should be imposed for the $i - th$ cable force, considering the maximum torque that the correspondent winch can apply

$$\bar{f}_{c,i} \leq \bar{f}_{c_i,max}. \tag{3.16}$$

Taking into account (3.15) and (3.16), and considering the vector of bounding forces $\bar{f}_{c,max} = \begin{bmatrix} \bar{f}_{c1,max} & \bar{f}_{c2,max} & \dots & \bar{f}_{c_{n_c},max} \end{bmatrix}^T$, the following constraint should be considered within the MPC

$$0 \leq u \leq \bar{f}_{c,max}. \tag{3.17}$$

This constraint is enforced by projecting the inputs onto the feasible set in the forward rollout of the SLQ-MPC algorithm.
It is important to mention that the resulting optimization problem is highly nonlinear and non-convex. Classical MPC guarantees on recursive feasibility and stability can thus not be provided. This is the reason why, as previously mentioned, the sequential linear quadratic (SLQ) algorithm is used.
This algorithm, in each iteration, alternates between two steps: the forward pass, where the system dynamics are forward integrated over the time horizon using the feedback policy of the previous step, and the backward pass where the local linear quadratic (LQ) approximation of the non-linear optimization problem is constructed, allowing to efficiently find a solution of the problem by solving the Ricatti's differential equation.
Moreover, it allows designing a continuous controller for a non-linear system with a linear computational complexity with respect to the optimization time horizon.
Using the SLQ method, the update for the controller has the form

$$u(t, x) = \bar{u} + \alpha(I(t)) + I_e(t)) + L(t)(x - \bar{x}), \tag{3.18}$$

with $\bar{u}$ and $\bar{x}$ the input and state nominal trajectories. $L(t)$, $I(t)$ and $I_e(t)$ are the LQR gains and the feedforward inputs for the cost reduction and the constraint correction, respectively. The parameter α is the learning rate for the feedforward inputs [33].

3.5 Experiments

In the following, some experiments are presented to validate the controller. The controller has been tested on a robot built at the Robotics System Lab, ETH Zurich. The robot has four cables, and the position of the connection points is known, while the position of the robot is retrieved from the measurement of an IMU sensor, using a Kalman filter as state estimator. The maximum force for the cable tension is $F_{max} = 800$ N.
The MPC runs with a frequency of $100Hz$, the state estimation has instead a frequency of $200Hz$.
The MPC has been realized using the *OCS2* toolbox[1]. In the following, some details about the robot will be provided.
The MPC is compared with a classical control based on the solution of an inverse geometric problem.

3.5.1 Floating robot

The floating robot used for these experiments has been built at the Robotics System Lab, ETH Zurich, from the spin-off, Floating Robotics[2] (Fig. 3.2).
This CDPR offers mobility and manipulation on large scales. It brings cable winches inside and offers easy deployment and compactness.
Cables can be taken out and installed on four poles, whose tips correspond to the connection point of the cable to the environment. The robot is for gardening applications in rough terrain, such as vineyards. The tasks of the robot are local spraying, cutting, and monitoring. Thus, the robot allows harvesting in optimal conditions. Then, the robot is endowed with four cables, so $n_c = 4$ and with four coupled onboard actuators. The coupling of the actuators is realized by a differential system mounted within a cylindrical structure. The differential system relies on a differential mechanism constructed with bevel gears. The actuators are connected to the differential mechanism by means of side contact between the actuator gearbox output and the bevel gear's circumferential area. Commanding a torque to these actuators, the tension in the cables is modulated and the cables can be wound and unwound inside the robot allowing to move it around.

[1] https://leggedrobotics.github.io/ocs2/
[2] https://floatingrobotics.com/

Figure 3.2. The floating robot, used for the experiments, during a locomotion task within a vineyard.

3.5.2 Inverse Geometric Problem of a Cable-Driven Parallel Robot with four cables

In order to show a comparison with a different control method, and to introduce a tension algorithm able to give the desired u_{des} to use in (3.14), the solution of the inverse geometric problem of the used robot will now be introduced [16].
The employed robot has $n_c = 4$ cables, so it is under-constrained.
Usually, for an under-constrained robot only either a desired position or a desired orientation of the robot can be commanded [16]. As previously said, the robot tends to approach the configuration of minimum gravitational potential energy. So, if a target position is commanded, it is possible to compute the orientation the robot will have in a static equilibrium configuration once it reached the desired position.
Let consider (3.7) and (3.8), the static equilibrium condition can be written as

$$\begin{bmatrix} 0 \\ 0 \\ mg \\ 0 \\ 0 \\ 0 \end{bmatrix} + W \begin{bmatrix} f_{c_1} \\ f_{c_2} \\ f_{c_3} \\ f_{c_4} \end{bmatrix} = 0, \tag{3.19}$$

where the matrix $W \in \mathbb{R}^{6\times 12}$ is a wrench matrix mapping the cables tension into the wrench of the CoM.
Rearranging and decomposing into force and torque equations yield to the following for the forces equation

$$\begin{bmatrix} 0 \\ 0 \\ mg \end{bmatrix} = H \begin{bmatrix} \hat{f}_{c_1} \\ \hat{f}_{c_2} \\ \hat{f}_{c_3} \\ \hat{f}_{c_4} \end{bmatrix}, \tag{3.20}$$

where $H = \begin{bmatrix} p_{c_1} - p_{b_1} & p_{c_2} - p_{b_2} & p_{c_3} - p_{b_3} & p_{c_4} - p_{b_4} \end{bmatrix} \in \mathbb{R}^{3\times 4}$, and $\hat{f}_{c_i} = \dfrac{\bar{f}_{c_i}}{\|p_{c_i} - p_{b_i}\|}$.
Instead, the torques equation is

$$\begin{bmatrix} 0 \\ 0 \\ 0 \end{bmatrix} = \begin{bmatrix} M_1 & M_2 & M_3 & M_4 \end{bmatrix} \begin{bmatrix} \hat{f}_{c_1} \\ \hat{f}_{c_2} \\ \hat{f}_{c_3} \\ \hat{f}_{c_4} \end{bmatrix}, \tag{3.21}$$

where $M_i = R_b r_i \times (p_{c_i} - p_{b_i}) \in \mathbb{R}^3$. Substituting (3.20) in (3.21) the following equation is obtained

$$\begin{bmatrix} 0 \\ 0 \\ 0 \end{bmatrix} = \begin{bmatrix} M_1 & M_2 & M_3 & M_4 \end{bmatrix} H^{-1} \begin{bmatrix} 0 \\ 0 \\ mg \end{bmatrix}. \tag{3.22}$$

In order to solve the inverse geometric problem, (3.22) must be solved for the orientation Θ.
It should be noticed that H is not invertible either if the cables are parallel to each other or if they are coplanar, so this situation is avoided [16].
Once the orientation is known, the equation relative to the static equilibrium (3.19) has only the cable tensions as unknown variables. These tensions can be computed through an optimization problem, as in the fol-

lowing [78]

$$\underset{u}{\text{minimize}} \quad \|u\|_2, \tag{3.23}$$

$$\text{subject to} \quad Au = b, \tag{3.24}$$

where u is the vector of cable tensions and (3.24) coincides with the static equilibrium condition (3.19). Moreover, once obtained the orientation of the robot Θ, the lengths of the $i-th$ cable can be retrieved as $l_i = p_{c_i} - (R_b r_i + d)$.
Usually, the solution of the inverse geometric problem can be employed within a control algorithm in combination with the solution of the problem in (3.23) [60]. Indeed, considering $x_{com,des} \in \mathbb{R}^3$ as a desired position, the desired orientation of the robot in a static equilibrium can be retrieved from the inverse problem. This orientation can be employed to realize a standard control approach. For example, once the orientation is obtained, the desired cable length $l_{i,des}$ of each cable can be computed. Considering $\bar{f}^*_{c_i}$ as the result of (3.23) for the $i-th$ cable, a simple control law for the force of each cable can be the following PD

$$\bar{f}_{c_i} = K_p e_{l,i} - K_d v_{l,i} + \bar{f}^*_{c_i}, \tag{3.25}$$

where $e_{l,i} = l_{i,des} - l_i$ is the error of cable length, while $v_{l,i}$ is the current velocity of the cable, coinciding with the velocity of the winch actuating the cable, and $\bar{f}^*_{c_i}$ can be considered as a gravity compensation.

Recalling the vector of desired cable tensions u_{des} introduced in (3.14), a choice of this vector can be computed as the tensions of the static equilibrium, meaning the solution of 3.23. Indeed, the result of this problem coincides with the desired cables tension u_{des} for a configuration of equilibrium once the desired target is reached. This equilibrium input could be injected into the MPC as desired tension.

3.5.3 Experiments results

To demonstrate the validity of the proposed approach, some results are going to be presented.
In order to understand the capability of the model predictive controller for such a robot to improve the performance of the CDPRs, it should

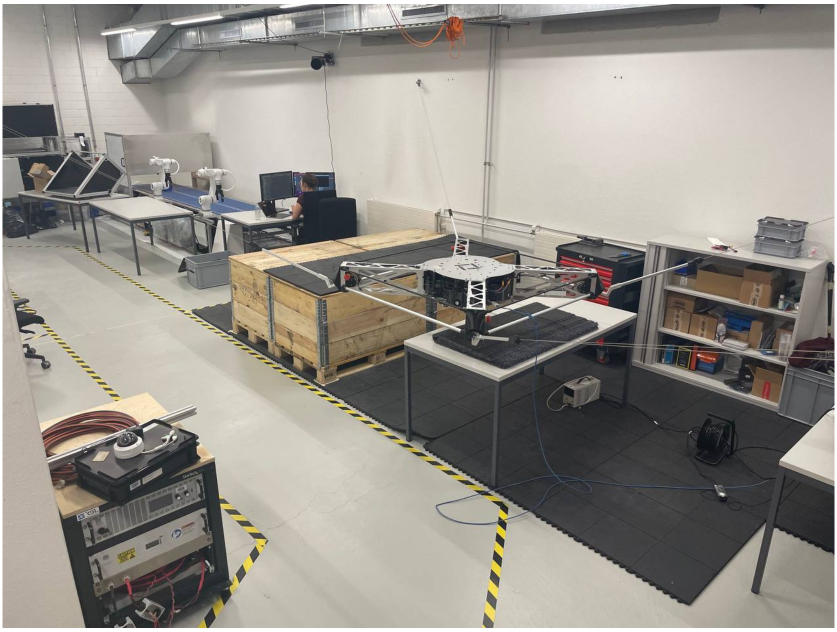

Figure 3.3. The setup of the experiments, the four cables are attached to the wall with four hooks, that are positioned in order to create a parallelogram whose dimension is 7×9 m.

be highlighted that two main problems characterize other state-of-the-art control strategies [78]:

- Oscillations caused by the cables are not damped during the movement;

- Tension in the cables is not constrained to remain within the boundaries so that the cable could be near to become slack or impose too much power on the motor.

The robot has been tested within an empty environment, with no obstacles (Fig. 3.3), and the position of all the connection points is known.

Damping cables oscillations

A fixed circular trajectory has been performed through three different control approaches:

- **MPC with equilibrium input**: the vector u_{des} obtained through (3.23) is employed as desired tension;

- **MPC without desired input**: The vector u_{des} consists entirely of zeros, thereby ensuring that cable tensions are always minimized while remaining positive, in compliance with the unilaterality constraint (3.17);

- **PD**: the PD presented in (3.25) is employed.

Analysing the cable tension of the different approaches gives a measure of the smoothness obtained through the control, and of the mechanical safety of the actuator, given by the capability of the approach to maintain the forces within the mechanical limits. Since the behaviour of the different cables revealed to be similar, in Fig. 3.4 only the tension of one cable is shown for all the approaches. As it can be noticed the forces are always contained within the bounds in every case. However, the two results obtained through the MPC show the capability to obtain a force that is more contained within the bounds. It can also be noticed that whenever an equilibrium input is given to the MPC, the cable tension appears to be smoother than in case this value is not provided.
About this aspect, another value can be taken into account to understand the safety guaranteed by the robot during the task.
This measure regards the derivative of the magnitude of the cable tension $\dot{f}_{c,i}$. Indeed, this value can be taken as a measure of the aggressiveness of the control method.
In Fig. 3.5, the derivatives of the tension of one cable (the same as Fig. 3.4) are shown.
It can be noticed that the control that guarantees smoother and less aggressive behaviour is the MPC with the equilibrium input.
This is given by the fact that within the MPC not only the constraint that guarantees the tautness of the cable is taken into account but also a reference for the tension itself is provided.

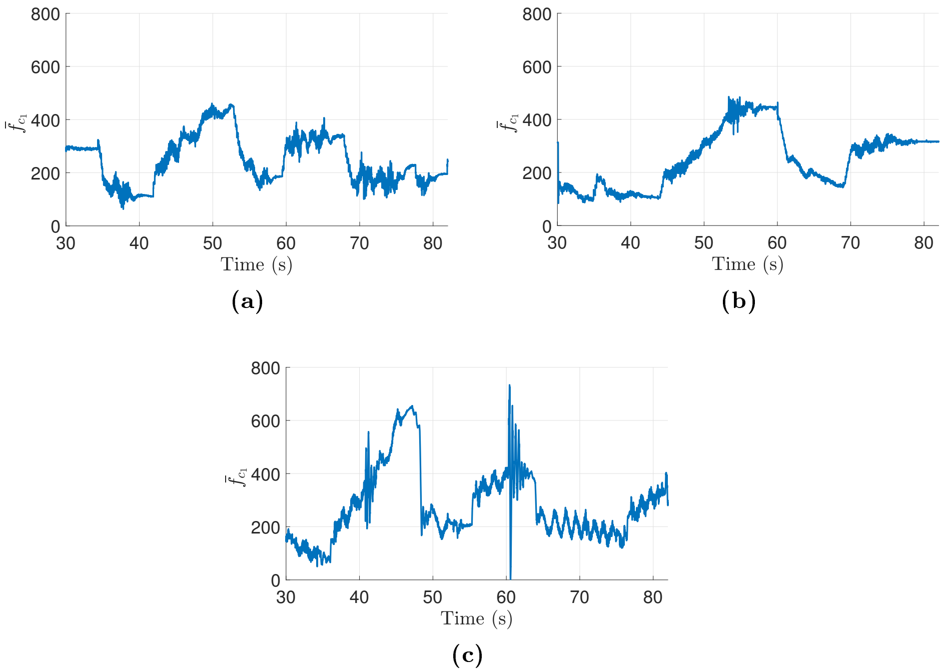

Figure 3.4. Force of cable 1 during the task: (a) MPC with no desired input (b) MPC with equilibrium input (c) PD.

Differently, the other two approaches are more aggressive. Indeed, using the PD a high push of the cable can be obtained when the robot is not able to track precisely the reference and the error of the cable length becomes major.

Using the MPC without equilibrium input, the controller always tries to minimize cable tensions. For this reason, after giving a hard pull to the cable to reach the desired target, the controller usually tries to bring the torque of the motor again towards zero, making this force highly discontinuous with respect to the case of MPC with equilibrium input. Having cable tension within the limits guarantees the safety of the hardware, while a less aggressive control can guarantee the safety of both the hardware and the environment in which the robot is working. Nevertheless, using an MPC guarantees to take into account the latest behaviour of the robot, comput-

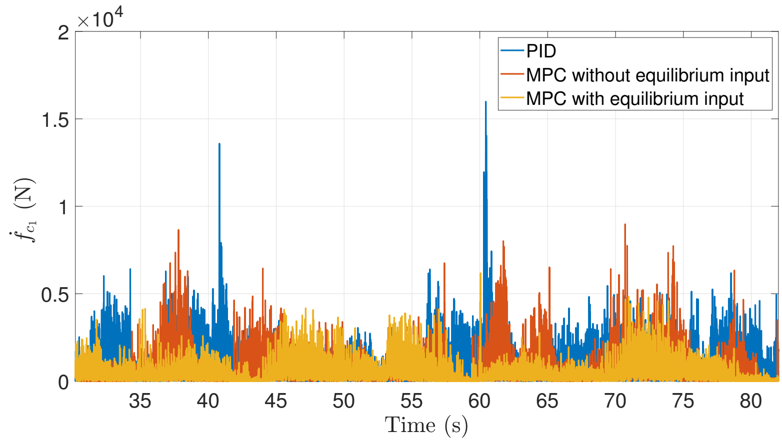

Figure 3.5. Force derivative for cable 1.

ing the new control action on the base of the history of the state of the robot. For this reason, it can be supposed that MPC can be able to damp the oscillations that are usually caused by the flexibility of the cables. To validate this aspect, the angles of roll, pitch and yaw of the robot during the task are presented in Fig. 3.6.
Observing the orientation during the movement, it can be noticed that the PD approach, the only one not taking into account the history of the movement, is not able to reject these oscillations, which are constantly happening during the whole task.
Comparing the two MPC approaches, the one employing the equilibrium input handles the oscillations in the best way, as can be observed in Fig. 3.6b. In the plot, the oscillations are rarely happening, and they are immediately rejected.
The difference between the two MPC approaches in handling vibrations can be related to the aggressiveness of the control. As previously seen, the MPC without equilibrium input is more aggressive, and the discontinuities in the command forces reduce the capability of the approach to dampen the vibrations given by the cables' flexibility. A second criterion to evaluate the smoothness of the trajectory is to consider the acceleration of the robot. The norm of the linear acceleration of the CoM $\|\ddot{x}_{com}\|$ can be observed in Fig. 3.7. In this case, the two MPC are comparable, while

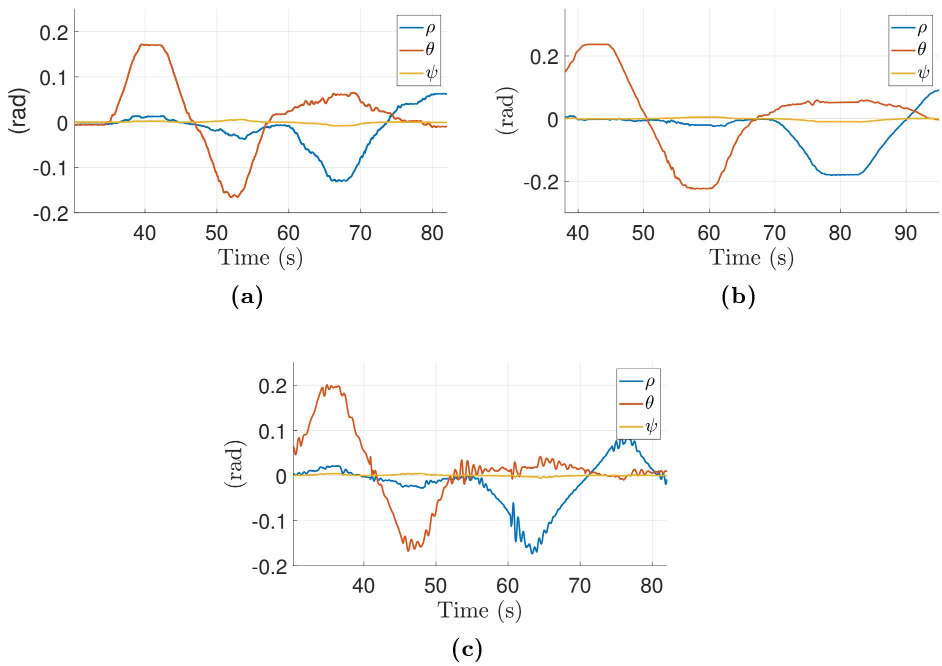

Figure 3.6. Euler angles during the task: (a) MPC with no desired input (b) MPC with equilibrium input (c) PD.

the optimal solution does not guarantee a smooth trajectory.

Rejection of external disturbance

This experiment aims to demonstrate the capability of external disturbance rejection of the MPC.
Given the results of the previous section, which demonstrated the better performance obtained using the MPC with equilibrium input, only this approach will be compared to the PD approach in this section.
For this experiment, a mass of 5 kg has been attached to the robot and suddenly released to obtain a perturbation.

In Fig. 3.8, the perturbation of the components x_c and y_c is presented. It can be observed that using the MPC the perturbation is damped in a

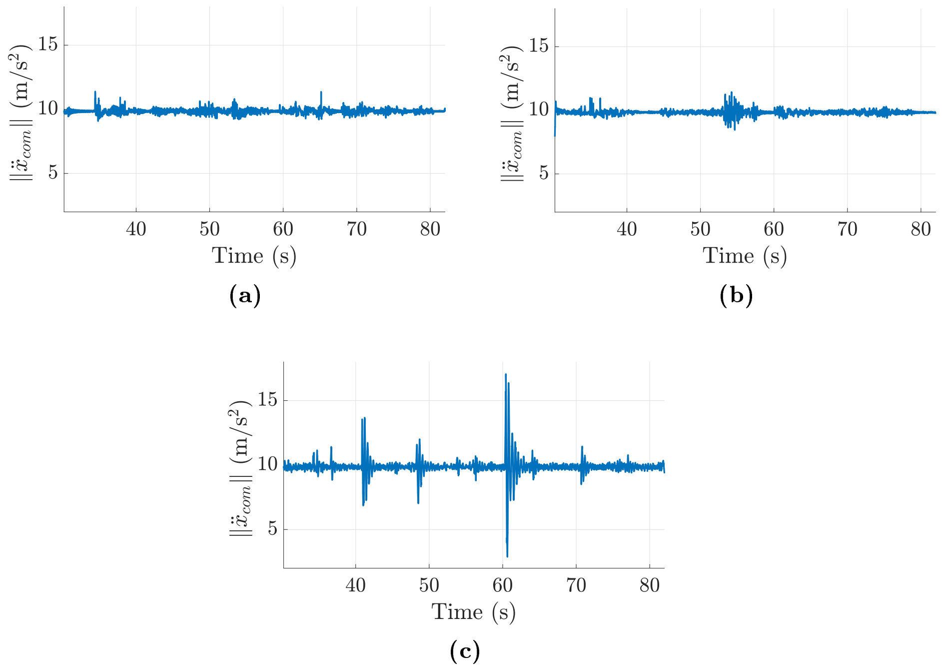

Figure 3.7. Linear acceleration during the task: (a) MPC with no desired input (b) MPC with equilibrium input (c) PD.

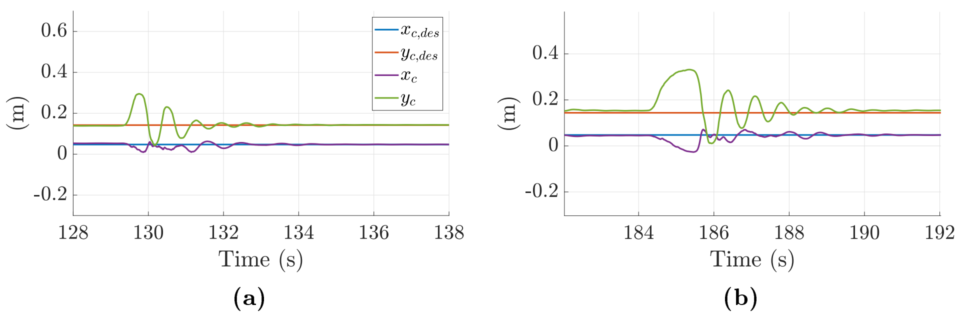

Figure 3.8. x and y component during the task: (a) MPC with equilibrium input (b) PD.

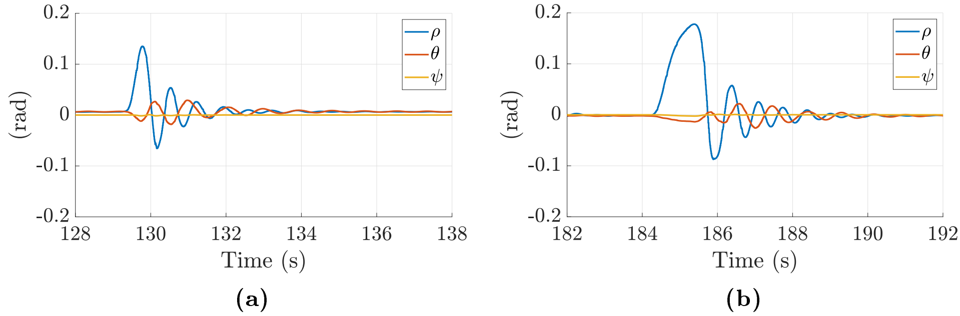

Figure 3.9. Euler angles during the task: (a) MPC with equilibrium input (b) PD.

smaller time. Let consider t_d the dampening time, that is the time in which the oscillations' amplitude becomes smaller than a certain threshold, here chosen as 0.02. the experiments showed that using MPC it is $t_d \simeq 4$ s, while the PD approach gives $t_d \simeq 7$ s. Moreover, it can be noticed that MPC is able to give an immediate response to the disturbance. Differently from the PD approach, the amplitude of oscillations obtained with MPC is always smaller, demonstrating its ability to improve the response to the disturbance.

Recalling the results of the previous case study, it can be understood that the vibrations caused by the flexibility of cables, which PD is not able to handle, increase the oscillations caused by external disturbances, making the damping slower when this approach is employed.

For completeness, in Fig. 3.9 the angles of roll, pitch and yaw are shown, to observe also the damping capabilities related to the orientation for both approaches. Here, the same observation made for the linear components of the CoM can be made, both regarding the damping time and the oscillations' amplitude.

Chapter 4

Conclusions and Future Study

An overview of the results presented in this thesis is reported in this chapter. Afterwards, some possible future developments are presented.

4.1 Main Results

The problem of robustness control for limbed parallel robots is faced within this thesis. Two kinds of robots are the object of interest in this work

- *Quadruped Robots*;
- *Cable-Driven Parallel Robots.*

As it has been demonstrated, quadruped robots are often subject to external disturbances caused by either the irregularities of the terrain or the presence of obstacles within the environment. In literature, disturbances acting directly on the swinging legs are usually neglected. However, these disturbances could make the robot lose its balance and fall in some situations.
For this reason, a disturbance-observer-based whole-body controller has been presented in this work. Two observers are integrated within the controller to take into account both the disturbances acting on the CoM and the ones affecting the movement of the legs.
The observer acting on the CoM is composed of an acceleration-based observer for the translational part and a momentum-based observer for the

angular one. Given its combination of two observers, it is here identified as *hybrid*. The observer acting on the legs' dynamics is momentum-based. The observation coming from these observers is compensated within the whole-body controller to reject disturbances and parametric uncertainties. The presented observers have been tested against other state-of-the-art observers, demonstrating satisfactory performance in reacting to time-varying external forces. Indeed, they appear to reduce the error to the planned robot's CoM and improve the stability, even when the swing leg or the CoM are affected by large and impulsive external unpredicted forces. The proposed approach was also tested with random forces, demonstrating its robustness against an unexpected variation of the application point and parametric uncertainties. The controller resulted in being robust against noisy measurement and irregular terrain.

The observer acting on the legs dynamics demonstrated to allow the locomotion of a legged robot inside an unstructured environment where a collision could happen. Indeed, if a swing leg impacts an object, it can have a wide foot drift. It causes a reduction of the support polygon, unbalancing the robot. The presented controller compensated directly for those disturbances acting on the moving legs, minimizing the drift. Beyond obstacles, the controller guarantees good performance when irregularities in the terrain cause disturbance.

The hybrid observer, instead, demonstrated to allow the locomotion of a legged robot in case an unknown force is acting on the robot's torso. This capability revealed to be useful in a care assistance application, where the observer allows to identify the force that a visually impaired person is impressing on the robot through a leash connecting it to the human. Through the estimation of this force, a supervisor can modify the behaviour of the robot on the basis of the intention of the human.

Instead, cable-driven parallel robots are characterized by the presence of cables instead of rigid links. These cables introduce in the dynamic of the robot a flexibility that causes several vibrations and oscillations. Usually, the desired wrench is computed and commanded for the robot's movement. However, during the computation of this wrench, some limits for the cable tensions play a crucial role, since the cables must not become slack and have tension limits. Nevertheless, the proposed control strategies are often not able to handle these constraints within the motion controller,

and they use a cable tension distribution algorithm, which acts only after the desired wrench is computed. Thus, if the computed desired wrench is unfeasible, the controller can not realize the movement. To overcome this problem, an MPC has been presented in this work. The MPC considers the constraints related to the cable tension to obtain a feasible solution. However, to adapt the MPC to be used with an under-constrained robot, the MPC is combined with a tension algorithm that computes the tension for an equilibrium configuration after solving the inverse geometric problem of the cable-driven parallel robot. The equilibrium configuration is used within the MPC as desired tensions.
The results of this MPC have been compared to the ones obtained through a classical PD approach, demonstrating the capability of the presented method to improve the rejection of both oscillations given by the flexibility of cables and external disturbance. Moreover, the MPC has also been tested without using the tension of the equilibrium configuration, obtaining rejection of disturbances and a more aggressive control.

4.2 Future Developments

The combination of the observers acting on the CoM and the legs opens some possible developments in legged robotics. Indeed, the employed decoupled model and the use of two different observers could be employed for a legged manipulator to widen the tasks that this kind of robot can perform. An idea could be to consider the arm as an external disturbance to control the robot's locomotion separately from the manipulation tasks. Combining the two observers allows for rejecting a broader range of external disturbances and unmodelled dynamics. Thus, if the arm is considered an external disturbance, and its dynamics is unknown to the controller of the legged robot, its movement during a manipulation task will be compensated through the observers.

Also in the case of the cable-driven parallel robots, the possibility to endow them with a manipulator should be considered. Indeed, in order to work in an industrial or agricultural field, an arm could be mounted on the robot. Since manipulation tasks usually require high precision, the flexibility of cables and their oscillations could affect the performance of these tasks. With the dampening of oscillations and the rejection of external disturbances obtained through the MPC, the manipulation task can be performed without being affected by the low stiffness of the system. Moreover, the movement of the arm, and the manipulation task, could be introduced within the MPC, obtaining a unified framework.

Bibliography

[1] Farhad Aghili. A unified approach for inverse and direct dynamics of constrained multibody systems based on linear projection operator: Applications to control and simulation. *IEEE Transactions on Robotics*, 21(5):834–849, 2005.

[2] Alireza Alikhani and Mehdi Vali. Sliding mode control of a cable-driven robot via double-integrator sliding surface. In *2012 International Conference on Control, Robotics, and Cybernetics*, 2012.

[3] Jeremy Begey, Loic Cuvillon, Maximilien Lesellier, Marc Gouttefarde, and Jacques Gangloff. Dynamic control of parallel robots driven by flexible cables and actuated by position-controlled winches. *IEEE Transactions on Robotics*, 35(1):286–293, 2018.

[4] C Dario Bellicoso, Christian Gehring, Jemin Hwangbo, Péter Fankhauser, and Marco Hutter. Perception-less terrain adaptation through whole body control and hierarchical optimization. In *2016 IEEE-RAS 16th International Conference on Humanoid Robots*, pages 558–564, 2016.

[5] C Dario Bellicoso, Fabian Jenelten, Péter Fankhauser, Christian Gehring, Jemin Hwangbo, and Marco Hutter. Dynamic locomotion and whole-body control for quadrupedal robots. In *2017 IEEE/RSJ International Conference on Intelligent Robots and Systems*, pages 3359–3365, 2017.

[6] C Dario Bellicoso, Fabian Jenelten, Christian Gehring, and Marco Hutter. Dynamic locomotion through online nonlinear motion optimization for quadrupedal robots. *IEEE Robotics and Automation Letters*, 3(3):2261–2268, 2018.

[7] Lénaïck Besnard, Yuri B Shtessel, and Brian Landrum. Quadrotor vehicle control via sliding mode controller driven by sliding mode disturbance observer. *Journal of the Franklin Institute*, 349(2):658–684, 2012.

[8] Gerardo Bledt, Patrick M Wensing, Sam Ingersoll, and Sangbae Kim. Contact model fusion for event-based locomotion in unstructured terrains. In *2018 IEEE International Conference on Robotics and Automation*, pages 4399–4406, 2018.

[9] Gerardo Bledt, Patrick M Wensing, and Sangbae Kim. Policy-regularized model predictive control to stabilize diverse quadrupedal gaits for the MIT Cheetah. In *2017 IEEE/RSJ International Conference on Intelligent Robots and Systems*, pages 4102–4109, 2017.

[10] Q. Bombled and O. Verlinden. Indirect foot force measurement for obstacle detection in legged locomotion. *Mechanism and Machine Theory*, 57:40–50, 2012.

[11] Johann Borenstein and Iwan Ulrich. The guidecane-a computerized travel aid for the active guidance of blind pedestrians. In *Proceedings of International Conference on Robotics and Automation*, volume 2, pages 1283–1288. IEEE, 1997.

[12] Roger BostelMan, James Albus, Nicholas Dagalakis, ADAM Jacoff, et al. Robocrane [r] project: An advanced concept for large scale manufacturing. In *AUVSI-PROCEEDINGS-*, pages 509–522, 1996.

[13] Roger Bostelman, James Albus, Nicholas Dagalakis, Adam Jacoff, John Gross, et al. Applications of the nist robocrane. In *Proceedings of the 5th International Symposium on Robotics and Manufacturing*, volume 5, page 1, 1994.

[14] Mounir Bousbia-Salah and Mohamed Fezari. A navigation tool for blind people. In *Innovations and advanced techniques in computer and information sciences and engineering*, pages 333–337. Springer, 2007.

[15] Guy Campion and Woojin Chung. Wheeled robots. In *Springer handbook of robotics*, pages 391–410. Springer, 2008.

[16] A Capua, A Shapiro, and S Shoval. Spiderbot: a cable-suspended walking robot. *Mechanism and Machine Theory*, 82:56–70, 2014.

[17] Diego S Carrasco and Graham C Goodwin. Feedforward model predictive control. *Annual Reviews in Control*, 35(2):199–206, 2011.

[18] Marco Carricato and Jean-Pierre Merlet. Stability analysis of underconstrained cable-driven parallel robots. *IEEE Transactions on Robotics*, 29(1):288–296, 2012.

[19] Wen-Hua Chen, Jun Yang, Lei Guo, and Shihua Li. Disturbance-observer-based control and related methods—an overview. *IEEE Transactions on industrial electronics*, 63(2):1083–1095, 2015.

[20] Chris Chesher. Robots and the moving camera in cinema, television and digital media. In *Cultural Robotics: First International Workshop, CR 2015, Held as Part of IEEE RO-MAN 2015, Kobe, Japan, August 31, 2015. Revised Selected Papers 1*, pages 98–106. Springer, 2016.

[21] Z. Cong, A. Honglei, C. Wu, L. Lang, Q. Wei, and M. Hongxu. Contact force estimation method of legged-robot and its application in impedance control. *IEEE Access*, 8:161175–161187, 2020.

[22] Jared Di Carlo, Patrick M Wensing, Benjamin Katz, Gerardo Bledt, and Sangbae Kim. Dynamic locomotion in the mit cheetah 3 through convex model-predictive control. In *2018 IEEE/RSJ International Conference on Intelligent Robots and Systems*, pages 1–9, 2018.

[23] Navid Dini and Vahid Johari Majd. Sliding-mode tracking control of a walking quadruped robot with a push recovery algorithm using a nonlinear disturbance observer as a virtual force sensor. *Iranian Journal of Science and Technology, Transactions of Electrical Engineering*, pages 1–25, 2019.

[24] Navid Dini and Vahid Johari Majd. An MPC-based two-dimensional push recovery of a quadruped robot in trotting gait using its reduced virtual model. *Mechanism and Machine Theory*, 146, 2020.

[25] Navid Dini, Vahid Johari Majd, Farid Edrisi, and Mehran Attar. Estimation of external forces acting on the legs of a quadruped robot using two nonlinear disturbance observers. In *2016 4th International Conference on Robotics and Mechatronics*, pages 72–77, 2016.

[26] Wenqian Du, Mohamed Fnadi, and Faiz Benamar. Rolling based locomotion on rough terrain for a wheeled quadruped using centroidal dynamics. *Mechanism and Machine Theory*, 153, 2020.

[27] Brian Due and Simon Lange. Semiotic resources for navigation: A video ethnographic study of blind people's uses of the white cane and a guide dog for navigating in urban areas. *Semiotica*, 2018(222):287–312, 2018.

[28] Rhiannon Tudor Edwards. "forward!" the experience of a new guide dog owner. *Bmj*, 325(7356):171, 2002.

[29] Gamal El-Ghazaly, Marc Gouttefarde, and Vincent Creuze. Adaptive terminal sliding mode control of a redundantly-actuated cable-driven parallel manipulator: Cogiro. In *Cable-Driven Parallel Robots: Proceedings of the Second International Conference on Cable-Driven Parallel Robots*, pages 179–200. Springer, 2015.

[30] Johannes Englsberger, George Mesesan, and Christian Ott. Smooth trajectory generation and push-recovery based on divergent component of motion. In *2017 IEEE/RSJ International Conference on Intelligent Robots and Systems*, pages 4560–4567, 2017.

[31] Shamel Fahmi, Carlos Mastalli, Michele Focchi, and Claudio Semini. Passive whole-body control for quadruped robots: Experimental validation over challenging terrain. *IEEE Robotics and Automation Letters*, 4(3):2553–2560, 2019.

[32] Raouf Fareh, Sofiane Khadraoui, Mahmoud Y Abdallah, Mohammed Baziyad, and Maamar Bettayeb. Active disturbance rejection control for robotic systems: A review. *Mechatronics*, 80:102671, 2021.

[33] Farbod Farshidian, Michael Neunert, Alexander W Winkler, Gonzalo Rey, and Jonas Buchli. An efficient optimal planning and control framework for quadrupedal locomotion. In *2017 IEEE International Conference on Robotics and Automation (ICRA)*, pages 93–100. IEEE, 2017.

[34] Eric Feron and Eric N Johnson. Aerial robotics. In *Springer handbook of robotics*. Springer, 2008.

[35] Jonathan Fink, Nathan Michael, Soonkyum Kim, and Vijay Kumar. Planning and control for cooperative manipulation and transportation with aerial robots. *The International Journal of Robotics Research*, 30(3):324–334, 2011.

[36] Michele Focchi, Romeo Orsolino, Marco Camurri, Victor Barasuol, Carlos Mastalli, Darwin G Caldwell, and Claudio Semini. Heuristic planning for rough terrain locomotion in presence of external disturbances and variable perception quality. In *Advances in Robotics Research: From Lab to Market*, pages 165–209. 2020.

[37] A Gasparetto and L Scalera. From the unimate to the delta robot: the early decades of industrial robotics. In *Explorations in the History and Heritage of Machines and Mechanisms*, pages 284–295. Springer, 2019.

[38] Ruben Grandia, Farbod Farshidian, René Ranftl, and Marco Hutter. Feedback mpc for torque-controlled legged robots. In *2019 IEEE/RSJ International Conference on Intelligent Robots and Systems (IROS)*, pages 4730–4737. IEEE, 2019.

[39] Kaveh Akbari Hamed, Vinay R Kamidi, Wen-Loong Ma, Alexander Leonessa, and Aaron D Ames. Hierarchical and safe motion control for cooperative locomotion of robotic guide dogs and humans: A hybrid systems approach. *IEEE Robotics and Automation Letters*, 5(1):56–63, 2019.

[40] B. Henze, C. Ott, and M.A. Roa. Posture and balance control for humanoid robots in multi-contact scenarios based on model predictive control. In *2014 IEEE/RSJ International Conference on Intelligent Robots and Systems*, pages 3253–3258, 2014.

[41] Jane Holland, Liz Kingston, Conor McCarthy, Eddie Armstrong, Peter O'Dwyer, Fionn Merz, and Mark McConnell. Service robots in the healthcare sector. *Robotics*, 10(1):47, 2021.

[42] Michael A Hopkins, Dennis W Hong, and Alexander Leonessa. Compliant locomotion using whole-body control and divergent component of motion tracking. In *2015 IEEE International Conference on Robotics and Automation*, pages 5726–5733, 2015.

[43] Marco Hutter, Hannes Sommer, Christian Gehring, Mark Hoepflinger, Michael Bloesch, and Roland Siegwart. Quadrupedal locomotion using hierarchical operational space control. *The International Journal of Robotics Research*, 33(8):1047–1062, 2014.

[44] Sung Wook Hwang, Jeong-Hyeon Bak, Jonghyun Yoon, Jong Hyeon Park, and Jong-Oh Park. Trajectory generation to suppress oscillations in underconstrained cable-driven parallel robots. *Journal of Mechanical Science and Technology*, 30:5689–5697, 2016.

[45] Qimi Jiang and Vijay Kumar. Determination and stability analysis of equilibrium configurations of objects suspended from multiple aerial robots. 2012.

[46] Shuuji Kajita and Bernard Espiau. Legged robot. In *Springer handbook of robotics*. Springer, 2008.

[47] Rafal Kamocki. Pontryagin maximum principle for fractional ordinary optimal control problems. *Mathematical Methods in the Applied Sciences*, 37(11):1668–1686, 2014.

[48] Mohammad A Khosravi and Hamid D Taghirad. Robust pid control of fully-constrained cable driven parallel robots. *Mechatronics*, 24(2):87–97, 2014.

[49] Jonas Koenemann, Andrea Del Prete, Yuval Tassa, Emanuel Todorov, Olivier Stasse, Maren Bennewitz, and Nicolas Mansard. Whole-body model-predictive control applied to the hrp-2 humanoid. In *2015 IEEE/RSJ International Conference on Intelligent Robots and Systems*, pages 3346–3351, 2015.

[50] Moharam Habibnejad Korayem, Hami Tourajizadeh, and Mahdi Bamdad. Dynamic load carrying capacity of flexible cable suspended robot: robust feedback linearization control approach. *Journal of Intelligent & Robotic Systems*, 60:341–363, 2010.

[51] Hosang Lee, Yisoo Lee, and Jaeheung Park. Contact-consistent disturbance observer for floating-base robots. In *International Symposium on Experimental Robotics*, pages 475–484, 2018.

[52] Jay H Lee. Model predictive control: Review of the three decades of development. *International Journal of Control, Automation and Systems*, 9(3):415–424, 2011.

[53] Jay H Lee and Zhenghong Yu. Worst-case formulations of model predictive control for systems with bounded parameters. *Automatica*, 33(5):763–781, 1997.

[54] MV Levskii. Pontryagin's maximum principle in optimal control problems of orientation of a spacecraft. *Journal of Computer and Systems Sciences International*, 47(6):974–986, 2008.

[55] Z. Li, S.S. Ge, and S. Liu. Contact-force distribution optimization and control for quadruped robots using both gradient and adaptive neural networks. *IEEE Transactions on Neural Networks and Learning Systems*, 25(8):1460–1473, 2013.

[56] Abhijit Mahapatra, Shibendu Shekhar Roy, and Dilip Kumar Pratihar. *Multi-Legged Robots—A Review*, pages 11–32. Springer Singapore, Singapore, 2020.

[57] Liheng Mao, Feng Gao, Yuan Tian, and Yue Zhao. Novel method for preventing shin-collisions in six-legged robots by utilising a robot–terrain interference model. *Mechanism and Machine Theory*, 151, 2020.

[58] Alexandra Markis, Maximilian Papa, David Kaselautzke, Michael Rathmair, Vinzenz Sattinger, and Mathias Brandstötter. Safety of mobile robot systems in industrial applications. In *Proceedings of the ARW & OAGM Workshop*, pages 26–31, 2019.

[59] David Q Mayne. Model predictive control: Recent developments and future promise. *Automatica*, 50(12):2967–2986, 2014.

[60] Ramin Mersi, Sina Vali, Ghasem Abbasnejad, Mehdi Tale Masouleh, et al. Design and control of a suspended cable-driven parallel robot with four cables. In *2018 6th RSI International Conference on Robotics and Mechatronics (IcRoM)*, pages 470–475. IEEE, 2018.

[61] Nathan Michael, Jonathan Fink, and Vijay Kumar. Cooperative manipulation and transportation with aerial robots. *Autonomous Robots*, 30:73–86, 2011.

[62] Michael Mistry and Ludovic Righetti. Operational space control of constrained and underactuated systems. *Robotics: Science and systems VII*, pages 225–232, 2012.

[63] Viviana Morlando and Fabio Ruggiero. Disturbance rejection for legged robots through a hybrid observer. In *2022 30th Mediterranean Conference on Control and Automation (MED)*, pages 743–748. IEEE, 2022.

[64] Viviana Morlando, Ainoor Teimoorzadeh, and Fabio Ruggiero. Whole-body control with disturbance rejection through a momentum-based observer for quadruped robots. *Mechanism and Machine Theory*, 164:104412, 2021.

[65] Michael Neunert, Markus Stäuble, Markus Giftthaler, Carmine D Bellicoso, Jan Carius, Christian Gehring, Marco Hutter, and Jonas Buchli. Whole-body nonlinear model predictive control through contacts for quadrupeds. *IEEE Robotics and Automation Letters*, 3(3):1458–1465, 2018.

[66] Christian Ott, Maximo A Roa, and Gerd Hirzinger. Posture and balance control for biped robots based on contact force optimization. In *2011 11th IEEE-RAS International Conference on Humanoid Robots*, pages 26–33. IEEE, 2011.

[67] Zoran Pandilov and Vladimir Dukovski. Comparison of the characteristics between serial and parallel robots. *Acta Technica Corviniensis-Bulletin of Engineering*, 7(1), 2014.

[68] Jaehwan Park, Ohung Kwon, and Jong Hyeon Park. Anti-sway trajectory generation of incompletely restrained wire-suspended system. *Journal of Mechanical Science and Technology*, 27:3171–3176, 2013.

[69] Andreas Pott and Tobias Bruckmann. *Cable-driven parallel robots*. Springer, 2013.

[70] Lal Bahadur Prasad, Barjeev Tyagi, and Hari Om Gupta. Optimal control of nonlinear inverted pendulum system using pid controller and lqr: performance analysis without and with disturbance input. *International Journal of Automation and Computing*, 11:661–670, 2014.

[71] Sen Qian, Bin Zi, Wei-Wei Shang, and Qing-Song Xu. A review on cable-driven parallel robots. *Chinese Journal of Mechanical Engineering*, 31(1):1–11, 2018.

[72] Oscar E Ramos, Nicolas Mansard, and Philippe Soueres. Whole-body motion integrating the capture point in the operational space inverse dynamics control. In *2014 IEEE International Conference on Humanoid Robots*, pages 707–712, 2014.

[73] Ludovic Righetti, Jonas Buchli, Michael Mistry, and Stefan Schaal. Inverse dynamics control of floating-base robots with external constraints: A unified view. In *2011 IEEE international conference on robotics and automation*, pages 1085–1090. IEEE, 2011.

[74] Helena Sofia Rodrigues, M Teresa T Monteiro, and Delfim FM Torres. Optimal control and numerical software: an overview. *arXiv preprint arXiv:1401.7279*, 2014.

[75] Fabio Ruggiero. Decentralized control of aerial manipulators through a momentum-based estimator. In *Aerial Robotic Manipulation*, pages 159–174. Springer, 2019.

[76] Fabio Ruggiero, Jonathan Cacace, Hamid Sadeghian, and Vincenzo Lippiello. Passivity-based control of vtol uavs with a momentum-based estimator of external wrench and unmodeled dynamics. *Robotics and Autonomous Systems*, 72:139–151, 2015.

[77] Haydar Sahin and Levent Guvenc. Household robotics: autonomous devices for vacuuming and lawn mowing [applications of control]. *IEEE Control Systems Magazine*, 27(2):20–96, 2007.

[78] João Cavalcanti Santos, Ahmed Chemori, and Marc Gouttefarde. Model predictive control of large-dimension cable-driven parallel robots. In *Cable-Driven Parallel Robots: Proceedings of the 4th International Conference on Cable-Driven Parallel Robots 4*, pages 221–232. Springer, 2019.

[79] Emre Sariyildiz, Roberto Oboe, and Kouhei Ohnishi. Disturbance observer-based robust control and its applications: 35th anniversary overview. *IEEE Transactions on Industrial Electronics*, 67(3):2042–2053, 2019.

[80] Christian Schenk, Carlo Masone, Andreas Pott, and Heinrich H Bülthoff. Application of a differentiator-based adaptive super-twisting controller for a redundant cable-driven parallel robot. In *Cable-Driven Parallel Robots: Proceedings of the Third International Conference on Cable-Driven Parallel Robots*, pages 254–267. Springer, 2018.

[81] Stefano Seriani, Paolo Gallina, and A Wedler. A modular cable robot for inspection and light manipulation on celestial bodies. *Acta Astronautica*, 123:145–153, 2016.

[82] Bruno Siciliano, Lorenzo Sciavicco, Luigi Villani, and Giuseppe Oriolo. *Robotics: modelling, planning and control*. Springer, 2010.

[83] Ruizhuo Song and Frank L Lewis. Robust optimal control for a class of nonlinear systems with unknown disturbances based on disturbance observer and policy iteration. *Neurocomputing*, 390:185–195, 2020.

[84] Susumu Tachi, Kazuo Tanie, Kiyoshi Komoriya, Yuji Hosoda, and Minoru Abe. Guide dog robot—its basic plan and some experiments with meldog mark i. *Mechanism and Machine Theory*, 16(1):21–29, 1981.

[85] Lewei Tang, Xiaoqiang Tang, Xiaoling Jiang, and Clément Gosselin. Dynamic trajectory planning study of planar two-dof redundantly actuated cable-suspended parallel robots. *Mechatronics*, 30:187–197, 2015.

[86] Yuval Tassa, Tom Erez, and Emanuel Todorov. Synthesis and stabilization of complex behaviors through online trajectory optimization. In *2012 IEEE/RSJ International Conference on Intelligent Robots and Systems*, pages 4906–4913, 2012.

[87] Chuck Thorpe and Hugh Durrant-Whyte. Field robots. In *Proceedings of the 10th International Symposium of Robotics Research (ISRR'01)*, 2001.

[88] Marco Tognon, Rachid Alami, and Bruno Siciliano. Physical human-robot interaction with a tethered aerial vehicle: Application to a force-based human guiding problem. *IEEE Transactions on Robotics*, 37(3):723–734, 2021.

[89] Teodor Tomić, Christian Ott, and Sami Haddadin. External wrench estimation, collision detection, and reflex reaction for flying robots. *IEEE Transactions on Robotics*, 33(6):1467–1482, 2017.

[90] Yuh-Shyang Wang, Nikolai Matni, and John C Doyle. Localized lqr optimal control. In *53rd IEEE Conference on Decision and Control*, pages 1661–1668. IEEE, 2014.

[91] Xavier Weber, Loic Cuvillon, and Jacques Gangloff. Active vibration canceling of a cable-driven parallel robot using reaction wheels. In *2014 IEEE/RSJ International Conference on Intelligent Robots and Systems*, pages 1724–1729. IEEE, 2014.

[92] Xavier Weber, Loic Cuvillon, and Jacques Gangloff. Active vibration canceling of a cable-driven parallel robot in modal space. In *2015 IEEE International Conference on Robotics and Automation (ICRA)*, pages 1599–1604. IEEE, 2015.

[93] Alexander W Winkler, Dario C Bellicoso, Marco Hutter, and Jonas Buchli. Gait and trajectory optimization for legged systems through phase-based end-effector parameterization. *IEEE Robotics and Automation Letters*, 3:1560–1567, 2018.

[94] Alexander W Winkler, Farbod Farshidian, Michael Neunert, Diego Pardo, and Jonas Buchli. Online walking motion and foothold optimization for quadruped locomotion. In *2017 IEEE International Conference on Robotics and Automation*, pages 5308–5313, 2017.

[95] Anxing Xiao, Wenzhe Tong, Lizhi Yang, Jun Zeng, Zhongyu Li, and Koushil Sreenath. Robotic guide dog: Leading a human with leash-guided hybrid physical interaction. In *2021 IEEE International Conference on Robotics and Automation (ICRA)*, pages 11470–11476. IEEE, 2021.

[96] Guiyang Xin, Hsiu-Chin Lin, Joshua Smith, Oguzhan Cebe, and Michael Mistry. A model-based hierarchical controller for legged systems subject to external disturbances. In *2018 IEEE International Conference on Robotics and Automation*, pages 4375–4382, 2018.

[97] Guiyang Xin, Wouter Wolfslag, Hsiu-Chin Lin, Carlo Tiseo, and Michael Mistry. An optimization-based locomotion controller for quadruped robots leveraging Cartesian impedance control. *Frontiers in Robotics and AI*, 7:1–12, 2020.

[98] Hao Xiong, Lin Zhang, and Xiumin Diao. A novel control strategy for cable-driven parallel robots with unknown jacobians. In *2019 IEEE International Conference on Advanced Robotics and its Social Impacts (ARSO)*, pages 79–83. IEEE, 2019.

[99] James E Young, Youichi Kamiyama, Juliane Reichenbach, Takeo Igarashi, and Ehud Sharlin. How to walk a robot: A dog-leash human-robot interface. In *2011 RO-MAN*, pages 376–382. IEEE, 2011.

[100] Xuanqi Zeng, Songyuan Zhang, Hongji Zhang, Xu Li, Haitao Zhou, and Yili Fu. Leg trajectory planning for quadruped robots with high-speed trot gait. *Applied Sciences*, 9(7), 2019.

[101] Nan Zhang and Weiwei Shang. Dynamic trajectory planning of a 3-dof under-constrained cable-driven parallel robot. *Mechanism and Machine Theory*, 98:21–35, 2016.

[102] Bin Zi, Jun Lin, and Sen Qian. Localization, obstacle avoidance planning and control of a cooperative cable parallel robot for multiple mobile cranes. *Robotics and Computer-Integrated Manufacturing*, 34:105–123, 2015.

[103] Nathaniel Zoso and Clément Gosselin. Point-to-point motion planning of a parallel 3-dof underactuated cable-suspended robot. In *2012 IEEE International Conference on Robotics and Automation*, pages 2325–2330. IEEE, 2012.

Author's Publications

- **Viviana Morlando**, Ainoor Teimoorzadeh, Fabio Ruggiero
  "Whole-body control with disturbance rejection through a momentum-based observer for quadruped robots",
  Mechanism and Machine Theory, vol. 164 , pp. 104412, 2021,
  DOI: https://doi.org/10.1016/j.mechmachtheory.2021.104412

- **Viviana Morlando**, Mario Selvaggio, Fabio Ruggiero
  "Nonprehensile Object Transportation with a Legged Manipulator",
  2022 International Conference on Robotics and Automation (ICRA),
  Philadelphia, Pennsylvania, May 2022, pp. 6628-6634, IEEE,
  DOI: https://doi.org/10.1109/ICRA46639.2022.9811810

- **Viviana Morlando**, Fabio Ruggiero
  "Disturbance rejection for legged robots through a hybrid observer",
  2022 30th Mediterranean Conference on Control and Automation (MED)
  Athens, Greece, June 2022, pp. 743-748, IEEE,
  DOI: https://doi.org/10.1109/MED54222.2022.9837169

- **Viviana Morlando** , Mario Selvaggio, Fabio Ruggiero
  "Robotic Non-prehensile Object Transportation",
  Conferenza I-RIM 3D 2022, 4 Conferenza Italiana di Robotica e Macchine Intelligenti Roma,
  Italia, Oct. 2022

- **Viviana Morlando**, Fabio Ruggiero, Vincenzo Lippiello
  "Tethering a Human with a Quadruped Robot: A Guide Dog to Help Visually Impaired People",
  Submitted to 2023 31th Mediterranean Conference on Control and Au-

tomation (MED) ,
Cyprus, 2023

- **Viviana Morlando**, Gianluca Neglia, Fabio Ruggiero,
"Drilling task with a quadruped robot for silage face measurements,"
Submitted to the 2023 IEEE International Workshop on Measurements and Applications in Veterinary and Animal Sciences,
Naples, Italy, 2023